# Formation evaluation of the Jurassic Stø and Nordmela formations in exploration well 7220/8-1, Barents Sea, Norway

*Johan Kristensson*

**Dissertations in Geology at Lund University,**

**Master's thesis, no 493**

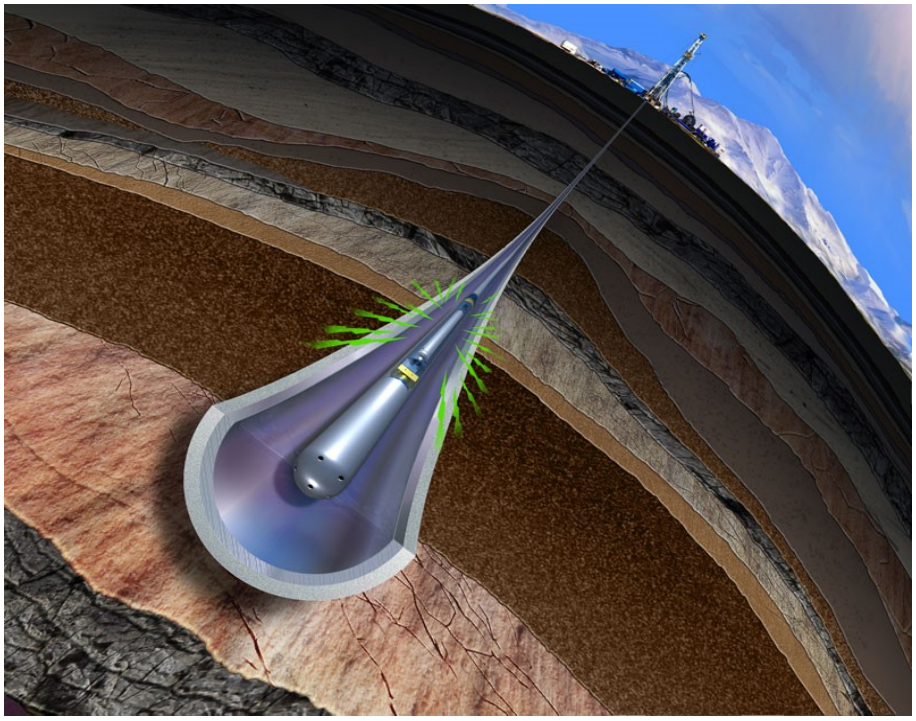

**Department of Geology**

**Lund University**

**2016**

# Formation evaluation of the Jurassic Stø and Nordmela formations in exploration well 7220/8-1, Barents Sea, Norway

Master's thesis

Johan Kristensson

Department of Geology
Lund University
2016

# Contents



**Cover Picture:** A drill string with well log tools sampling subsurface data (www.drillingcontractor.org).

# Formation evaluation of the Jurassic Stø and Nordmela formations in exploration well 7220/8-1, Barents Sea, Norway

JOHAN KRISTENSSON

Kristensson, J. 2016: Formation evaluation of the Jurassic Stø and Nordmela formations in exploration well 7220/8-1, Barents Sea, Norway. *Dissertations in Geology at Lund University*, No. 493, 57 pp. 45 hp (45 ECTS credits) .

Abstract: Evaluating reservoirs with alternating sequences of sand and shale meet the challenge of quantifying the effect from clay minerals. The clay minerals have an impact on logging tools and the resulting data. When not considering the effects, a formation evaluation will present incorrect results on e.g. porosity and water saturation leading to management decisions based on poor quality interpretations. One of the most challenging tasks for a petrophysicist is to determine the water saturation (Sw) in the formation. This is a crucial step because the assumption is that the hydrocarbon saturation are the remaining fluids whenever the water saturation is lower than 100% (1-Sw). This work present a formation evaluation on logging data from exploration well 7220/8-1, in the Barents Sea. It is based on the comparison between conventional evaluation techniques and techniques which compensate for the clay mineral effect. Results from Archie's water saturation are compared to Indonesia water saturation and Archie´s equation containing an alternative formation resistivity based on data from the triaxial induction tool, referred to as "sand resistivity". The conventional Archie´s method uses bulk resistivity affected by the conductive properties from both sand and lithologies built by clay minerals. Using sand resistivity as opposed to the bulk resistivity compensates for the clay mineral effect. The results show significantly lower water saturation when compensating for the clay mineral effects. The faster and cheaper sand resistivity approach could be validated by conducting special core analysis providing data for the Waxman-Smits water saturation equation. Comparable results would be in favor of the cheaper and faster method. The petrophysical effects on logging tools are tied to the regional geological evolution revealing the need for a multidisciplinary approach when evaluating potential reservoirs within the petroleum industry.

**Keywords:** Formation evaluation, shale effect, sand resistivity, Barents Sea, Stø Formation, Nordmela Formation, Lower Jurassic, Middle Jurassic, petroleum exploration, 7220/8-1, Schlumberger Techlog.

**Supervisor(s):** Mikael Erlström & Per Ahlberg

**Subject:** Bedrock Geology

*Johan Kristensson, Department of Geology, Lund University, Sölvegatan 12, SE-223 62 Lund, Sweden. E-mail: johankristensson778@hotmail.com.*

# Utvärdering av de jurassiska Stø- och Nordmelaformationerna i undersökningsborrningen 7220/8-1, Barents hav, Norge

JOHAN KRISTENSSON

Kristensson, J. 2016: Utvärdering av de jurassiska Stø- och Nordmelaformationerna i undersökningsborrningen 7220/8-1, Barents hav, Norge. *Examensarbeten i geologi vid Lunds universitet*, Nr. 493, 57 sid. 45 hp.

Sammanfattning: När petroleumföretag letar efter nya oljefyndigheter har de möjligheten att på själva borrsträngen fästa instrument som mäter olika egenskaper i berggrunden. En del instrument används för att bestämma hur stor andel mikroskopiska porer den sedimentära berggrunden består av och vilken vätska som ockuperar porerna. Porositeten ockuperas alltid av en vätska - formationsvatten, olja eller gas. Dessa vätskor förekommer också tillsammans, sorterade vertikalt beroende på vätskornas densitet. Denna studie behandlar en utvärdering av en petroleumreservoar belägen i Barents hav utanför Norges kust. Ett av målen är att bestämma hur mycket av varje vätska som förekommer i reservoaren för att i slutändan räkna ut det kommersiella värdet. Detta gjordes med hjälp av ett dataset insamlat från en undersökningsborrning i Barents hav. Datan bearbetades sedan i en mjukvara framtagen speciellt för utvärdering av berggrundens fysiska egenskaper, Schlumberger Techlog 2015.3. Reservoaren som studerades består av två berggrundsenheter, Stø och Nordmela. Dessa formationer består till huvuddelen av sandsten varvat med skiffer. Skiffer består av lermineral vilka har egenskapen att binda stora mängder formationsvatten. Instrumenten som används för att samla in data har låg upplösning vilket gör det problematiskt att bestämma vatten- och petroleumhalten i berggunden eftersom det endast är önskvärt att utvärdera sandstenen som är själva reservoaren. Empiriska formler för att bestämma vattenhalten är utarbetade och används frekvent. Tas det inte hänsyn till lermineralen och dess vattenhållande egenskaper, blir resultatet en för hög beräkning av vattenmättnaden vilket i slutändan kan innebära att man inte väljer att producera reservoaren då det inte anses lönsamt. Det är därför viktigt att kvantifiera lermineralen för att kunna göra bättre beräkningar. Detta kan inte utföras under datainsamlingen på grund av begränsningar i instrumenten, utan sker under utvärderingsfasen. Archies ekvation är den konventionella och traditionella metoden för att bestämma vattenhalten i berggrunden. Resultat från denna metod jämförs med resultaten från två andra metoder som kvantifierar och bortser från lermineralens egenskaper—Indonesia och Archie/Clavaud ekvationerna. Resultaten visar att Archies ekvation beräknar högst vattenmättnad följd av Indonesia. Lägst vattenmättnad ger Archie/Clavaud-metoden som bygger på att mjukvaran alternerar mellan olika värden i ekvationen beroende på de vertikala och horisontella egenskaperna i berggrunden. Metoden möjliggör upptäckt av tunna sandstensavsnitt som annars varit svåra att upptäcka där de alternerar med skiffer. Traditionellt har det varit relativt enkelt att hitta och producera olja och gas. Denna process blir alltmer en utmaning och så korrekta utvärderingar som möjligt krävs. Petroleum behövs till energi, men den kommer inte produceras om inte företagen går med vinst. I vilken slags berggrund och hur den är utformad beror på den geologiska utvecklingen där globala, regionala och lokala processer har betydelse. Att studera den geologiska utvecklingen är vitalt för att få en uppfattning om vad som kan förväntas i berggrunden. Detta möjliggör en mer ingående planering av vilka instrument, undersökningar och beräkningar som krävs för att uppnå ett resultat så nära sanningen som möjligt. I slutändan ger detta underlag till företagsledningen som kan ta korrekta beslut.

**Nyckelord:** Formation, utvärdering, lermineral, sandresistivitet, Barents hav, Støformationen, Nordmelaformationen, jura, 7220/8-1, Schlumberger Techlog.

**Handledare**: Mikael Erlström & Per Ahlberg

*Johan Kristensson, Geologiska institutionen, Lunds universitet, Sölvegatan 12, 223 62 Lund, Sverige. E-post: johankristensson778@hotmail.com.*

# 1 Introduction

Current challenges for the petroleum industry include the evaluation and appraisal of new discoveries. Historically, vast amounts of petroleum has been explored and produced with relative simplicity globally. The current and future petroleum discoveries are found in geologically more complex areas and the costs of producing such discoveries are significantly higher. The ability to make as correct evaluations as possible of petroleum reservoirs, and estimate the potential profit is therefore vital. Such framework determines whether or not a project will have a closure or a continuation.

This study meet the challenge of performing a formation evaluation with data from exploration well 7220/8-1 located offshore Norway in the southwestern Barents Sea. The main target of the drilling, and the reservoir comprised by the Lower and Middle Jurassic Nordmela and Stø formations, is evaluated using Schlumberger Techlog 2015.3 software. The result gives the pay interval and the hydrocarbon saturation. The knowledge of these two factors gives us the ability to calculate potential revenues.

The Stø and Nordmela formations are sandstone units containing shale. The shale content increases in the lower parts of the Stø- and in most parts of the Nordmela formation.

The shale, built by clay minerals, has an impact on the data retrieved from petrophysical logging tools. Techniques compensating for shale in sandstone reservoirs will be discussed and implemented into the formation evaluation. The results reveal the need for a multidisciplinary approach within the petroleum industry when evaluating potential petroleum reservoirs. The Barents Sea reservoirs and the petrophysical impact on logging tools, related to regional geological setting are discussed.

## 1.1 Locality/study area

The studied exploration well 7220/8-1 is located in the Norwegian sector of the southwestern Barents Sea (72°29'28.92 N/20°20'2.25 E). The Barents Sea constitutes a shallow shelf area with an intracratonic setting between the Atlantic Ocean, Bjørnøya, Svalbard archipelago, Frans Josef Land and Novaya Zemlya archipelago (Barrére 2009; Dore 1995; Edvardsen et al. 2014; Fig. 1).

Seismic surveys with the purpose to locate hydrocarbon reservoirs have been carried out since the 1970´s, and drilling in the area began in 1980. The first hydrocarbon-producing field in the Norwegian

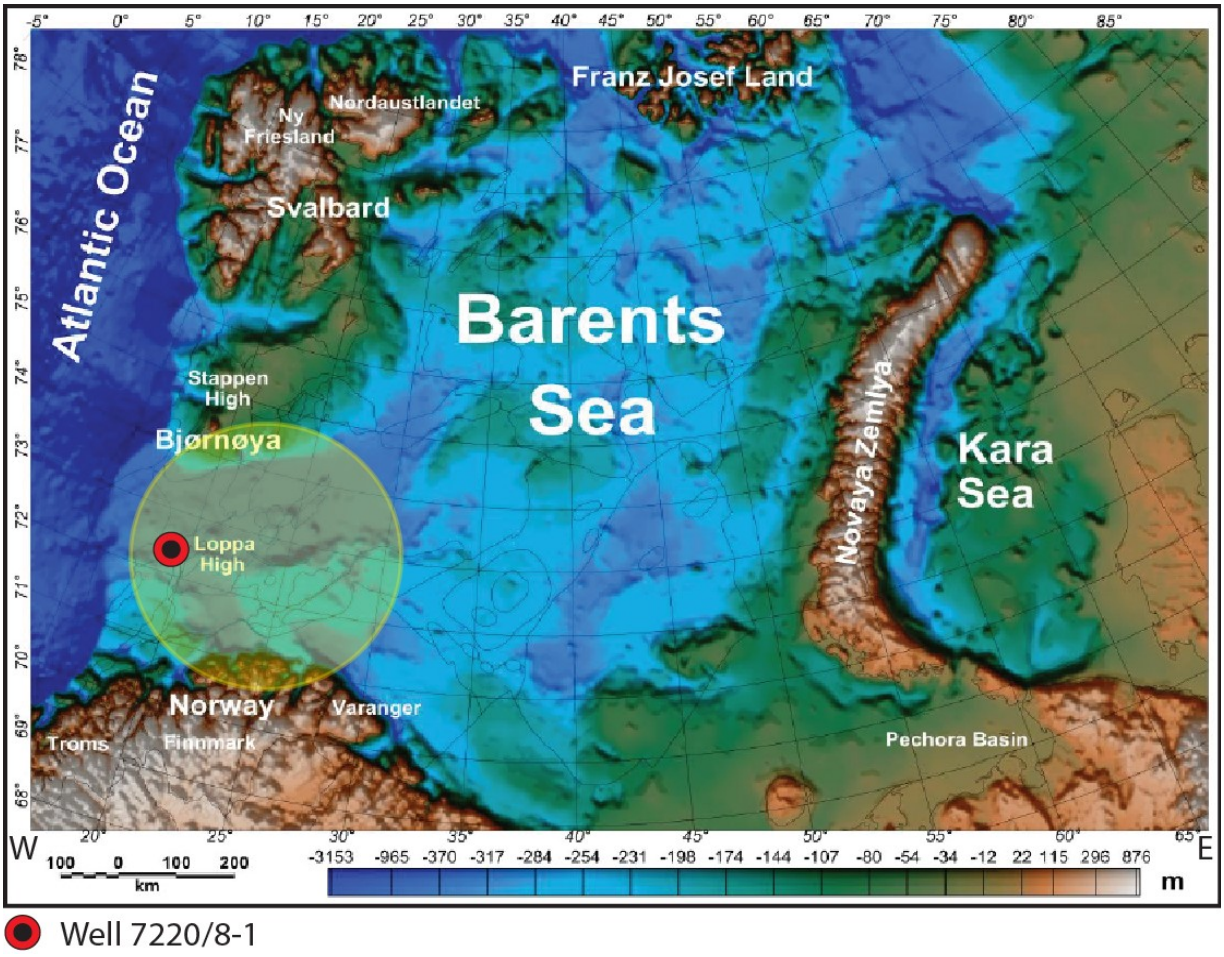


*Fig. 1. Map showing relative depths of the Barents Sea and surrounding landmasses. The Barents Sea is situated between Norway, Russia, Novaya Zemlya, Franz Josef Land, Svalbard, Bjørnøya and the Atlantic Ocean. The main study area, SW Barents Sea, marked by the red and black circle (modified from Barrére 2009).*

sector is the Snøhvit field, still producing today. Later, additional fields have been discovered, such as the Skrugard and Havis fields, and recently, by Lundin A/S, the Gohta field. The hydrocarbons of the Gohta field are found in Late Permian carbonate reservoirs. The Barents Sea hydrocarbon fields display a great variety of reservoirs, not only a majority of sandstone reservoirs as in the North Sea, but also carbonate reservoirs (Smelror et al. 2009; Lundin 2013).

The studied well is situated in the Skrugard fault block in the PL532 drilling license (Fig. 2A). The Skrugard fault block is the main target within the Bjørnøyrenna fault complex, an area with several tilted and rotated fault blocks ranging from north to south (Fanavoll et al. 2014; Lindberg et al. 2013; Løseth et al. 2013; Fig. 2B).

The Lower Jurassic Nordmela Formation is found between 1354 m and 1511 m depth and is overlain by the Middle Jurassic Stø Formation which forms the top of the reservoir at 1276 m in the 7220/8-1 well (Lindberg et al. 2013; Halland et al. 2013).

## 1.2 Geological evolution

During Ordovician through early Devonian times, the Caledonian orogeny (490-390 Ma) initially started to form what would become the Barents Sea through a collision event between the Laurentian, Laurussian and Baltic paleocontinental plates. The complex evolution of the area is described by e.g. Gabrielsen (1984), Dore (1991, 1995), Ryseth et al. (2003), Ritzmann & Faleide (2007), Gee et al. (2008) and Gernigon et al. (2014). Important framework of the Barents Sea frequently used in geological research has been carried out by e.g. Faleide et al. (1984) and Smelror et al. (2009).

The collision and merging of the Baltic and Laurentian plates resulted in closure of the Iapetus Ocean and the formation of the Laurussian continent (Faleide et al. 1984; Smelror et al. 2009; Fig. 3A). During the Devonian, extensive post-orogenic erosion took place. A compressional phase in the area shifted towards a left-lateral shearing, resulting in large scale strike-slip movements creating folding and Graben structures during the Late Devonian (Harland 1965; Faleide et al. 1984; Smelror et al. 2009; Fig. 3B). During Carboniferous, the left-lateral movements changed into an extensional regime still active in early Permian (Gjeldberg & Steel 1981; Fig. 3C).

During Late Palaeozoic and Mesozoic times, an extensional regime dominated in the area. An exception to this is the Uralian orogeny (280-240 Ma) forming the eastern margin of the Barents Sea (Dore 1995).

Post-orogenic evolution includes late Silurian to Early Devonian widespread extension (Fossen 2000, 2010), late Devonian to Carboniferous intracratonic rifting (Worsley 2006) and early Permian subduction forming an extensive carbonate platform (Stemmerik & Worsley 2005). During the Permian subduction, eastern and western Barents Sea was separated by a structural high. The climate varied and eustatic sea level changes, characterized by high frequency and amplitude, determined the depositional regime in the area (Worsley et al. 2006; Smelror et al. 2009; Henriksen et al. 2011).

During late Permian and throughout Triassic times the area was subjected to rapid subsidence due to the accumulation of siliciclastic sediments (Johansen et al. 1992). During the Jurassic, a rifting episode caused block faulting in the western Barents Sea resulting in the formation of major structural highs and lows (Gabrielsen 1990). Cretaceous rifting and subsidence occurred in western Barents Sea while the eastern parts were subjected to moderate subsidence (Johansen et al. 1992; Figs. 4A, 4B).

The Norwegian-Greenland Sea was opened at approximately 56 Ma. The subsequent sea floor spreading had great impact on the Cenozoic geological evolution of the Barents Sea (Eldholm et al. 1987; Johansen et al. 1992; Fig. 4C). The sea floor spreading was initially characterized as a sheared margin where most deformation occurred west of the Loppa High and

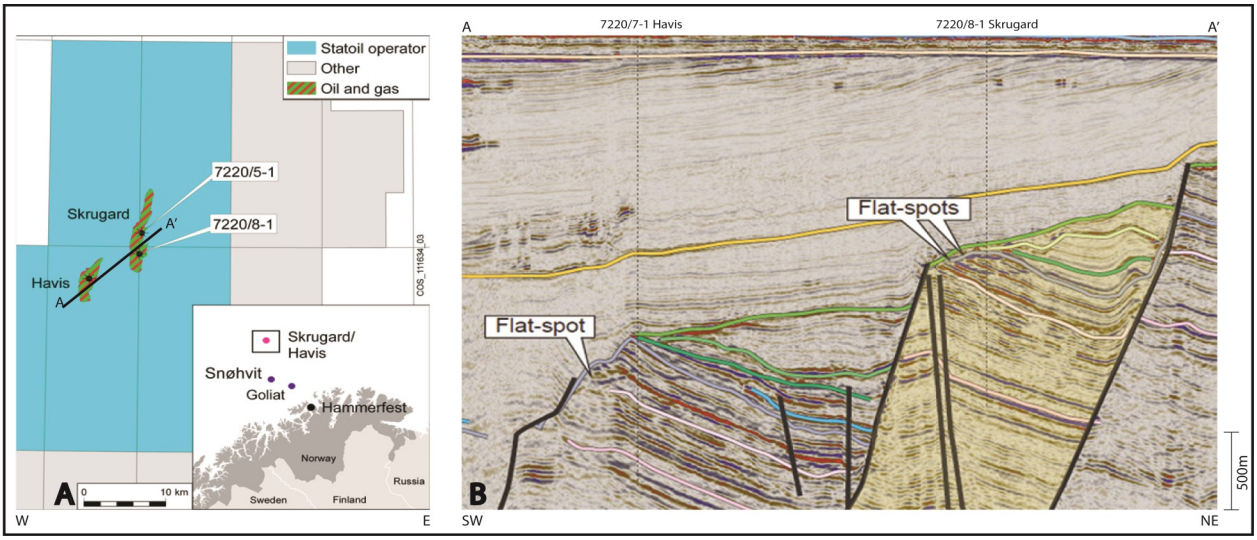


*Fig. 2. A. Drilling license map showing the Skrugard and Havis field developments. Study well 7220/8-1 is situated in the Skrugard field in the SW Barents Sea. The profile A-A' is shown in B (modified from Norwegian Petroleum Directorate). B. Seismic section showing the profile A-A' in figure 2A. The highlighted Skrugard fault block penetrated by exploration well 7220/8-1 (dotted line) is part of the Bjørnøyrenna Fault Complex. The differently coloured seismic horizons indicate the interpreted top and base of different geological formations. The interpreted "Flat-spots" indicate fluid contacts (modified from Carstens 2013).*

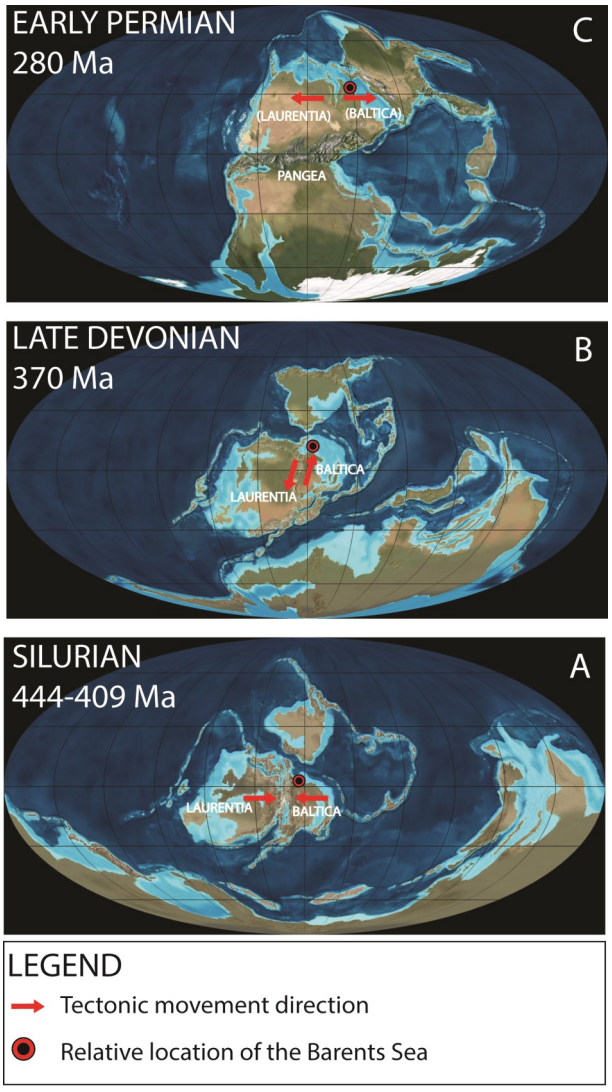


*Fig. 3. Palaeogeographic maps with main direction of tectonic movements indicated by the red arrows affecting the Barents Sea area during A: Silurian, B: Devonian and C: Permian (modified from www.sepmstrata.org).*

Senja Ridge illustrated in Fig. 5 and 6. The westernmost basins in the Barents Sea continued to subside and sediment from the local highs and the uplifted eastern and northern shelf areas accumulated in the basins (Johansen et al. 1992; Faleide et al. 1996; Ryseth et al. 2003). The sheared margin formation evolves during three main stages. First, the rift stage caused by continent-continent shearing, followed by the drift stage during continent ocean transition. The final stage results in a passive margin characterized by a continent-ocean fracture zone boundary. The margin tends to be relatively narrow. As sea floor spreading occurs along the margin, thermal uplift produces a ridge which is able to trap sediments. Thick sedimentary sequences are common in association with the sheared margin (Bird 2001).

During the Paleogene to Neogene, compressive deformation occurred in the western Barents Sea. During the mid-Miocene, the Barents Sea was regionally uplifted (Dengo & Røssland 1992; Worsley 2006; Smelror et al. 2009).

### 1.3 Structural geology

The Skrugard prospect, and wildcat well 7220/8-1, is situated west of the structural elements Polheim Sub-Platform and Loppa High in the Barents Sea (Fig. 5). The Skrugard fault block, containing the petroleum prospect, is one of several rotated fault blocks belonging to Bjørnøyrenna Fault Complex (Lindberg et al. 2013; Løseth et al. 2013; Halland et al. 2013; Fanavoll et al. 2014; Fig. 6).

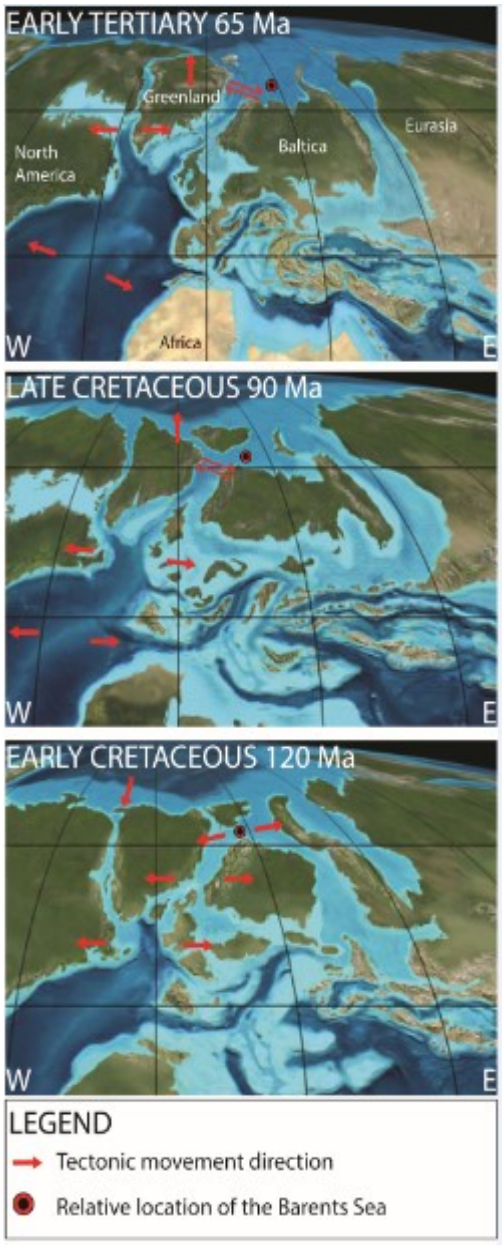


*Fig. 4. Tectonic movements in the northern hemisphere during (A) Early Cretaceous, (B) Late Cretaceous and (C) Early Tertiary (modified from www.sepmstrata.org).*

The Polheim Sub-Platform, a block-faulted area, situates between the Loppa High to the east and the Bjørnøyrenna and Ringvassøy-Loppa Fault Complex to the west. The Loppa High, an isolated and elongated structural high in the southwestern Barents Sea, borders the Hammerfest Basin to the south in an area referred to as the Asterias Fault Complex. To the west, there is an area separating the Loppa High and the

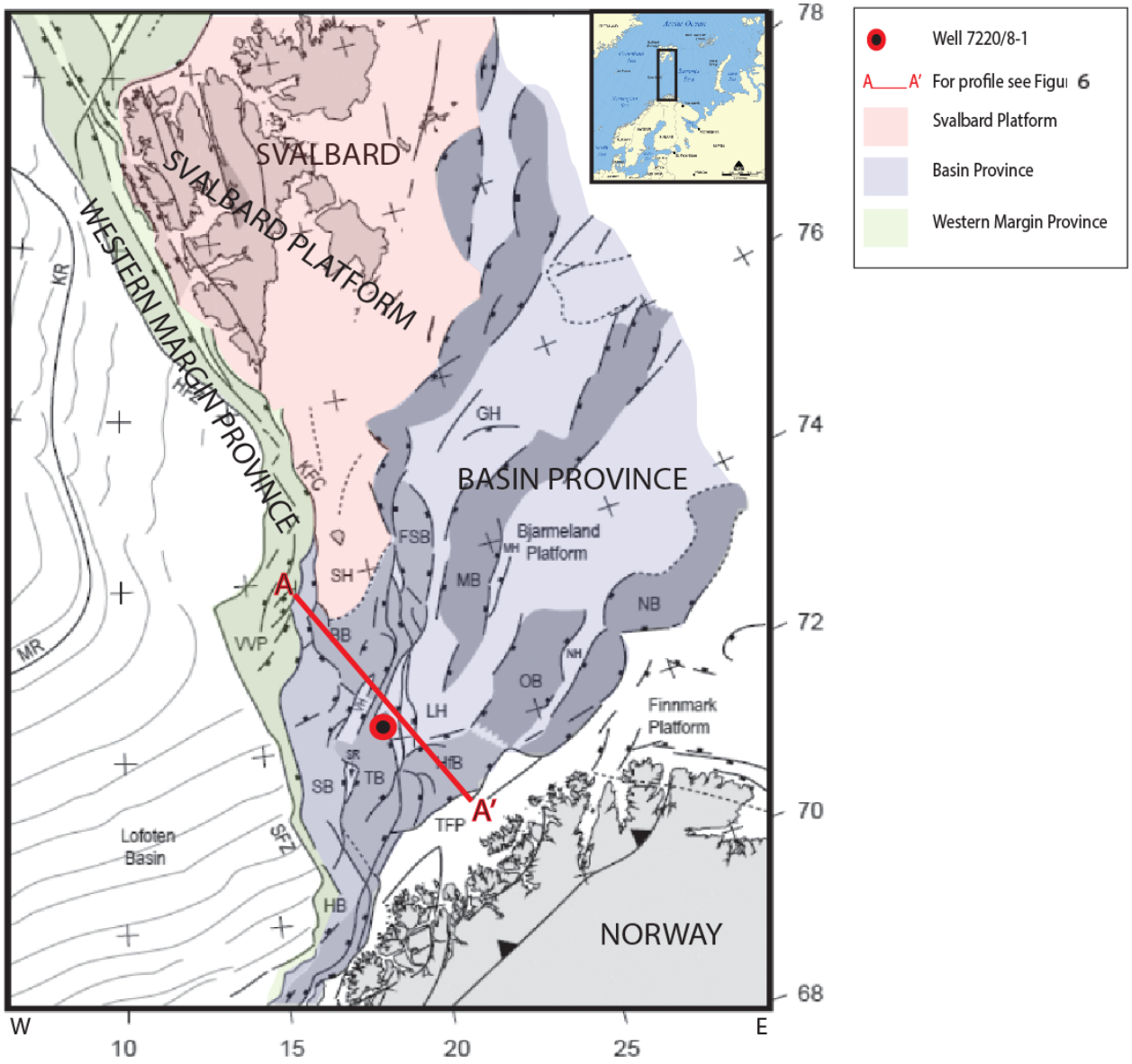


*Fig. 5. Map showing the main structural elements in SW Barents Sea approximately divided into three geological provinces: The Western Margin, The Svalbard platform and the Basin Province. The profile A-A' is illustrated in Figure 6 (modified from Faleide et al. 2010). Abbreviations: Basins: BB = Bjørnøya Basin, FSB = Fingerdjupet Sub Basin, HB = Harstad Basin, HFB = Hammerfest Basin, MB = Maud basin, NB = Nordkapp Basin, OB = Ottar Basin, SB = Sørvestnaget Basin, TB = Tromsø BasinFracture Zones: HFZ = Hornsund Fault Zone, SFZ = Senja Fracture Zone. Structural Highs: GH = Gardarbakken High, KR = Knipovich Ridge, LH = Loppa High, MH = Mercurius High, MR = Mohs Ridge, NH = Nordsel high, SH = Stappen High, SR = Senja Ridge, TFP = Troms-Finnmark Platform, VVP = Veslemøy High.*

Tromsø Basin known as the rotated fault blocks comprising the Ringvassøy-Loppa Fault Complex. In the northwest area, the Loppa High is separated from the Bjørnøya Basin, by the Bjørnøyrenna Fault Complex. (Figs. 5, 6). The structural geology of the western Barents Sea is well documented by e.g. Rønnevik et al. (1984), Wood et al. (1989), Gabrielsen (1990), Stemmerik et al. (1995), Larssen et al. (2005), Glørstad et al. (2010), Lindberg et al. (2013), Løseth et al. (2013), Halland et al. (2013) and Fanavoll et al. (2014).

The NE-SW facing Bjørnøyrenna Fault Complex acts as boundary between the Loppa High to the southeast and Bjørnøya Basin to the northwest and terminates in the Tromsø Basin to the south. Extension and vertical displacement forming this complex is recognized by normal faults and large throws associated with minor doming. Seismic studies reveal signs of inversion, dome features, deformed fault planes, reverse faulting and deformation of footwall blocks, all of them contributing to the complexity in this area (Gabrielsen 1990; Fig. 5).

Faults were active during the Late Jurassic–Early Cretaceous and reactivated during Late Cretaceous–Paleogene. Larssen et al. (2002) states that the main faults originate from the Palaeozoic and that they were reactivated several times during the Mesozoic and Ter tiary. Deformed fault planes, reverse faults and footwall block deformation are related to two separate

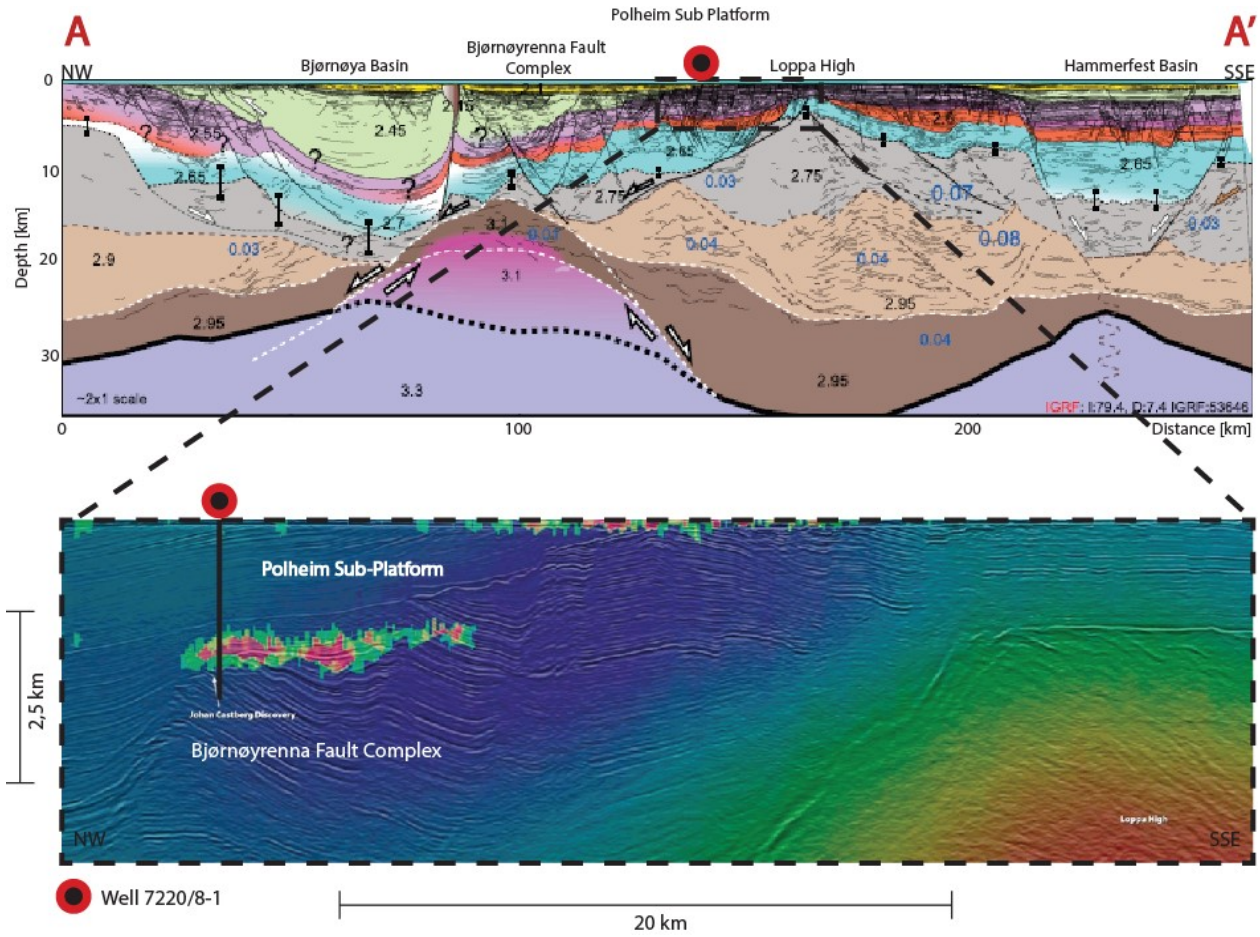


*Fig. 6. Profile A-A' marked in figure 5 crosscutting, e.g., well 7220/8-1 and the surrounding structural elements responsible for shaping the trap mechanism. The image is an interpreted geoseismic section where structural elements and formations are determined on the basis of seismic data (modified from Gernigon et al. 2014). The image below shows a close up section with the Loppa High in the southeast and the Polheim Sub-Platform and Bjørnøyrenna Fault Complex with the Johan Castberg discovery in the northwest. Well 7220/8-1 is seen penetrating the Johan Castberg discovery. The image is created on the basis of electromagnetic data. The technique is heavily used for exploration studies (modified from McKay et al. 2014).*

stages of inversion documented by Gabrielsen et al. (1997). The first stage is correlated with a strike-slip movement during the Early Cretaceous, and the second, during the Late Cretaceous and early Tertiary, is associated with a compressional regime.

## 1.4 Stratigraphy

A general stratigraphy of the sedimentary succession in the SW Barents Sea is shown in Fig. 7. The stratigraphy in the exploration well 7220/8-1, is illustrated in Fig. 8 and 13. The stratigraphic subdivision in the area is based on the work of sequence stratigraphical interpretation by e.g. Cecchi et al. (1995), Sattar et al. (2012), Halland et al. (2013) and Smelror, (1994) together with data from seismic surveys carried out by e.g. van Veen et al. (1993) and Sattar et al. (2012). The definition of formation boundaries has also been refined by data from spectral gamma ray studies (Halland et al. 2013). Correlation throughout the structurally complex area is based on well- and seismic correlation and compared to equivalent sequences in USA and on Svalbard (Cecchi et al. 1995; Smelror 1994).

Several biostratigraphical studies including work on spores, pollen, dinoflagellates, foraminifera and palynomorphs by Hochuli et al. (1989), Vigran et al. (1998), Nagy et al. (2004) and Radmacher et al. (2014) contribute to the biostratigraphical zonation of the sedimentary bedrock in the Barents Sea.

### Palaeozoic stratigraphy

The general Palaeozoic succession of the strata, overlying the Caledonian basement, includes the Billefjorden, Gipsdalen, Bjarneland and Tempelfjorden groups. The strata range from siliciclastic rocks derived from the Caledonides to carbonate sediments deposited in shallow marine environments (Dalland et al. 1988, 1989; Mørk et al. 1989; Faleide et al. 1991, 1993; Smelror et al. 2009).

### Mesozoic stratigraphy

The Mesozoic succession comprises the Sassendalen, Kapp Toscana, Adventdalen and Nygrunnen groups. The reservoir formations in well 7220/8-1 which are the focus of this study, the Nordmela and Stø formations (Figs. 8, 13), belong to the Kapp Toscana Group. These formations are described and discussed below. The source rock, the Hekkingen Formation, from which the petroleum has migrated into the reser-

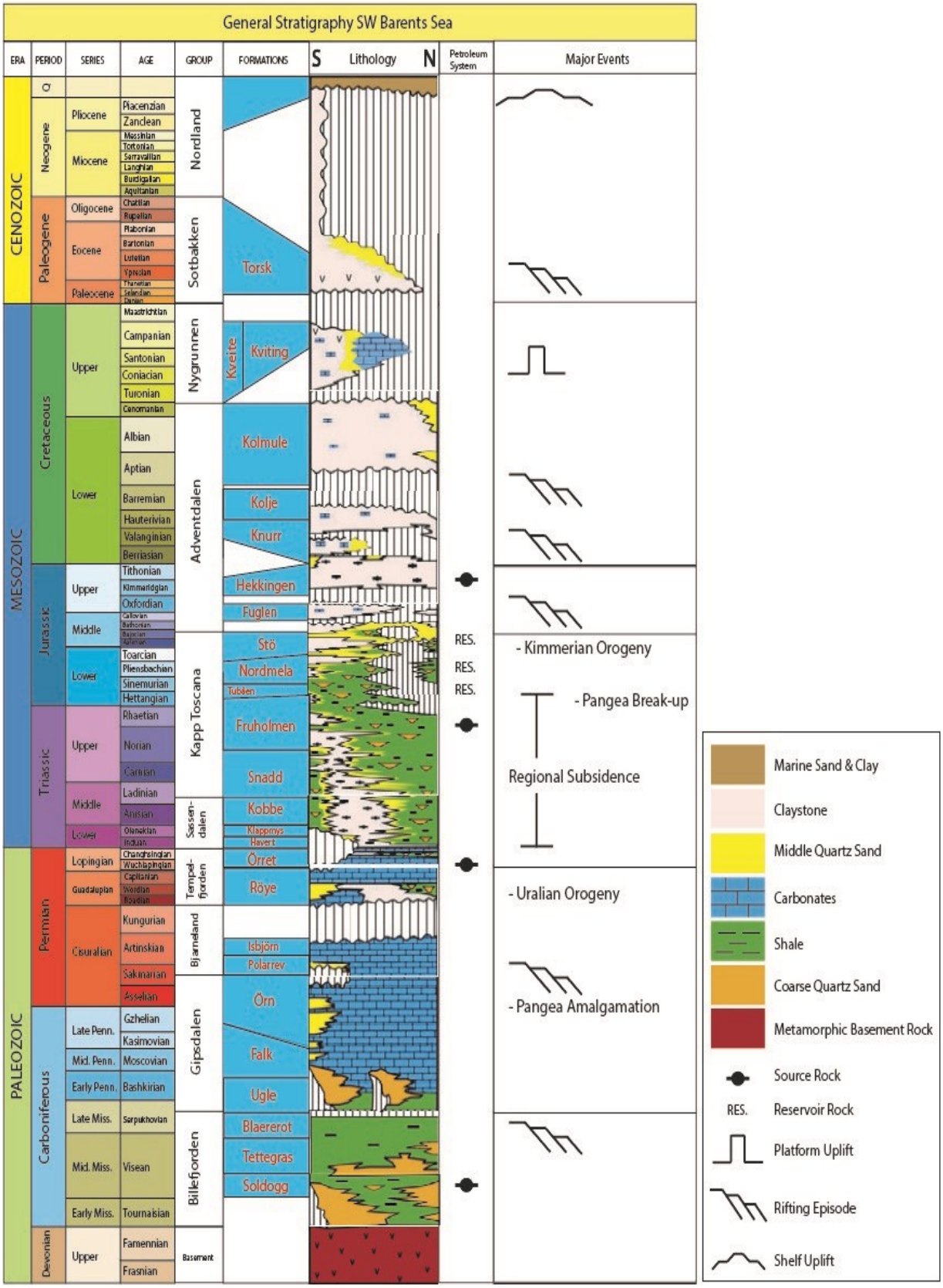


*Fig. 7. General stratigraphy of the SW Barents Sea showing the lithostratigraphic classification, formations, groups, major tectonic events and petroleum systems (after Glørstad-Clark et al. 2010).*

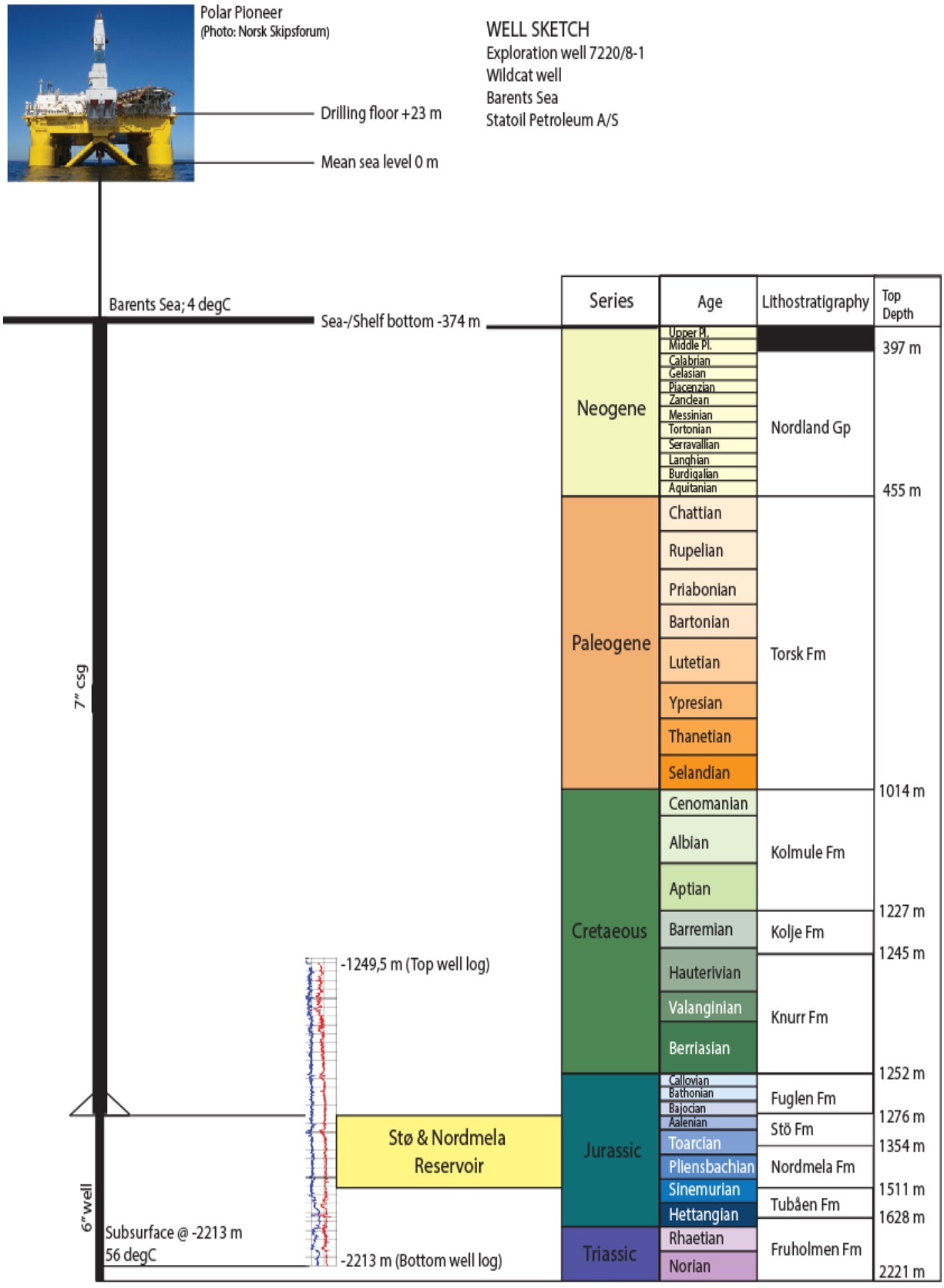


*Fig. 8. Well sketch showing exploration well 7220/8-1 with measurements, temperature, logging interval and the stratigraphic subdivision. The main objectives for this study: Stø and Nordmela formations, are highlighted in yellow.*

voir, overlies the reservoir formations and belongs to the same group (Dalland et al. 1988, 1989; Faleide et al. 1991, 1993; Smelror et al. 2009; Fig 14).

### Cenozoic stratigraphy

The youngest sedimentary rocks in the Barents Sea are of Neogene and Quaternary age. The Nordland Group. overlies the Paleogene Sotbakken Group, the latter comprising the Torsk Formation which is composed of greenish–gray claystone with thin laminae of silt- and limestone. Horizons with volcanic tuff are known from the lowermost parts of the unit. The strata are interpreted as having been deposited in open to deep marine shelf environments during the Paleocene through the Oligocene (Worsley 1988; Dalland et al. 1989).

## 1.5 Study formations

### Study Formation 1: Nordmela – Secondary reservoir unit

The Nordmela Formation (Figs. 10, 11) is composed of a succession of strata with alternating beds of siltstone, sandstone, shale and claystone. Together with minor occurrences of coal the formation indicate deposition in tidal flat and flood plain settings during the Sinemurian to late Pliensbachian. The formation is underlain by the Tubåen Formation and overlain by the Stø Formation (Dalland et al. 1989; Smelror et al. 2009). Isolated sandstone units are suggested to indicate estuarine and tidal channel environments (Halland et al. 2013). The amount of sandstone beds increases upsection towards the base of the Stø Formation. In the Hammerfest Basin, a wedge of strata similar to the

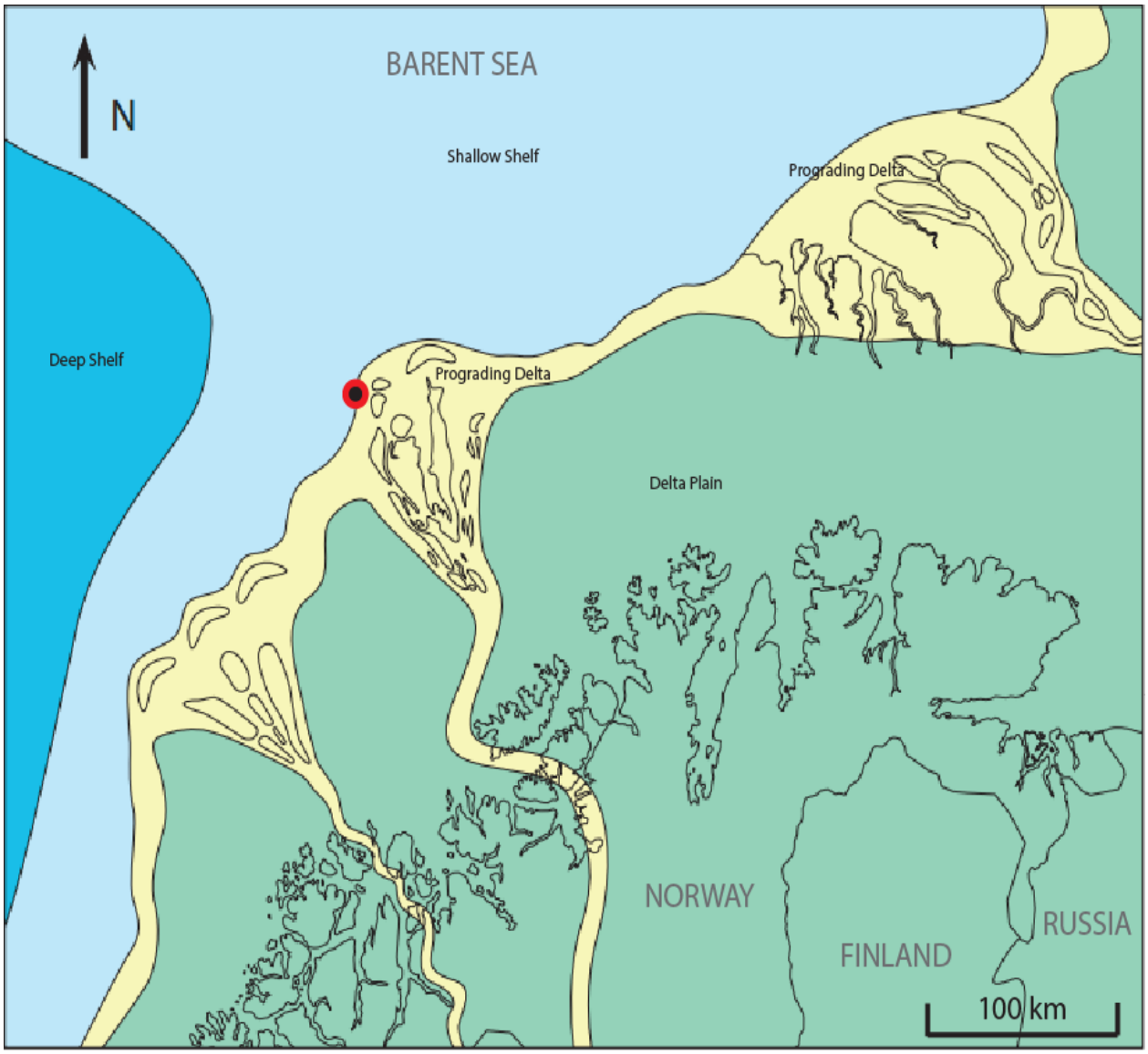


*Fig. 9. Conceptual sketch showing prograding deltas in a northern direction during deposition of Stø Formation. The Nordmela Formation was deposited prior to the Stø Formation during an interval with less supply of material deposited and more frequent tidal episodes (modified from Norwegian Petroleum Directorate).*

underlying Tubåen Formation has been recognized. The wedge thickens towards the southwest. The formation is diachronus becoming younger towards the east (Halland et al. 2013).

The thickness of the formation is 62 m in the type well (7121/5-1) and 202 m in the reference well (7119/12-2). The variation in thickness between the type- and reference wells coincides with the suggested wedge, thickening toward soutwest (Halland et al. 2013). A general westward thickening of the sedimentary succession is recognized in formations belonging to the Lower and Middle Jurassic. A suggested explanation for this is subsidence during the Kimmerian orogeny and tilting towards the Tromsø and Bjørnøya basins (Halland et al. 2013).

In the geophysical wire-line data the base of the Nordmela Formation is marked by a gamma ray increase in comparison to the underlying boxcar to blocky bell-shaped pattern. The boxcar gamma ray response curve indicates aggrading units of relative clean sandstone units while the bell shaped response signals a fining upward sequence while retrograding (Catuneanu et al. 2011). The base is also marked by a bulk density increase continuing upward. The top of the formation is characterized by a distinct decrease in the gamma ray of the overlying, cleaner sandy Stø Formation. Nordmela Formation is considered the secondary reservoir unit in the southwestern Barents Sea.

### Study Formation 2: Stø – Primary reservoir unit

The dominant lithology described by Dalland et al. (1988) comprises moderately to well- sorted mineralogically mature sandstones with distinct shale and siltstone horizons (Figs. 10,12). In some wells, especially in the upper parts of the formation, a phosphatic lag conglomerate is encountered. Sedimentation occurred during the late Pliensbachian to Bajocian. The base is diachronous in the Hammerfest Basin, and becomes younger from west to east in comparison with Nordmela Formation. Stø is overlying Nordmela Formation and is overlain by Fuglen Formation.

The sands were deposited when the coast prograded northward, suggested by a variety of linear clastic coastal lithofacies (Figs. 9, 10). The shale and siltstone horizons were formed during the late Toarcian and late Aalenian regional transgressions. Three depositional sequences are recognized. The base of the formation has only been encountered in the western parts of the Hammerfest Basin. The overlying sequence represents a maximum regional transgression followed by a variable sequence affected by syn-depositional uplift and differential erosion at the top (Dalland et al. 1988; Halland et al. 2013).

The type section is from well 7121/5-1 and measures 77 m from 2445–2368 m while the reference well, 7119/12-2, measures 145 m between 1517 and 1372 m (Dalland et al. 1988).

Geophysical data reveals a base defined by the clear transition from regular to serrated gamma ray patterns of the underlying Nordmela unit towards blocky and smooth patterns in the Stø unit indicating a more well sorted sandstone formation upward. The serrated pattern indicates horizons of different rock types (Catuneanu et al. 2011). A gradual density decrease across the boundary is visible (Dalland et al. 1988; Halland et al. 2013).

As part of the exploration led by the operator Statoil AS, Moosefinn (2011) performed a conventional core analysis (CCA) from the well 7220/8-1 with main focus on the Stø Formation. There are, in addi-

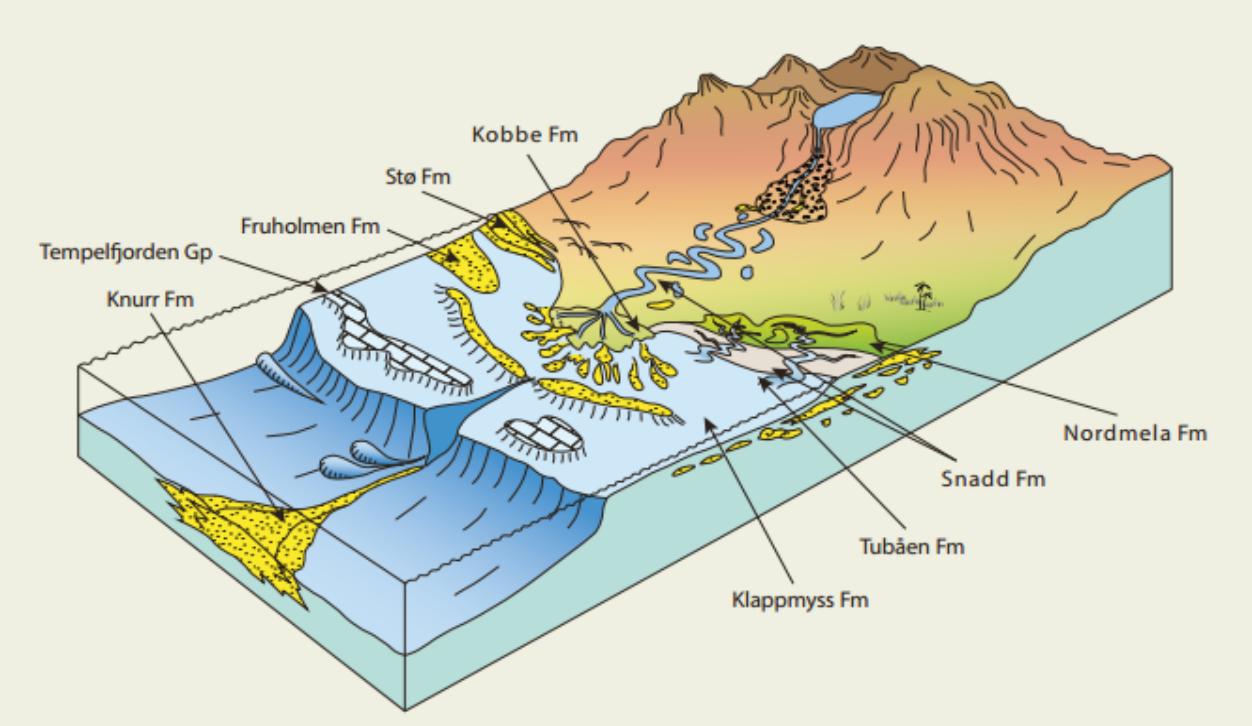


*Fig. 10. Depositional environments for the major reservoir formations in the SW Barents Sea (Norwegian Petroleum Directorate).*

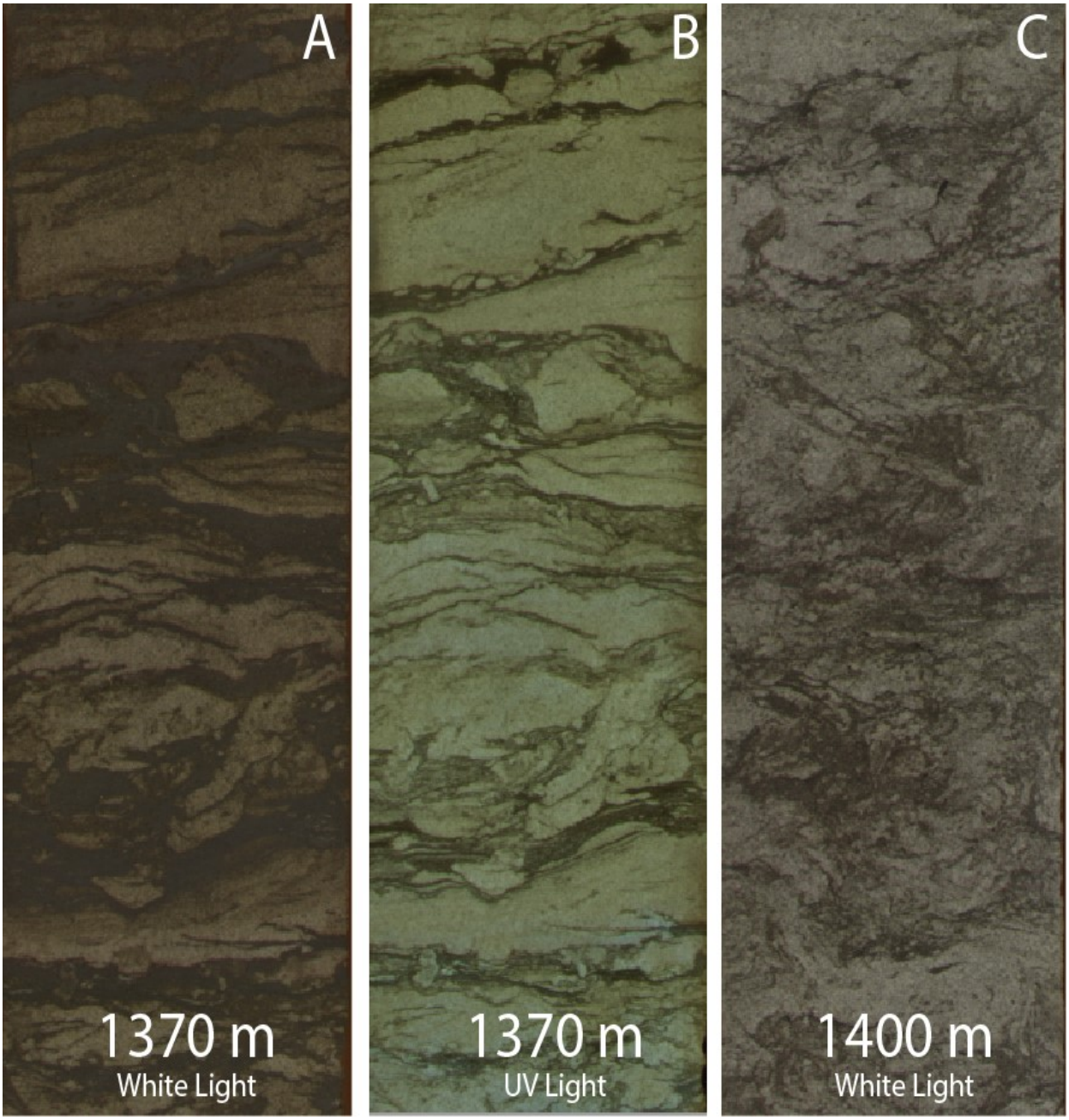


*Fig. 11. Core photos from the Nordmela Formation (well 7220/8-1) showing a sandstone with flaser to lenticular bedding. The clay mineral content is substantial compared to the Stø Formation. Visually, photo A and B indicate petroleum content while C at 1400 m, in the water zone, indicates brine content (modified from Statoil AS).*

tion, core data available for the upper part of the Nordmela Formation. These data are used for a comparison with the results derived from the well log analysis presented in this study. The assumption is that the data will be representative for the Nordmela reservoir as well since the upper part comprises the most potential reservoir sandstones in the Nordmela Formation. The core data from the Stø and Nordmela formations are summarized in Appendix II.

### 1.6 Study Well, Borehole History: 7220/8-1

#### General

The exploration well 7220/8-1 was drilled with the objective of finding hydrocarbons of commercial value. The well is located west of the Polheim Subplatform and Loppa High in the Barents Sea. In addition, the objective was to clarify the gas/oil- and oil/water contacts in the Stø and Nordmela formations within the Skrugard Fault Block for evaluation and future production purposes. The prospect fault block is one of many rotated fault blocks within the Bjørnøyrenna Fault Complex (Statoil; Figs. 8, 13).

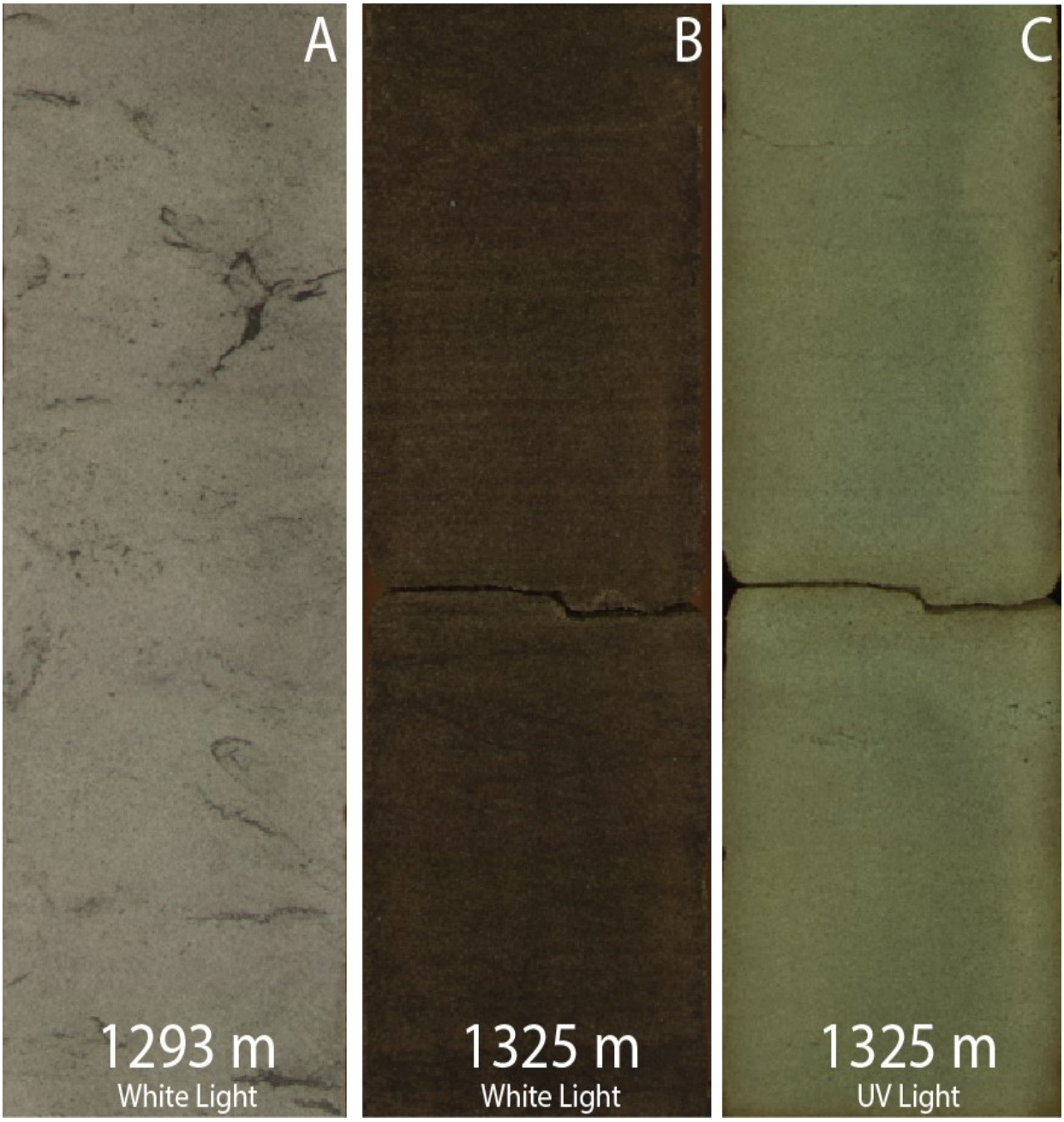


*Fig. 12. Core photos from the Stø Formation (well 7220/8-1) revealing a relatively clean sandstone reservoir. B shows a darker sandstone due to oil saturation. The oil show is confirmed in C since organic matter glows in UV light (modified from Statoil AS).*

## Operations and results

A pre-investigation well, referred to as 7220/8-U-1, was initially drilled and logged down to 955 m with the intention to detect shallow gas. The location of the borehole was based on a seismic anomaly visible in the area. However, no shallow gas was encountered. Even though no gas was indicates the drilling of the study well started in February 2011 and included a drilling down to the total vertical depth (TVD) at 2221 m, penetrating the Late Triassic Snadd Formation using the semi-submersible Polar Pioneer drilling rig. Spud-mud, based on guar gum or salt gel in offshore drillings, was used for the first 850 m followed by KCl/Polymer/Glycol-based mud from 850 m, through the reservoir interval to the TVD (Norwegian Petroleum Directorate 2013).

A table summarizing general drilling operation data is found in Appendix I.

The well penetrated the following stratigraphical units and rock types:

- Tertiary and Cretaceous clay- and sandstone.
- Upper Jurassic claystone.
- Jurassic sandstone in the reservoir unit belonging to Stø, Nordmela and Tubåen formations (Fig. 13).
- Triassic Fruholmen and Snadd formations.

The main target of the drilling, the top of the Stø Formation, was encountered at 1276 m, and the top of the Nordmela Formation at 1354 m. The formations con-

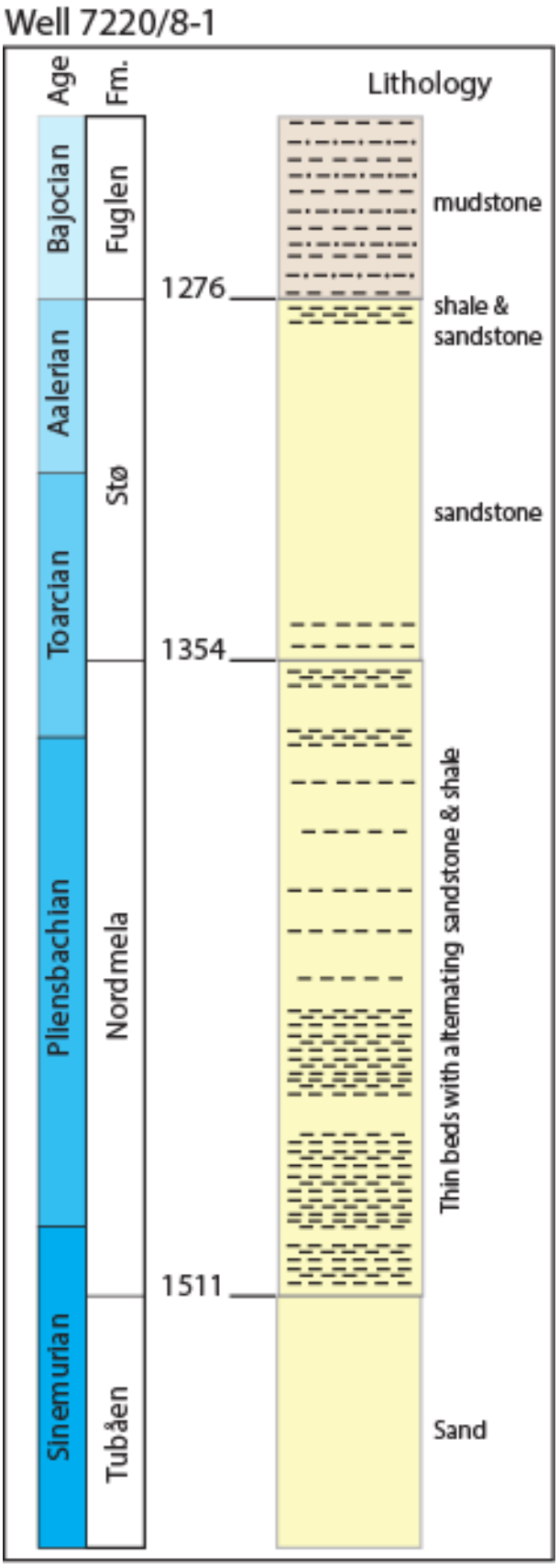


*Fig. 13. Interval illustrating the reservoir formations, Stø and Nordmela in exploration well 7220/8-1*

tained a 37 m thick gas column with a gas-oil contact at 1312 m and an 83 m thick oil column with the oil-water contact at 1395 m. These findings are consistent with interpreted flat spots from seismic studies. The flat spot is seen on seismic sections as a horizontal line in contrast to the surroundings and indicate the boundary between fluids with different characteristics. The Snadd Formation was reached 35 m shallower than expected, at 2221 m TVD. All depths are recorded in metres below drilling floor (Norwegian Petroleum Directorate 2013).

Oil was recorded in Stø and Nordmela formations, both in the core and in cuttings (Figs. 11, 12). Gas was detected in the drilling mud using a gas chromatograph. No other shows were encountered in core samples and cuttings, below 1400 m (Statoil).

Five cores representing the Stø and Nordmela formations were cut between 1292.5 and 1405.5 m depth, with a 97,8% recovery using a Schlumberger single probe modular formation dynamics tester. Oil samples were collected at 1320.6 m, 1336.8 m and 1380.5 m in both reservoir formations. On 2 May 2011 the well was abandoned and presented as an oil and gas discovery (Norwegian Petroleum Directorate 2013).

### 1.7 Petroleum systems in the Barents Sea

A petroleum system is defined by a once active, or still active, source rock generating petroleum raw-products such as gas and crude oil. Furthermore, the system includes the geological processes and/or prerequisites necessary for petroleum accumulation. These processes comprise the presence of a source rock, a reservoir rock with a suitable seal and overburden rock together with petroleum migration during a critical period of time. The processes must occur in a sequential order of sequences as to achieve successful accumulation (Magoon et al. 1994; Al Saeed et al. 2009; Fig. 15).

The petroleum is generated within the source rock when, once buried and preserved, organic material is exposed to a temperature and pressure equivalent to the area-specific oil- and gas window. This usually takes place in an organic-rich shale- or mudstone but could be generated in other sedimentary rocks as well (Magoon et al. 1994; Al Saeed et al. 2009).

Prior to petroleum generation the organic matter takes the state of kerogen, a waxy compound mixture of organic matter from different organic facies. The accumulated organic material is predominantly derived from marine plankton, bacteria and terrestrial plants. Different kerogen types will receive different Hydrogen/Carbon- and Oxygen/Carbon ratios thus having higher or lower petroleum potential. Type I kerogen stems from algae where lipids are enriched from bacterial activity. Type II kerogen contains mostly marine plankton and other lipid rich organic matter. Type I and II kerogen gives oil prone source rocks. Type III kerogen is mostly derived from terrestrial plants and give gas prone source rocks. Type IV kerogen contains reworked and oxidized organic material. This type of kerogen has the lowest quality and will not give petroleum prone source rocks (Gluyas and Swarbrick 2004; Bjørlykke 2010).

Due to overburden pressure, petroleum escapes the source rock and start to migrate. The migration could


*Fig. 14. Core photo from the Hekkingen Formation (well 7219/8-1S) showing a 1 m interval with laminated dark grey to black shale. The high TOC value, 3-13%, indicates a good potential source rock (modified from*

occur in any direction but normally upwards toward the surface due to the lower density of petroleum compared to formation water. The lighter petroleum will replace and push water away from the pores in a permeable reservoir rock (Magoon et al. 1994; Al Saeed et al. 2009).

The petroleum accumulates in porous reservoir rocks only if a suitable trap has evolved before migration takes place, known as the critical moment. The trap is usually made up by a seal rock, an impermeable or low-permeable sedimentary rock such as shale, claystone or evaporite. Tectonic events are important for the formation of traps, and can for instance generate anticlines, which have great potential for petroleum accumulation. The reservoir rock is usually a porous and permeable sandstone or grainstone, but numerous variations occur. The reservoir rock could be more or less damaged by cementation or a high content of clay. In contrast, diagenetic processes could also enhance reservoir properties (Magoon et al. 1994; Al Saeed et al. 2009).

Henriksen et al. (2011) recognize three different petroleum systems in the Barents Sea: Paleozoic, Early to Mid-Triassic and Late Jurassic petroleum systems. The study area for this article and exploration well 7220-8/1 is situated in Bjørnøya Basin belonging to the Late Jurassic petroleum system.

## Source rocks

Lower Carboniferous, upper Permian, Upper Triassic and Upper Jurassic source rocks have been identified in SW Barents Sea. Carboniferous source rocks consist of shale and mudstone, mostly gas prone, but oil prone shales also exist. Upper Permian source rocks have good potential as oil prone source rocks. Triassic source rocks are oil- and gas prone having good petroleum potential. Jurassic source rocks are considered the best source rocks with excellent petroleum potential. The thermal maturity, measured as vitrinite reflectance, for source rocks in the SW Barents Sea ranges between 0.6 and 1.3 %Ro, and the oil window for this region is thought to be located between 2500–5000 m. Source rocks located within this depth interval have great potential for generating petroleum (Johansen et al. 1992; Fig. 16).

In SW Barents Sea, the source rocks comprise the Jurassic Hekkingen Formation, being the main source for e.g. the Hammerfest-, Tromsø- and Bjørnøya basins. The Hekkingen Formation consists of a thick succession of dark, organic-rich shales deposited during deep marine anoxic conditions (Fig. 14). The depositional condition is a result of the Kimmerian Orogeny when barriers to water circulations were created (Dore 1995). Petroleum from Triassic shales may occur, but is considered of minor importance in this area (Johansen et al. 1992). The petroleum in the Bjar meland platform and Nordkapp basin is derived from the Lower to Middle Triassic Steinkobbe Formation.

The Hekkingen Formation has a substantial Total Organic Carbon (TOC) value and hence petroleum potential, important for the generation of petroleum. In the Hammerfest Basin the Triassic source rocks generated oil when the Hekkingen Formation was in an early mature stage. When the Hekkingen Formation generated oil, i.e. being within the oil window, the Triassic source rocks generated gas while exposed to higher temperature and pressure at greater depths (Johansen et al. 1992).

During the Hammerfest basin evolution, area uplift lowered the temperatures critical for hydrocarbon generation i.e. the source rock was displaced from the oil- and gas windows, and is considered immature. This indicates that the organic-rich source rock had not reached its full potential for generating hydrocarbons in the uplifted areas (Dalland et al. 1988; Dore 1995). Studies by Awuah et al. (2013) indicates a paleodepth of approximately 2000–2700 m for the Upper Jurassic source rocks in the Hammerfest basin. This is to be compared to the main oil window considered to be within an interval of 2500–3400 m (Fig. 16).

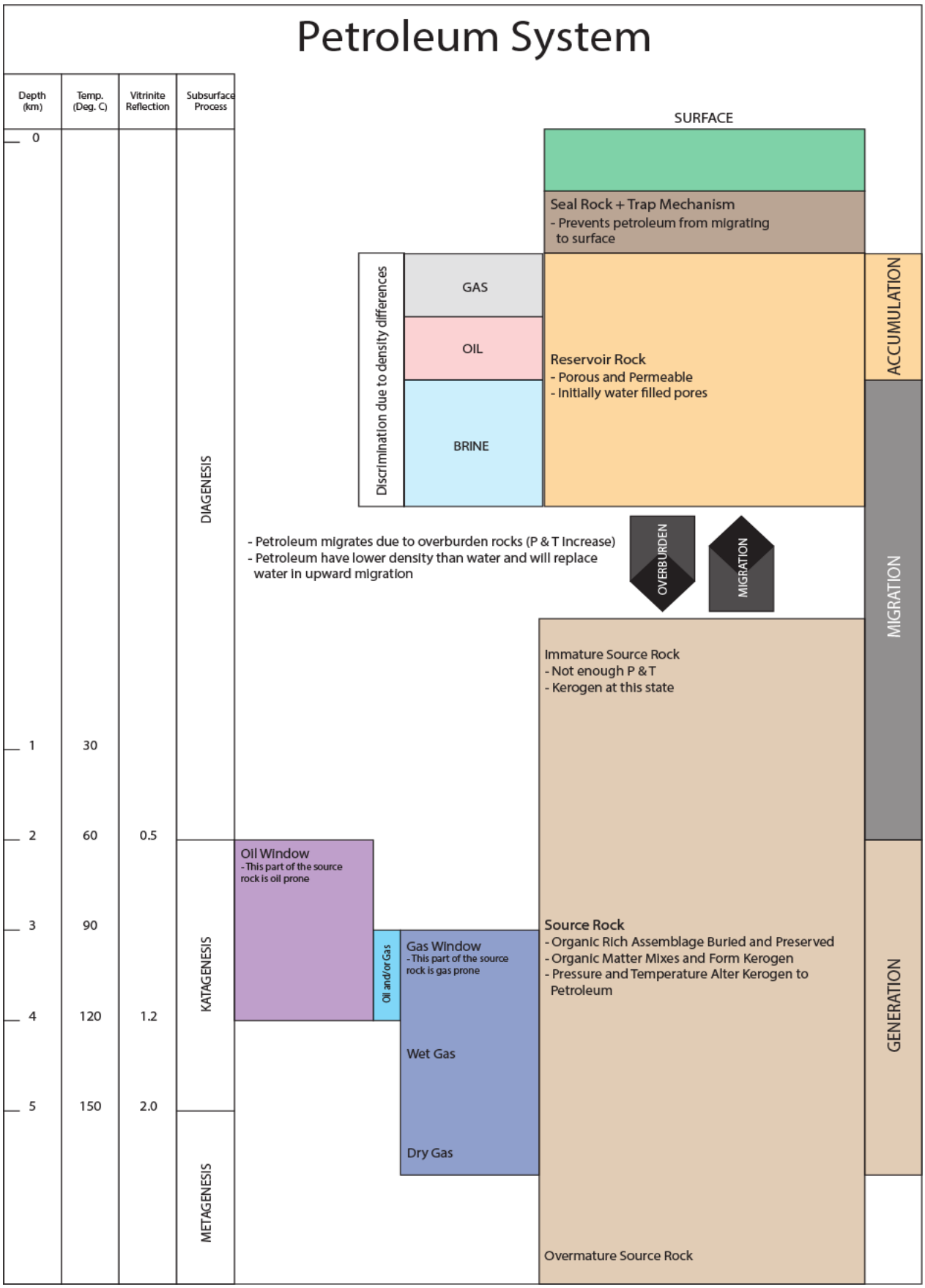


*Fig. 15. Schematic sketch explaining the general, major essential processes, in relation to each other, of a petroleum system.*

### Reservoir rocks

The most interesting and significant reservoir rocks belong to the Lower–Middle Jurassic Stø Formation, which is believed to comprise approximately 85% of the reservoir rocks within the Norwegian sector of the Barents Sea. Most of the reservoirs are anticipated to generate natural gas when produced. The formation consists of mature sandstone intercalated by thin shale- and siltstone beds. It was deposited in prograding coastal areas interrupted by minor transgressive episodes represented by clays (Dalland et al. 1988; Dore 1995).

Other reservoir rocks, expected to hold hydrocarbons, include the Lower Jurassic Nordmela and Tubåen formations which have relatively good reservoir properties. These formations were deposited in coastal, deltaic, marine and shoreface settings (Dalland et al. 1988; Dore 1995).

The Nordmela Formation is characterized by lenticular and/or flaser bedding, and was deposited in a subtidal to tidal channel. The formation is known to have low vertical permeability, but horizontally there is great connectivity and the unit serve as a good reservoir. The major challenge here lies in estimating correct reservoir quantities due to the high presence of non-reservoir shale (Dalland et al. 1988; Dore 1995).

The Tubåen Formation is comprised of sandstone with subordinate shales and minor coals recognized by Spencer et al. (2008). It is considered a better reservoir unit in comparison to the Nordmela Formation due to its fine– and medium grained sandstones. The decrease in reservoir quality is related to deeper burial and associated diagenetic alterations (Dalland et al. 1988; Dore 1995).

Trapping mechanisms in the SW Barents Sea are mainly created by rotated fault blocks and horst structures. In the Nordkapp Basin, there are stratigraphic traps created by salt diapirs. Since the Nordmela and Stø formations decrease in thickness toward the NE, this area demand a cap rock with low permeability and a spatial distribution large enough to prevent leakage. Tilting of strata and reactivation of faults have caused both preservation and trapping of petroleum as well as leakage throughout geologic time. Cenozoic uplift resulted in erosion of surficial strata and truncation of structures, possibly causing leakage and biological degradation of petroleum (Doré 1995; Dalland et al. 1998; Halland et al. 2013).

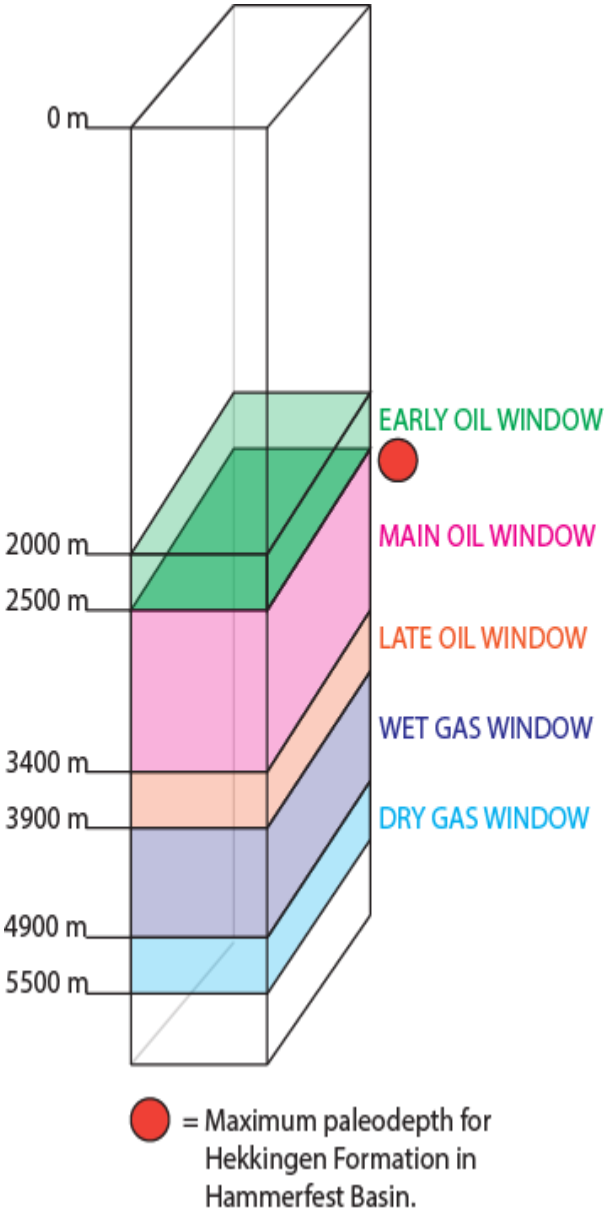


*Fig. 16. Schematic image showing the oil- and gas window depths in the SW Barents Sea. This is a general view and the conditions can be different in certain basins or areas.*

### 1.8 Well Logging

Well logging is a in situ method to examine the physical properties of rock. The technique was developed as complement to the geological descriptions and measurements on cuttings and core samples. The cuttings are always somewhat mixed and contaminated and coring is vastly expensive, while well logging is fast and favorable. LWD tools, Logging While Drilling, collect real-time data on petrophysical properties of the bedrock. Examples of LWD tools are Gamma Ray, Density and Neutron tools. The name of the tool indicates the parameter measured by the tool. Interpretations of the LWD data are used in formation evaluation, which is the focus of this study. The concept of formation evaluation is described below. MWD tools, Measuring While Drilling, are used in monitoring various drilling parameters, such as rate of penetration (ROP) and gas detection. MWD is used for drilling operation optimization. The MWD data are surveyed and documented by e.g. a mud logger. A mud logger is a type of field engineer who also collects and documents cuttings in order to evaluate in which formation the drilling takes place for the moment (Gluyas & Swarbrick 2004; Ellis & Singer 2008).

In general the tools indirectly measure rock characteristics including porosity and permeability. Interpretation of log data provides an estimation of subsurface rock characteristics. The techniques are continuously refined and today we are able to get reliable interpreta-

tions when performed with care (Gluyas & Swarbrick 2004; Ellis & Singer 2008).

For formation evaluation purposes, the necessary and basic logging tool suite includes the gamma ray, neutron porosity, density and resistivity tools. As the measurements from each tool supplement each other it is not recommended to use one tool only. The tools are also sensitive to the environment they operate in. These effects must be considered and corrected for in the evaluation. The environmental effects are, e.g., borehole size, mud type and mud weight, mud cake thickness, borehole salinity, borehole temperature, pressure, formation salinity, depth of invasion and tool standoff. Most logs require environmental corrections. These are made in specific software such as Schlumberger Techlog or Paradigm Geolog (Gluyas & Swarbrick 2004; Ellis & Singer 2008; Fig. 17). Manual corrections can be made using, e.g., graphic log interpretation charts from Schlumberger (2009). A brief explanation of the most common tools is given below.

## Gamma Ray

Described by, e.g., Gluyas & Swarbrick (2004) and Ellis & Singer (2008), a gamma ray tool detects and measure natural gamma radiation in the formation. Pure quartz sandstones have low gamma radiation due a low content of minerals containing potassium, thorium and uranium. These minerals are the main source for the gamma radiation. Argillaceous rock types, such as shale and claystone, are in contrary rich in clay minerals containing potassium and yields consequently significantly higher values compared to a pure sandstone. The gamma ray tool is therefore considered one of the most useful lithology tools. Type values for different lithologies do exist, but should be used with care and interpretation is best carried out together with other logging tools. Shale laminated sandstones or sandstones with dispersed clay will, e.g., have a mixed gamma ray value, which makes interpretation more of a challenge. A somewhat mixed lithology should always be considered.

Gamma radiation is recorded as American Petroleum Industry (API) units. The tools are calibrated in a test pit at the University of Houston, USA. The relative difference between high and low radioactivity are defined as 200 API units.

The tool is often used for correlation with offset wells, identification of lithology, volume of shale or shaliness, depth correlation between different log runs, depth correlation for fluid sampling and perforation and depth correlation when coring. The shape of the log response could be used for the identification of depositional facies. For example, a fining upward sequence would have coarser and clean sandstone with low gamma ray values gradually shifting toward higher values as the clay mineral content increases up the log. The coarsening upward sequence would be displayed as the opposite log response and the unmixed formation would have stabile low or high values.

The gamma ray log have to be corrected for borehole size, mud weight, mud type and cased hole formation. In a large borehole, with heavy mud or a casing the uncorrected tool would display too low values. If a KCl-based mud is used, the uncorrected log shows too high values.

The natural gamma ray tool separates the potassium, thorium and uranium components in the rock and may help in the process of evaluating different clay mineral groups present in the sandstone (Gluyas & Swarbrick 2004; Ellis & Singer 2008). Together with interpretation charts, plotting the content of the radioactive components may indicate the type of clay mineral. Kaolinite has, for instance, high concentrations of thorium and low concentrations of potassium. The chart has the highest potential of determining mineral type when there is a strong dominance from one radioactive mineral only (Schlumberger 2009).

## Neutron Tool

The neutron tool is, e.g., used in evaluations of lithology, fluid type and porosity. The tool emits neutrons from a cesium source which interacts with the concentration of hydrogen ions in the formation. A higher concentration of ions in the formation yields a higher signal compared to low concentrations. The assumption is that the detected hydrogen ions are a component of formation water or hydrocarbons, and indirectly porosity.

The neutron logging is an interaction with energy versus time. High energy emissions of neutrons are emitted from the tool. The neutrons interact with the formation and thereby loose energy i.e. they are slowed down. The process of slowing down continues until the neutrons reach thermal energy levels. The thermal state neutrons are eventually captured by an atom emitting gamma rays, as the nucleus gets excited. Different atoms have various ability of capturing the neutrons.

If not captured or absorbed, the high energy neutron scatters elastically in contact with a hydrogen nucleus. Each collision with other nuclei slows the neutron down and the time for the returning neutron is recorded by the tool. Hydrogen has the greatest ability to slow neutron energy down. A higher concentration of hydrogen will slow the neutron down more compared to a low concentration. Hydrogen is most abundant in pores and the slowing down rate is a function of porosity.

The tool is often used together with the density tool on the log trace and crossplots in order to determine porosity and lithology (Gluyas & Swarbrick 2004; Ellis & Singer 2008; Schlumberger 2009).

## Density Tool

The density tool emits and detects gamma radiation. The principle is that when density increases, fewer emitted gamma rays reach the detector. The tool has heavy shieldings preventing the emitted gamma rays to arrive directly from source to detector. The natural gamma radiation from the formation has much lower concentrations and will not affect the measurement. (Gluyas & Swarbrick 2004; Ellis & Singer 2008).

Electron density can be used as an indicator of true formation density. Formation mass is not determined by electrons but merely by neutrons and protons. The assumption is that in most cases a proton and a neutron roughly equals to two electrons providing a relationship between mass and electron density.

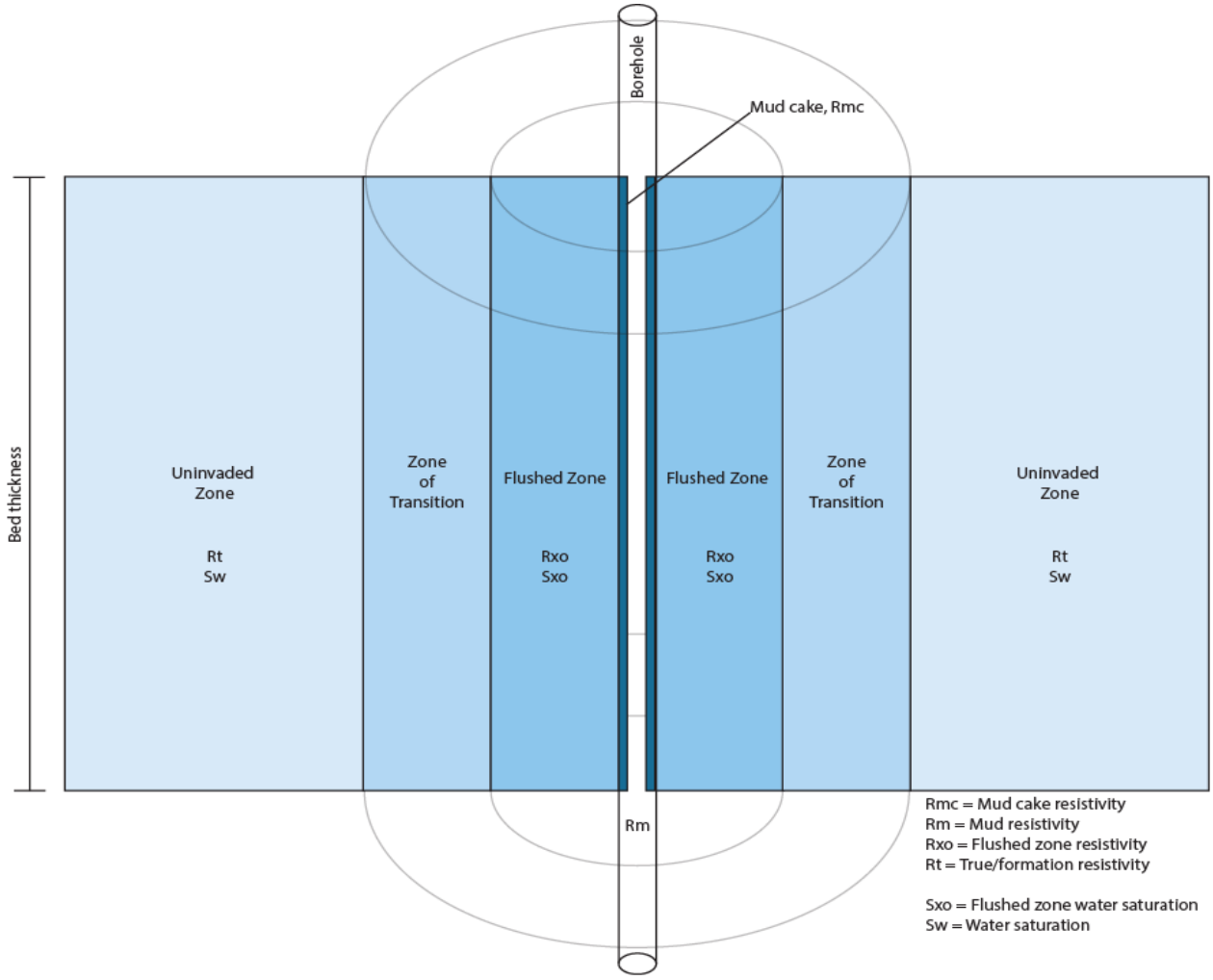


*Fig. 17. Sketch showing a generalized situation for the borehole environment. A drilling fluid invades all zones except the uninvaded zone. The drilling fluid affect log readings from different penetration depths from the borehole. In order to receive true formation log data, measurements are taken from different penetration depths (after Schlumberger 2009).*

The tool is normally used as a lithology and porosity indicator. Together with the neutron tool placed in the same log trace, reservoir units could be graphically detected. When the density has low and the neutron high values, this is an indicator of a fluid-filled porous formation. The relative separation between the neutron and density log responses could indicate the amount of porosity and fluid contacts. A porous interval with gas would have greater separation compared to a porous interval with oil, which in turn have greater separation than water filled interval.

## Resistivity Tool

The primary applications for the resistivity logs are fluid saturations, hydrocarbon thickness, or net pay, and permeability indication. In a porous and permeable formation, mud will invade the formation from the borehole. Resistivity is therefore measured at different penetration depths from the borehole wall in order to discriminate the resistivity in different zones. Resistivity of the mud, mudcake, flushed zone close to the the borehole, and the mixed zone and uninvaded zone furthest away from the borehole is usually measured. The uninvaded, or virgin, zone is considered to hold true formation properties (Fig. 17).

Resistivity is defined as the material's ability not to conduct electricity. Plastic has no conducting ability and thus high resistivity while saltwater, which is an excellent conductor, have low resistivity. When performing formation evaluation, the common assumption is that the rock matrix does not conduct electricity in non-shaly formations. Resistivity is thus a function of formation fluid conductivity. Oil and gas do not conduct electricity while formation water will. The conductivity of the formation water depends on salinity, temperature and ion type. This determines formation water resistivity, or $R_w$. There are several charts from Schlumberger (2009) where the researcher could determine $R_w$ from knowing salinity and temperature. The higher concentration of ions in the formation fluid, the higher salinity and thus lower resistivity. Salinity differs between different formations locally, regionally and globally, and is vital to determine (Gluyas & Swarbrick 2004; Ellis & Singer 2008).

When the resistivity tool emits electricity into the formation, the electricity reaches the detector with more or less ease. The ease is determined by the material which is an interaction between lithology and formation fluid and/or cementation.

When discriminating between the different resistivity depths, an invasion profile has to be established. The profile indicates how much of the drilling mud that has penetrated the formation. This is also a permeability indicator; the more invaded the more permeable formation. Using the Caliper tool, which measures borehole size, indicates the ability of mud cake formation. Permeable intervals would have a build-up of a mud cake in the borehole decreasing borehole size.

Drilling mud could hold different properties depending on the purpose. Oil-based mud will yield high near-borehole resistivity compared to low formation resistivity, $R_t$, in a water filled reservoir. Things could get complicated when oil based mud invades an oil-filled reservoir. The oil saturation could be overestimated. Mud type used for different intervals should always be specified in the log header.

Porosity also affects resistivity. The resistivity increases in low porosity formations while a porous formation, maybe also affected by fractures, would have low resistivity in comparison. A high amount of isolated pores, vugs, increases the resistivity.

# 2 Methods

## 2.1 Formation evaluation

When performing a formation evaluation regarding its hydrocarbon potential, the objectives of the petrophysicist are to obtain the net reservoir column (net pay/pay interval), porosity, permeability and the fluid type/s occupying the potential pore space. The main purpose of such a study is estimation of hydrocarbon volumes. None of the necessary parameters described above are measured directly by the logging tools. The evaluation is based on interpretations and calculations of the log data. Obtaining the parameters is a relationship between log data and empirical relationships. The log data provide the necessary input to empirical formulas determining the parameter values. There are several classic frameworks covering the topic of formation evaluation such as those of Serra (1984, 1986), Bassiouni (1994) and Tiab & Donaldson (1996). Among more recent, up-to-date publications can be noted those of Gluyas & Swarbrick (2004) and Ellis & Singer (2007).

The gross rock volume is comprised by the rock intervals interpreted as a reservoir, such as clean, porous sandstone or grainstone together with formation fluids. Horizons or beds of impermeable rocks are not considered part of the net reservoir. Offshore formation fluids can either be brine, crude oil or natural gas, where brine is, by far, the main component in offshore sedimentological rock pores. The different fluids differ from each other vertically due to density differences. Combinations do occur in, e.g., water wet pore network with oil. The droplets from water and oil coexist in the same pore network but never mix. The saturation of water in the rock is a critical evaluation decision. Whenever the water saturation is less than 100%, the remaining fluids are considered hydrocarbons (Serra 1984, 1986; Bassiouni 1994; Tiab & Donaldson 1996; Gluyas & Swarbrick 2004; Hook 2003; Ellis & Singer 2007).

Porosity is the part of the rock containing formation fluids, and act as a measurement on how much fluid/gas a rock could hold. When the pores are connected, fluids have the ability to move in the rock. The ability for fluids to flow is a measure of the rock permeability, which is interesting for production purposes. In formation evaluation it is important to distinguish between two porosity types, total and effective porosity. Total porosity includes all pore space where fluids are occupied in a rock. This includes all mobile and isolated fluid space, capillary bound water and, in micropores, clay bound water. The only fluids not considered belonging to the total porosity is structurally bound water serving as part of the rock mineral structure. Effective porosity describes the pore space where we find mobile fluids suitable for production (Fig. 18). Log tools discriminating between mobile and immobile formation fluids exist. An example is the Nuclear Magnetic Resonace (NMR) logging tool, valuable for e.g. distinguishing between interlayer bound fluids, capillary bound fluids and free flowing fluids (Serra 1984, 1986; Bassiouni 1994; Tiab & Donaldson 1996; Hürlimann et al. 2002; Hook 2003; Gluyas & Swarbrick 2004; Ellis & Singer 2008).

The determination of the hydrocarbon volume is a multidisciplinary task. The petrophysicist interpret a net pay column of the reservoir, in meters, together with data on the quality of such a reservoir which are to be compared with data and evaluations from other wells. The areal extent of a reservoir is determined through seismic surveys. The formula for determine in place volumes of hydrocarbons (1) are determined by:

$$In\ Place\ Volumes = GRV \cdot \frac{N}{G} \cdot \varphi \cdot (1 - S_w) \quad (1)$$

*GRV = Gross Rock Volume [$m^3$]*
*N/G = Net to Gross [%]*
*$\varphi$ = Porosity [%]*
*$S_w$ = Water Saturation [%]*

The ability to produce from a reservoir depends on formation pressure together with the oil recovery techniques available for production. The amount of hydrocarbons considered producible, the reserves, depends on the recovery factor. When the reserves are determined, the number of barrels is calculated. One cubic meter is approximately equivalent to 6.3 barrels. The value of a barrel is determined by daily fluctuations in oil price. The reserves are determined by:

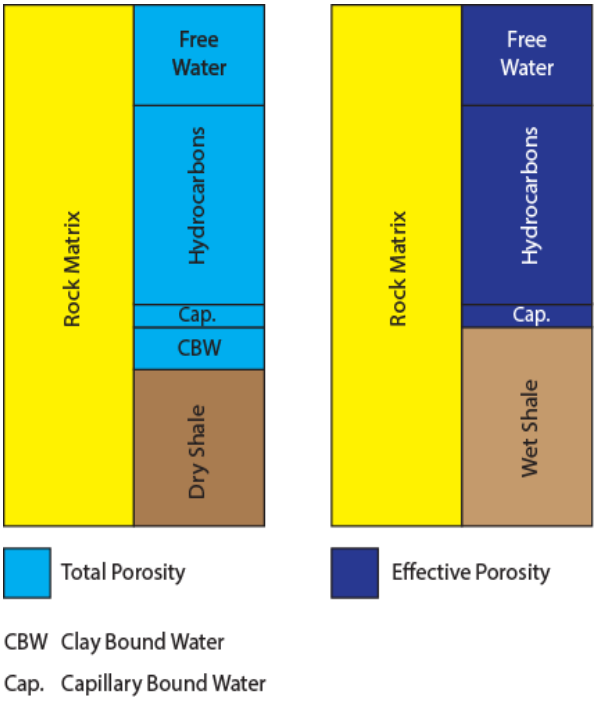


*Fig. 18. Block diagram illustrating the difference between total and effective porosity. The capillary bound water is tightly bound to the clay minerals in the shale and should not be considered a free flowing fluid. Thus, it is excluded from the effective porosity (after Schlumberger 2009).*

$$Reserves = In\ Place\ Volumes\ [m^3] \cdot Recovery\ Factor[\%] \quad (2)$$

The net to gross volume, porosity and fluid saturation are influenced or affected by clay minerals. When interpreting these key parameters for obtaining in place volumes and reserves, we have to consider techniques compensating for the shale- or clay effect (Serra 1984, 1986; Bassiouni 1994; Tiab & Donaldson 1996; Hook 2003; Gluyas & Swarbrick 2004; Ellis & Singer, 2007).

## 2.2 The shale/clay mineral effect

The presence of clay minerals in the formation often complicates the evaluation process. Variable amounts of clay minerals and the distribution of such minerals affects the log tool responses and the formation characteristics. Clay minerals behaves in different ways and could be part of the bulk rock volume as laminated shale horizons, part of the matrix as structural shale and/or dispersed in the pore network (Fig. 19). Strata consisting of clay minerals are impermeable with no effective porosity; they are not considered conventional reservoir rocks and should therefore be excluded from the net reservoir column in a conventional formation evaluation (La Vigne et al. 1994; Ellis & Singer 2007).

Resistivity measurements are vital for determination of the formation fluid saturation. Clay bound water is tightly geochemically attached to the clay. A small amount of clay could hold vast amounts of water due to extensive, low-permeable, microporosity. Due to low resolution of the logging tools, the results show bulk measurements affected by both reservoir rock and clay minerals in a laminated sequence (Fig. 19). The log tools therefore record an average response. Potential higher resolution of the resistivity log tools would result in a narrower formation investigation. However, a narrower investigation is also shallower. The log response will then most likely derive from drilling fluids invading the formation. Due to clay bound water, the log readings indicate a reservoir with higher water saturation in the reservoir units compared to reality. Whenever the clay is accounted for, we would receive true reservoir parameters. Not considering the clay content will mask net pay, which is critical since small differences have drastic effect on reserve estimations which, in the long run, could mean the closure of a project if not considered profitable (Ellis & Singer 2007).

When petroleum is produced, clay minerals in the formation easily get mobile and accumulate in pore throats having large impact on permeability. Techniques for dissolving accumulated clay particles exist but are costly and could possibly harm the environment and give permanent damage to the reservoir (Ellis & Singer 2007).

Clay particles have varying mineralogical composition and are differently distributed in the rock. The most common clay minerals encountered in formation evaluation dealing with the shaly sands offshore Norway are illite, kaolinite, smectite and chlorite. Mixed layer clays exist, most commonly illite/smectite (La Vigne et al. 1994; Gluyas & Swarbrick 2004; Ellis & Singer 2007).

Clay minerals can deform plastically, clog pore space and, hence, decrease the permeability. During stress the viscosity of clays increase and the minerals could be smeared destroying reservoir properties. Smectite has the ability to absorb large amounts of interlayer water to the crystal structure, creating a swelling effect affecting the porosity and permeability negatively.

Clay minerals split along the weaker x-axis which makes the mineral anisotropic regarding their ability to withstand pressure. Occurrence of laminated clay in reservoir sandstone could generate anisotropic permeability (P) properties ($P_v << P_h$) (La Vigne et al. 1994; Gluyas & Swarbrick 2004; Ellis & Singer 2007).

## 2.3 The shale effect on logging tools

All common clay minerals, such as kaolinite, illite, smectite and chlorite, contain a sufficient amount of hydrogen, due to their hydroxyl group content and tightly bound water, impacting on neutron porosity tools. The more clay mineral in a formation, the more hydrogen and higher neutron log readings overestimating neutron porosity. Overestimation of neutron porosity can also occur when lighter hydrocarbons occupy the pore space since they contain a higher H/C ratio

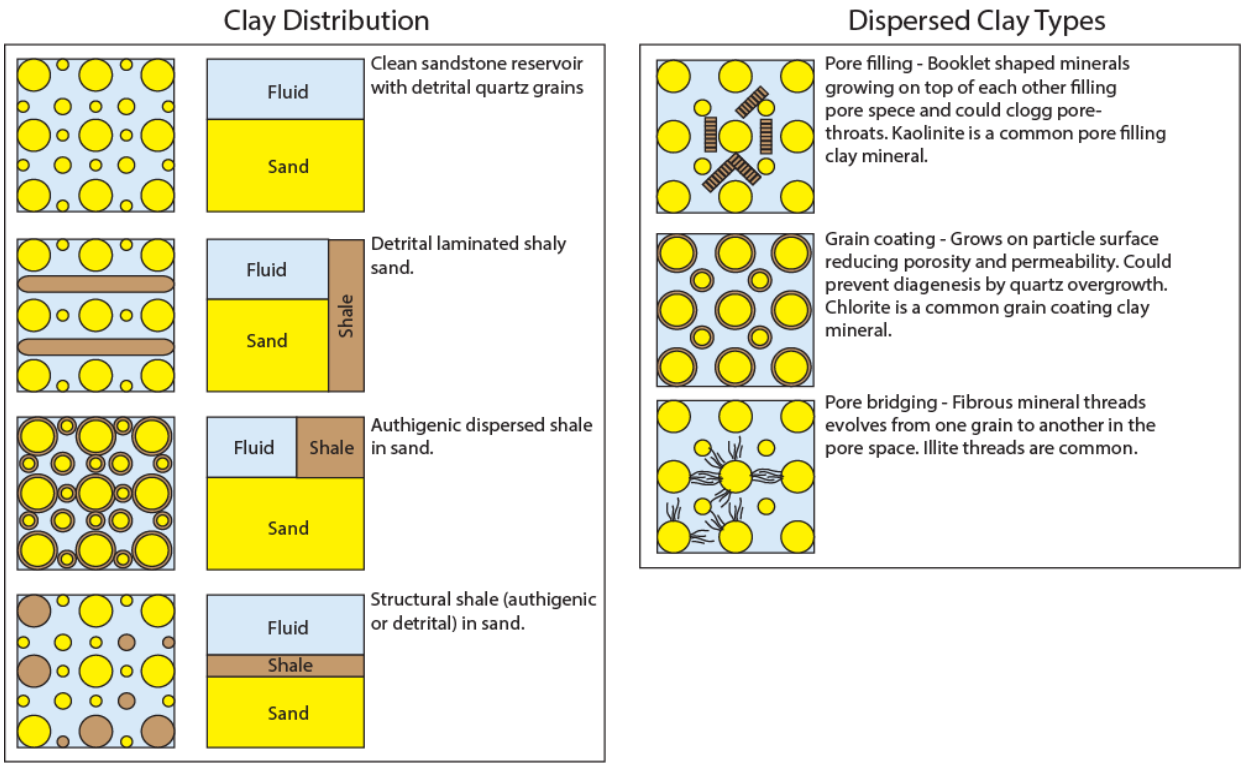


*Fig. 19. The image to the left shows how clay is distributed in a sandstone. The clay types can be distributed alone or in combinations. The figure to the right shows how clay can be dispersed in different ways in the pore system (after Schlumberger 2009).*

compared to heavier hydrocarbons (Hill et al. 1979; Ellis & Singer 2007).

Radioactive minerals, containing uranium, thorium or potassium, yield higher gamma ray values. These minerals could be part of the reservoir rock matrix as well as a constituent in clay minerals. Misinterpretations could lead to the assumption that radioactive minerals in a rock devoid of clay minerals are interpreted as shale or claystone. Clean reservoir intervals could therefore be misinterpreted and disregarded from the net pay (Ellis & Singer 2007)

The clay mineral surface is negatively charged and strives for chemical equilibrium. In order to eliminate the charge, the clays, possessing a large reaction surface due to the mineral sheet structure, react with its surroundings. The common clays contain abundant aluminum. Aluminum could be isomorphically substituted by another cation depending on the availability. The easier for the cation to be substituted the higher cation exchange capacity the clay inhabits. When cations of different valencies substitute the aluminum ion, a charge defect will occur. In order to compensate, $OH^-$ groups are bounded between the clay surface and the adsorbed cations creating a thin water film on the clay surface, known as clay bound water. Cations needed for charge equilibrium often comes from the salty formation brine due to large availability in offshore formations. The clay surface will then have a highly conductive surface overestimating conductivity readings from logging tools since conductivity will take the easiest, hence most conductive, path between source and receiver on the tool. A higher conductivity indicates a lower resistivity reading. Whenever low resistivity is encountered in a formation, the interpretation suggests water, or brine, as formation fluid. The effective porosity may contain hydrocarbons but will not be detected due to the preferential conductive path taken by the tool signal. This effect is larger in low salinity regions such as offshore Norway (≈35.000 ppm which is equivalent to the concentration in sea water), compared to high salinity regions such as in the USA where salinities as high as 300.000 ppm has been measured in carbonate reservoirs. Salinity normally increases with depth and trends are detected, but the oil companies use an average salinity when performing calculations. The petroleum content in a formation then tends to be underestimated when the log data is not compensated for the saline formation water attached to the clay mineral surface. The desired outcome is to completely rule out formations containing considerable amounts of clay minerals, and the properties associated, in order to determine and calculate on reservoir intervals only (Waxman & Smits 1968; Hill et al. 1979; Juhász 1981).

## 2.4 Water Saturation Calculation

### The Archie Equation

Essential for formation evaluation is to calculate and assess the water saturation in the reservoir. When the water saturation has been determined, the eventual remaining fluid is considered to consist of petroleum. Petroleum type and quality could be determined later. The different liquids could appear in separate phases or together in various combinations. The Archie water saturation was developed by Archie (1942, 1950,

1952) and is derived from the Archie Law and equation (3).

$$S_w = \left[\frac{a \cdot R_w}{\varphi^m \cdot R_t}\right]^{\left(\frac{1}{n}\right)}$$

(3)

$S_w$ = *Water saturation (Archie) [%]*
$a$ = *Lithology factor [unitless]*
$R_w$ = *Water resistivity [ohm-m]*

$\varphi$ = *Total porosity [%]*
$m$ = *Cementation factor [unitless]*
$R_t$ = *Bulk resistivity [ohm-m]*
$n$ = *Saturation exponent [unitless]*

## How to obtain the parameters for the Archie water saturation equation

### Porosity [ϕ]

Porosity is preferably determined from a good quality density log undisturbed from, or corrected for, environmental factors. The sonic or neutron logs can also be used for porosity determination but are not as straightforward as the density log. The sonic tool measure acoustic wave propagation which is a function of the elastic properties and bulk density in a formation. Neutron tool detect hydrogen in a formation. Hydrogen is present in all formation fluids and is a good indicator of the amount of fluids, and hence porosity, in a formation. The hydrogen present in clay bound water decrease the reliability of the neutron porosity tool in shaly formations since the clay bound water does not represent porosity that could be occupied with hydrocarbons. The porosity represented by clay bound water should be quantified and disregarded. Only the actual reservoir volume suitable for production should be considered. But one could in fact calculate sonic and neutron porosity in order to compare the results to density porosity. This is always valuable since it could reveal other characteristics of the formation. The total porosity value, used in the Archie water saturation equation is calculated from the density log by the formula (4) (Hook 2003; Ellis & Singer 2008):

$$\varphi_t = \frac{\rho_m - \rho_b}{\rho_m - \rho_{fl}}$$

(4)

$\varphi_t$ = *Total porosity [%]*

$\rho_m$ = *Matrix density [g/cm$^3$]*

$\rho_b$ = *Bulk density (from density log) [g/cm$^3$]*

$\rho_{fl}$ = *Fluid density [g/cm$^3$]*

The density tool measures the formation properties mainly in the invaded zone affected by mud filtrate. Hydrocarbons are less dense compared to water based mud, which should be considered. Significant presence of heavy minerals in the formation will increase the bulk density, which needs to be compensated for. The mineral constituents could be determined with a Gamma Ray Spectroscopy logging tool. In the log, minerals are determined due to the fractions of the different chemical elements present in the formation. This is not straightforward but with geological knowledge about the common minerals present in a certain region, a fair interpretation can be made (Ellis & Singer 2008).

Whenever there is core porosity data available, this value should be regarded as true total porosity when corrected for overburden effects. Cores and core analysis are, however, often not available due to the fact that coring is very expensive to perform and thus seldom executed (Ellis & Singer 2008; Andersen et al. 2013).

### Formation water properties

The composition of the formation water for the studied formation is not known. A Pickett plot is a method to empirically determine the formation water properties. To receive correct water properties, a clean sandstone zone free from shale, clay minerals or hydrocarbons, has to be identified in the logging suites. Non-shaly intervals could be determined by a simple gamma ray cut-off of for example <65 API (Pickett 1973).

Formation resistivity ($R_t$) is plotted against total porosity in a Pickett plot. Note that all values come from non-shaly zones. The plots will indicate a trend and cut the x-line at some point which gives a value of the formation water resistivity ($R_w$) in a specific lithology. The lithology is indicated by a lithology- or tortuosity factor (a). The lithology factor is an expression of the variation of pore structure and size and has a value ranging from 0.5 to 1.5. For simplicity reasons, a is normally set to 1.0 when calculating the Archie equation in North Sea sandstone reservoirs since the assumption is a small variation in the alterations of the lithology (Pickett 1973; Ellis & Singer 2008).

Using Schlumberger chart Gen-9 with values for $R_w$ and temperature given from a calculated temperature gradient will reveal the formation water salinity (Schlumberger 2009).

### Cementation factor and saturation exponent

The values from cementation factor (m) and saturation exponent (n) are preferably collected from Special Core Analysis data determined in laboratory settings. The cementation factor provides a measure of the consolidation of the rock. A higher m-value indicates a tightly consolidated rock whilst a low value indicates unconsolidated sediments. The rock itself is considered non-conductive, and when the rock contains a pore network the factor could be seen as an expression on how much it increases the resistivity in the rock. Also here, for simplicity reasons, the value for m is set to between 1.8 and 2.0 for consolidated sandstone reservoirs. A subsurface sandstone formation is considered consolidated if other log tools, such as the caliper tool, do not indicate a loose formation (Archie 1942, 1950, 1952; Ellis & Singer 2008).

The saturation exponent indicates the ratio of oil-wet versus water-wet rock and the distribution of them

in the rock pores. The saturation exponent varies as a function of water saturation and resistivity index. The resistivity index describes the ratio of resistivity of a hydrocarbon-bearing formation to the resistivity of a fully water-saturated formation. A more oil-wet rock gives a higher n-value. The oil wet rock is less conductive compared to the water wet rock. The value for n in the Archie equation is usually set to 2 since fixed values for different combinations of wettability in the rock is close to 2 (Archie 1942, 1950, 1952; Ellis & Singer 2008).

The formation resistivity, formation water resistivity, porosity, lithology factor, cementation factor and saturation factor are all the necessary input needed in order to calculate the Archie water saturation ($S_w$). All the input factors are related to the resistivity which in turn is used to determine the amount of different formation fluids in the formation (Ellis & Singer 2008).

## 2.5 Water saturation calculation in shaly sands

### Waxman-Smits

Whenever clay minerals are present in a formation, the Archie water saturation method is too simplistic and not reliable. A method quantifying the clay mineral effect is thus needed. The Waxman-Smits water saturation equation (Waxman & Smits 1968) corrects for eventual clay mineral conductivity with the outcome of too high water saturation values according to Archi'e equation described above. The conductivity of a water-filled rock formation containing clay could be expressed as:

$$C_o = \frac{C_w}{F} + C_s$$

(5)

*$C_o$ = Conductivity of water-filled rock [ohm-m]*
*$C_w$ = Conductivity of formation water [ohm-m]*
*$F$ = Formation factor [unitless]*
*$C_s$ = Excess clay conductivity [ohm-m]*

If $C_o$ and $C_w$ from the actual formation are plotted against each other and compared to a clean sandstone crossplot, the excess conductivity not being a part of the clean sandstone formation is visible graphically. This additional conductivity could be expressed as B·Qv where B = equivalent conductivity of clay exchange cations [mho/m] per [meq/cc] and Qv = cation exchange capacity per unit pore volume [meq/cc]. The BQv expresses how much extra conductivity is realted to the presence of clay minerals in the actual formation. The assumption in the workflow is that any cation considered as excessive belongs to clay minerals in the formation (Waxman & Smits 1968).

In a more controlled manner, it is possible to obtain BQv from Special Core Analysis (SCAL). The advantage is a BQv received at simulated reservoir conditions. This BQv value from special core analysis is preferred when accessible. The major disadvantage is that the method is expensive and time consuming (Waxman & Smits 1968; Lasswell 2006).

In addition to BQv as input for the Waxman-Smith water saturation equation, updated shaly sand lithology- (a*), cementation- (m*), and saturation (n*) factors are needed. These values are gathered from special core analysis data. m* is determined using core measured formation factor. n* is determined using core measured resistivity index. a* is established as a relationship between Qv and porosity (McPhee et al. 2015).

When these parameters for the Waxman-Smits equation (6) are calculated and modified, Waxman-Smits water saturation in shaly sand is determined by:

$$S_w^* = \left[\frac{a^* \cdot R_w}{\varphi^{m^*} \cdot R_t \cdot \left(1 + a^* \cdot R_w \cdot B \cdot \frac{Q_v}{S_w}\right)}\right]^{\left(\frac{1}{n^*}\right)}$$

(6)

*$S_w^*$ = Water saturation (Waxman-Smits) [%]*
*$S_w$ = Water saturation (Archies) [%]*
*$R_w$ = Water resistivity [ohm-m]*
*$R_t$ = Bulk resistivity [ohm-m]*
*$B$ = Equivalent conductivity of clay exchange cations [mho/m per meq/cc]*
*$Q_v$ = Cation exchange capacity per unit pore volume [meq/cc]*
*$\varphi$ = Porosity [%]*
*$a^*$ = Lithology factor (Waxman-Smits) [unitless]*
*$m^*$ = Cementation factor (Waxman-Smits) [unitless]*
*$n^*$ = Saturation factor (Waxman-Smits [unitless]*

In this formula, water saturation, $S_w$, is the result as well as input. The water saturation as input derives from the Archie water saturation which has to be calculated prior to Waxman-Smits. In order to decrease the error of the Waxman-Smits method, the equation is recalculated approximately eight times using the resulted $S_w^*$ as input in the following equation until there is little or no variation in results. A resulting lower Waxman-Smits water saturation value in comparison to the Archie value indicates shale in the formation. No difference indicates a clean sandstone formation (Waxman & Smits 1968; Ellis & Singer 2008).

### Poupon-Leveaux/Indonesia equation

The Poupon Leveaux or Indonesia equation (7) (Poupon & Leveaux 1971) is a method where the amount of clay and its properties are calculated separately and then disregarded in the water saturation calculation. The method is well known and widely used but is not build on empirical relationships. Anyhow, the method is interesting to carry out as a comparison to the Archie and Waxman-Smits methods, and could be helpful in determining the amount of clay in the formation. The Poupon-Levaux method determines water saturation in shaly sands according to following equation:

$$S_w = \left\{\left[\left(\frac{V_{clay}{}^{2-V_{clay}}}{R_{clay}}\right)^{1/2} + \left(\frac{\varphi_e^m}{R_w}\right)^{1/2}\right]^2 \cdot R_t\right\}^{-1/n}$$

(7)

*$S_w$ = Water saturation (Indonesia) [%]*
*$R_t$ = Bulk resistivity [ohm-m]*

*$V_{clay}$ = Clay/Shale volume [%]*
*$R_{clay}$ = Clay/Shale resistivity [ohm-m]*
*$\varphi_e$ = Effective porosity [%]*
*a = Lithology factor (From Archies) [unitless]*
*m = Cementation factor (From Archies) [unitless]*
*n = Saturation factor (From Archies) [unitless]*
*$R_w$ = Water resistivity [ohm-m]*

The first step is to identify what intervals contain clay and which ones that does not. This is not a straightforward procedure. It is primarily based on an interpretation by a skilled petrophysicist. When interpreting a clean clay or shale interval with i.e. the gamma ray, neutron/density, spontaneous potential (SP) or photoelectric factor (PEF) tool, it is possible to retrieve some formation properties, such as resistivity, from the specific interval. The formation resistivity for this interval serves as $R_{clay}$ in the equation (Poupon & Leveaux 1971).

The volume of clay, $V_{clay}$, can be determined using three different methods:

- Gamma Ray (Bhuyan & Passey 1994; Ellis & Singer 2008):

$$V_{clay_{GR}} = \frac{GR_{log} - GR_{clean\ sand}}{GR_{pure\ clay} - GR_{pure\ sand}}$$

(8)

*$V_{clay\_GR}$ = Volume of shale/clay derived from gamma ray logs [%]*
*$GR_{log}$ = Gamma ray data value from logs [API]*
*$GR_{clean\ sand}$ = Gamma ray value from interpreted clean sand interval/zone [API]*
*$GR_{pure\ clay}$ = Gamma ray value from interpreted pure clay interval/zone [API]*

- Density and Neutron (Bhuyan & Passey 1994; Ellis & Singer 2008):

$$V_{clay_{dn}} = \frac{NPHI_{log} + COR_{lith} - HI \cdot \varphi_t}{NPHI_{pure\ clay}}$$

(9)

*$V_{clay\_dn}$ = Volume of shale/clay derived from density and neutron logs [%]*
*$NPHI_{log}$ = Neutron data value from logs [API]*
*$COR_{lith}$ = Lithology correction when not handling limestone reservoir*
*HI = Hydrogen Index[S2/TOCx100]*
*$\varphi_t$ = Total porosity [%]*
*$NPHI_{pure\ clay}$ = Neutron value from interpreted pure clay interval/zone [API]*

- Spontaneous Potential (Ellis & Singer 2008):

$$V_{clay_{SP}} = \frac{SP_{log} - SP_{clean\ sand}}{SP_{pure\ clay} - SP_{clean\ sand}}$$

(10)

*$V_{clay\_SP}$ = Volume of shale/clay derived from spontaneous potential logs [%]*
*$SP_{log}$ = Spontaneous potential data value from logs [mV]*
*$SP_{clean\ sand}$ = Spontaneous potential value from interpreted clean sand interval/zone [mV]*
*$SP_{pure\ clay}$ = Spontaneous potential value from interpreted pure clay interval/zone [mV]*

Determination of the effective porosity, $\varphi_e$, from e.g. the density log is done by the following equation (Hook 2003; Ellis & Singer 2008):

$$\varphi_e = \varphi_t - (V_{clay} \cdot \varphi_{clay})$$

(11)

*$\varphi_e$ = Effective porosity [%]*
*$\varphi_t$ = Total porosity[%]*
*$V_{clay}$ = Clay/shale volume [%]*
*$\varphi_{clay}$ = Porosity from interpreted clay interval/zone [%]*

## The conventional water saturation determination techniques

The water saturation models have proven to be useful in formation evaluation. They have been, and are still being used frequently in petroleum exploration. The clay quantification techniques should be used with care, but they are the tools currently available for clay quantification. If the three water saturation equations described above have been carried out as instructed, Archie's equation should give the highest water saturation followed by Indonesia and then Waxman-Smits. The reasoning goes for saturation calculation when there is less than 100% water in the formation. The physical framework and empirical derivations of the empirical relationships are available in e.g. Archie (1942, 1950, 1952), Waxman & Smits (1968) and Poupon & Leveaux (1971).

## Water saturation from the triaxial induction logging tool

When there is no special core analysis data available an alternative method is needed. The triaxial induction tool has the advantage of letting the researcher calculate an alternative resistivity valid for sand fractions only in order to eliminate the effect from clay minerals. The necessary steps to retrieve the sand resistivity are elaborated later in the method section.

Due to the horizontal nature of sedimentation, the horizontal resistivity is considered homogenous parallel to strata. Formations with numerous thin beds of various lithologies, as in the case for many of the reservoirs offshore Norway, will have a vertical resistivity that differs from the horizontal resulting in resistivity anisotropy. When performing formation evaluation, only the beds containing reservoir properties are desired, and other beds should be disregarded. The formation resistivity ($R_t$) gives a value of the bulk resistivity and is always valid in a clean formation not disturbed by drilling fluid invasion. This scenario is rarely the normal case due to different lithologies and drilling mud invasion in permeable formations. The triaxial induction tool helps to solve the challenge of receiving a reservoir rock resistivity when operating in thin bed formations.

Anderson et al. (2008) describes an induction tool with tilted coils making it possible to measure the induction in X, Y and Z directions.

The challenge with measuring resistivity in laminated strata is that you measure different values in different lithologies, e.g. sandstone and shale would have different resistivity. Formation fluids complicate things even further since they also inhabit more or less conductive properties. When the bulk resistivity is measured, the lower resistivity in, e.g., waterfilled shale will dominate the log tool measurements and thus mask potential petroleum bearing reservoir sandstone with higher resistivity. Pay zones could be overlooked and/or underestimated, which in turn could have an effect on future project decisions. The challenge is taken on by measuring resistivity vertically in a sequence of alternating beds throughout the reservoir with measurements taken every 0.1524 m. The measurements are similar to the measurements of a series of circuits where the resistivity values are added together. In this case, a higher resistivity, which is the case with hydrocarbon bearing reservoir rock, is dominant. The triaxial induction tool does not always measure the accurate reservoir rock resistivity and is still somewhat influenced by shale, but the resistivity is more accurate compared to conventional formation resistivity measurements and additional pay zones are able to be discovered (Anderson et al. 2008).

The data derived from the triaxial induction tool makes it possible to calculate a sand resistivity using input as horizontal and vertical resistivity, shale and sand resistivity together with sand and shale fraction. Resistivity of sand could be derived using one of two equations:

$$\frac{1}{Rh} = \frac{Fs}{Rs\_h} + \frac{Fsh}{Rsh\_h} \quad (12)$$

$$Rv = [Fs \cdot Rs\_v] + [Fsh \cdot Rsh\_v] \quad (13)$$

*Rh = Horizontal resistivity*
*Rv = Vertical resistivity*
*Rs_h = Sand resistivity derived from Rh log*
*Rs_v = Sand resistivity derived from Rv log*
*Fsh = Shale fraction (=$V_{sh}$)*
*Fs = Sand fraction (=1-$V_{sh}$)*

## 2.6 Thesis workflow and parameters

Logging data from the well 7220/8-1 was converted into .DLIS file format and analyzed using the formation evaluation software Schlumberger Techlog 2015.3. Parameters necessary for evaluating three different methods of water saturation was calculated using: Archie, Indonesia and, a third method compensating for the thin alternating sand and shale beds, in this thesis referred to as the Archie/Clavaud method. The Archie/Clavaud method uses the sand resistivity described above. The petrophysical part of Techlog allows you to use your own choice of input and properties into the calculations. The input could be derived from the logs or from your own measurements, calculations and assessments. A workflow overview is presented in figure 20.

### Settings

A harmonized dataset was first created consisting of the logs containing the recorded information necessary for interpretable results. A sampling rate was set in order for the software to take readings/values from the logs every 0.1524 m/6 inch.

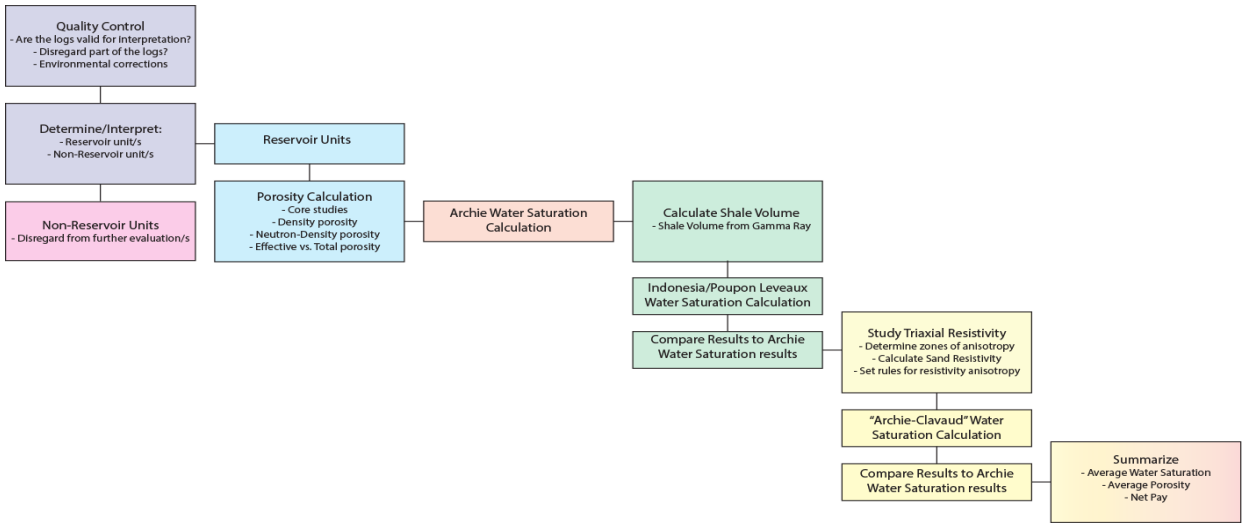


*Figure 20. The general workflow during the formation evaluation of well 7220/8-1. This workflow focusses on estimating the water-/hydrocarbon saturations and porosity.*

The logs were controlled to have suitable scales i.e. the resistivity curves should have a logarithmic scale from 0.2 to 2000 ohmm. Assigning the selected logs to a correct type of logging tool helps the software to identify the correct type of measurement.

The interval evaluated in the software consists of the entire Stø and Nordmela formations and is divided into five different zones primarily based on the gas-oil and oil-water fluid contacts. The fluid contacts are determined using formation pressure data. Plotting pressure point data with depth reveals subtle fluid gradients. The fluid contacts were already known from oil company reports (Norwegian Petroleum Directorate). Where these gradients overlap there is a fluid contact. In well 7220/8-1 there is a gas-oil contact as well as oil-water contact. The gas-oil contact is a bounding surface where predominately gas occurs above the contact and oil below. The oil-water contact is a bounding surface in the reservoir. Oil occurs predominantly above the contact, and water occurs predominantly below the contact. The fluid contacts are transitional and better defined as transitional zones rather than sharp boundaries (Dalland et al. 1988; Dore 1995).

The log zonation consists of a gas zone on the top of the oil zone, and a water zone at the base. The oil zone is divided into two parts, separated by a thick shale barrier. The shale barrier is defined as a separate zone in order to completely rule it out as a reservoir in later calculations.

## Shale volume

Using the environmentally corrected gamma ray curve (ECGR) as input provides a gamma ray curve for the entire studied reservoir interval. The other used parameters are default settings. The Volume of shale (Vsh) is then calculated by:

$$V_{sh} = \frac{GRlog - GRmin}{GRmax - GRmin} = \frac{ECGR - GRsand}{GRshale - GRsand}$$

(14)

## Total and effective porosity

The porosity is calculated using values from the density log (RHOZ) as well as the neutron-density log (NPHI). The density of sandstone, 2.65 g/cm$^3$, represented sandstone matrix and the density of water, 1.00 g/cm$^3$, except in the gas zone where the value was set to 0.81g/cm$^3$ due to the lower density of gas compared to both oil and brine.

The Volume of shale values was used as input in the porosity calculations. The equations used by the software in order to calculate the total and effective porosity are listed below.

Total porosity derived from density log:

$$\varphi_{tot/den} = \frac{\rho_{matrix} - \rho_{log}}{\rho_{matrix} - \rho_{fluid}} = \frac{2.65 - RHOZ}{2.65 - 1.00}$$

(15)

Effective porosity derived from density log:

$$\varphi_{\frac{eff}{den}} = \varphi_{\frac{tot}{den}} - (\varphi_{sh} \cdot V_{sh})$$

(16)

Total porosity derived from neutron log:

$$\varphi_{tot/neu} = \frac{\rho_{matrix} - \rho_{log}}{\rho_{matrix} - \rho_{fluid}} = \frac{2.65 - NPHI}{2.65 - 1.00}$$

(17)

Total porosity derived from neutron and density logs:

$$\varphi_{neu-den} = \frac{\varphi_{\frac{tot}{neu}} + \varphi_{\frac{tot}{den}}}{2}$$

(18)

Total porosity derived from neutron and density logs (for gas intervals):

$$\varphi_{neu-den} = \sqrt{\frac{\varphi_{neu} + \varphi_{den}}{2}}$$

(19)

Effective porosity derived from neutron and density logs:

$$\varphi_{eff\ neu-den} = \varphi_{tot\ neu-den} - (\varphi_{sh} \cdot V_{sh})$$

(20)

## Archie water saturation

The Archie water saturation method is a non-refined method and often uses default values for cementation (m), saturation (n) and lithology (a) factors in the absence of core analysis data. The default values of m=2, n=2 and a=1 were applied in the calculations. The Density porosity and Neutron porosity logs served as input in separate Archie water saturation calculations. The combination of Neutron and Density porosity logs were primarily used to limit the gas effect in zone 1, the gas zone. The formation resistivity ($R_t$) was taken from the RT_HRLT log. The water resistivity ($R_w$) was set to 0.039 ohm-m determined by the equation for apparent water resistivity with values derived from the water zone where Sw=1 (21):

$$Rwa = Rt \cdot \varphi^m$$

(21)

The Archie water saturation calculation was constructed and solved for as (22):

$$Sw_{Archie} = \frac{a \cdot Rw^{\,n}}{\varphi^{m} \cdot Rt} = \frac{1 \cdot 0.039^{\,2}}{\varphi^{2} \cdot RT_{HRLT}}$$

(22)

## Indonesia water saturation

All parameter values used in the Archie water saturation equation was held constant in the Indonesia equation, except for porosity. The Indonesia equation uses effective porosity in the right hand part of the equation since the microporosity is ruled out in the left hand part. The additional parameters are shale resistivity ($R_{sh}$) and volume of shale ($V_{sh}$). The latter is the results from the calculations according the equation mentioned above. The shale resistivity is the estimation of formation resistivity in clean shale intervals. These values are taken from zone 3, interpreted as a shale barrier, and set to 2.0 ohmm. The shale resistivity value is a mean of the formation resistivities measured in zone 3 between 1376 and 1380 m. Indonesia water saturation was then calculated (23) and compared to the results from the Archie water saturation.

$$Sw_{indo} = \left\{ \left[ \left( \frac{V_{clay}^{\,2-V_{clay}}}{R_{clay}} \right)^{\frac{1}{2}} + \left( \frac{\varphi_e^{\,m}}{R_w} \right)^{\frac{1}{2}} \right]^{2} \cdot R_t \right\}^{-\frac{1}{n}} \rightarrow$$

$$Sw_{indo} = \left\{ \left[ \left( \frac{V_{sh}^{\,2-V_{sh}}}{R_{sh}} \right)^{1/2} + \left( \frac{\varphi_e^{2}}{0.039} \right)^{1/2} \right]^{2} \cdot RT\_HRLT \right\}^{(-1/2)}$$

(23)

## Sand resistivity from Triaxial induction log tool

As input in the Archie/Clavaud water saturation equation, compensating for thin alternating beds, a sand resistivity curve is needed in order to compare the results to the Archie and Indonesia water saturation. The two logs, the vertical, RV54_1DF, and horizontal, RH54_1DF, resistivity curves were recorded by the triaxial induction tool for the studied interval. The logs are imported to the harmonized dataset in the same log trace with identical scale in order to study where the curves overlap and separate.

The sand resistivity is calculated from the horizontal resistivity log using the formula below (24):

$$\left[ \frac{1}{Rh} = \frac{Fs}{Rs_h} + \frac{Fsh}{Rsh_h} \right] = \left[ Rs\_h = \left[ \frac{Fsh}{Rsh\_h} + Fs \right] \cdot Rh \right]$$

(24)

The sand resistivity from vertical resistivity is calculated (25):

$$\left[ Rv = [Fs \cdot Rs_v] + [Fsh \cdot Rsh_v] \right] = \left[ Rs\_v = \frac{Rv - [Fsh \cdot Rsh\_v]}{Fs} \right]$$

(25)

The shale resistivity is obtained from the vertical and horizontal resistivity logs in shale zone 3. The fraction of shale, $F_{sh}$, is represented by the Volume of shale, $V_{sh}$, and fraction of sand by 1-$V_{sh}$.

The vertical resistivity curve is the most reliable and undisturbed in the dataset due to a better tool recording. The sand resistivity calculated from this curve is considered representative and used in later calculations.

## Archie/Clavaud water saturation

The equation (26) uses the same parameters as the Archie equation. However, the resistivity is the exception now represented by the vertical sand resistivity (Rs_v). In addition the vertical sand resistivity is labelled as sand resistivity or Rsand.

$$Sw_{Archie/Clavaud} = \frac{a \cdot Rw^{\,n}}{\varphi^{m} \cdot Rsand} = \frac{1 \cdot 0.039}{\varphi^{2} \cdot Rsand}$$

(26)

The sand resistivity is only valid in reservoirs where thin beds have an impact on the calculation of the water saturation. A homogenous sandstone unit has the same resistivity in all directions, indicating that the formation resistivity ($R_t$) readings are most valid here due to deeper penetration of the tool signal compared to the triaxial induction tool.

Therefore, a mathematical formula with certain conditions must be set in order to obtain the most representative values for the whole reservoir, including the sections in which formation resistivity is valid as well as the sections where the sand resistivity is valid. The point where the vertical and horizontal resistivity log curves separate from each other is an indication of resistivity anisotropy. Where the same log curves overlie each other is an indication of resistivity isotropy. When anisotropy occur an Archie/Clavaud water saturation calculation, using sand resistivity, is the most appropriate method to use. During isotropic conditions, such as in a homogeneous sand layer the Archie water saturation method is the most applicable method to determine the water saturation. An equation for this relationship was set up in the data editor in the Techlog software (27):

$$Sw_{conditional} = \left[ Sw_{Archie/Clavaud}\ IF\ Rv\_Rh_{Ratio} > 2\ ELSE\ Sw_{Archie} \right]$$

(27)

The result from the equation is a new log curve, $Sw_{conditional}$, representing a water saturation log where the thin beds are sand resistivity values. The consequence

is water saturation calculated from sand units only, ruling out shale units. Whenever the $Rv\_Rh_{ratio}$ is below 2, Archie water saturation is applied.

### Summaries in Techlog

The summary function in the Techlog software calculates the mean value for each parameter for the whole log or intervals set by the user. The parameters are later used in calculating Oil In Place and the economic value of the reservoir. Before the parameter summary executes the user has the ability to set preferred cut-off values. The cut-offs used, summarizing Archie, Indonesia and Archie/Clavaud water saturation, are summarized in Table 1.

**Table 1. Cut-off values used in the summaries from the water saturation calculations**

| Parameter | <Min. value | Max. value> |
|---|---|---|
| Porosity [%] | 10 | 50 |
| Water saturation [%] | 10 | 65 |
| Shale volume [%] | 0 | 50 |

# 3 Results

When using the summaries function in Techlog, the results are presented in tables. The five zones earlier interpreted and determined are each represented, and result values presented as the yellow row ROCK representing the volume made up by bedrock, the green row RES representing the intervals interpreted as reservoir rock and the red row PAY representing the intervals interpreted as reservoir rock containing hydrocarbons. The pay row indicates the economically viable intervals in the reservoir and these results are the most interesting in the formation evaluation since they later are used to calculate hydrocarbon volumes. Notable is that zone 3, the shale barrier, are excluded from the result calculations.

In order to interpret the tables, an explanation of the abbreviations used are summarized in Table 2. Whenever volume is stated this is not an expression of the whole reservoir, when measured in a borehole, but an expression of the vertical interval. Together with the areal extent of the reservoir, the volume could be estimated.

The results are presented in Table 3-8 below.

**Table 2. Explanation of the abbreviations used in the result tables.**

| Abbreviation | Name | Explanation |
|---|---|---|
| *Gross* | Gross Rock Volume | The intervals containing grains (bedrock) and pores |
| *Net* | Net Rock Volume | The intervals containing grains (bedrock) |
| *Net-Gross* | Net to Gross ratio | The ratio between the amount of bedrock and the bedrock together with porosity |
| *BVW* | Bulk Volume Water | The volume of water in relation to the total bulk volume of the rock |
| *POR-TH* | Pore Thickness | The total column of porosity (a sum of the porosity in the interval) |
| *HCPOR-TH* | Hydrocarbon Pore Thickness | The total column of the porosity occupied with hydrocarbons |
| *Avg_Shale* | Average Shale Volume | The average percent of bedrock consisting of shale |
| *Avg_Porosity* | Average Porosity | The average percent of porosity for the bedrock interval |
| *Avg_Sw* | Average Water Saturation | The average percent of water in relation to the porosity |

**Table 3. Results from Archie water saturation using density total porosity.**

| *Zone* | *Flag Name* | *Top [m]* | *Bottom [m]* | *Gross [m]* | *Net [m]* | *Net-Gross [ratio]* | *BVW* | *POR-TH [m]* | *HCPOR-TH [m]* | *Avg_Shale [%]* | *Avg_Porosity [%]* | *Avg_Sw [%]* |
|---|---|---|---|---|---|---|---|---|---|---|---|---|
| 1 | ROCK | n.a. | n.a. | n.a. | n.a. | n.a. | n.a. | n.a. | n.a. | n.a. | n.a. | n.a. |
| 1 | RES | n.a. | n.a. | n.a. | n.a. | n.a. | n.a. | n.a. | n.a. | n.a. | n.a. | n.a. |
| 1 | PAY | n.a. | n.a. | n.a. | n.a. | n.a. | n.a. | n.a. | n.a. | n.a. | n.a. | n.a. |
| 2 | ROCK | 1311.959 | 1375.760 | 63.801 | 60.327 | 0.946 | 1.358 | 17.132 | 15.774 | 0.185 | 0.284 | 0.079 |
| 2 | RES | 1311.959 | 1375.760 | 63.801 | 59.616 | 0.934 | 1.357 | 17.122 | 15.765 | 0.184 | 0.287 | 0.079 |
| 2 | PAY | 1311.959 | 1375.760 | 63.801 | 59.166 | 0.934 | 1.357 | 17.122 | 15.765 | 0.184 | 0.287 | 0.079 |
| 4 | ROCK | 1379.545 | 1395.142 | 15.597 | 10.617 | 0.681 | 0.662 | 3.200 | 2.538 | 0.264 | 0.301 | 0.207 |
| 4 | RES | 1379.545 | 1395.142 | 15.597 | 10.109 | 0.648 | 0.657 | 3.167 | 2.510 | 0.265 | 0.313 | 0.207 |
| 4 | PAY | 1379.545 | 1395.142 | 15.597 | 10.109 | 0.648 | 0.657 | 3.167 | 2.510 | 0.265 | 0.313 | 0.207 |
| 5 | ROCK | 1395.142 | 1516.724 | 121.582 | 39.878 | 0.328 | 9.654 | 10.368 | 0.714 | 0.337 | 0.260 | 0.931 |
| 5 | RES | 1395.142 | 1516.724 | 121.582 | 39.243 | 0.323 | 9.608 | 10.322 | 0.714 | 0.336 | 0.263 | 0.931 |
| 5 | PAY | 1395.142 | 1516.724 | 121.582 | 1.194 | 0.010 | 0.178 | 0.353 | 0.174 | 0.295 | 0.295 | 0.505 |



Table 3.
The results from Archie water saturation using total density porosity as input is not valid for zone 1, the gas zone. The gas zone is later examined using neutron-density porosity as input.

The average porosity for the oil and water zones ranges between 0.287 and 0.313. The water saturation is low in zone 2 and increases downward into the water zone.

**Table 4. Results from Indonesia water saturation using density effective porosity and Clavier calculated Vsh.**

| *Zone* | *Flag Name* | *Top [m]* | *Bottom [m]* | *Gross [m]* | *Net [m]* | *Net-Gross [ratio]* | *BVW* | *POR-TH [m]* | *HCPOR-TH [m]* | *Avg_Shale [%]* | *Avg_Porosity [%]* | *Avg_Sw [%]* |
|---|---|---|---|---|---|---|---|---|---|---|---|---|
| 1 | ROCK | n.a. | n.a. | n.a. | n.a. | n.a. | n.a. | n.a. | n.a. | n.a. | n.a. | n.a. |
| 1 | RES | n.a. | n.a. | n.a. | n.a. | n.a. | n.a. | n.a. | n.a. | n.a. | n.a. | n.a. |
| 1 | PAY | n.a. | n.a. | n.a. | n.a. | n.a. | n.a. | n.a. | n.a. | n.a. | n.a. | n.a. |
| 2 | ROCK | 1311.959 | 1375.760 | 63.801 | 63.242 | 0.991 | 1.219 | 15.817 | 14.598 | 0.109 | 0.250 | 0.077 |
| 2 | RES | 1311.959 | 1375.760 | 63.801 | 61.445 | 0.963 | 1.182 | 15.744 | 14.562 | 0.104 | 0.256 | 0.075 |
| 2 | PAY | 1311.959 | 1375.760 | 63.801 | 61.445 | 0.963 | 1.182 | 15.744 | 14.562 | 0.104 | 0.256 | 0.075 |
| 4 | ROCK | 1379.545 | 1395.142 | 15.597 | 14.982 | 0.961 | 0.963 | 3.512 | 2.549 | 0.211 | 0.234 | 0.274 |
| 4 | RES | 1379.545 | 1395.142 | 15.597 | 14.271 | 0.915 | 0.959 | 3.481 | 2.522 | 0.215 | 0.244 | 0.275 |
| 4 | PAY | 1379.545 | 1395.142 | 15.597 | 13.437 | 0.862 | 0.874 | 3.359 | 2.485 | 0.203 | 0.250 | 0.260 |
| 5 | ROCK | 1395.142 | 1516.724 | 121.582 | 58.032 | 0.477 | 9.567 | 10.411 | 0.844 | 0.252 | 0.179 | 0.919 |
| 5 | RES | 1395.142 | 1516.724 | 121.582 | 51.021 | 0.420 | 9.172 | 9.971 | 0.799 | 0.233 | 0.195 | 0.920 |
| 5 | PAY | 1395.142 | 1516.724 | 121.582 | 1.397 | 0.011 | 0.168 | 0.328 | 0.160 | 0.176 | 0.235 | 0.513 |



Table 4.

The Indonesia equation uses effective porosity as input in order to rule out any porosity belonging to shale. The overall effective porosity is lower compared to the total porosity in the Archie equation. The water saturation is lower in zone 2 and 5 but higher in zone 4.

**Table 5. Results from Archie/Clavaud water saturation using density total porosity.**

| *Zone* | *Flag Name* | *Top [m]* | *Bottom [m]* | *Gross [m]* | *Net [m]* | *Net-Gross [ratio]* | *BVW* | *POR-TH [m]* | *HCPOR-TH [m]* | *Avg_Shale [%]* | *Avg_Porosity [%]* | *Avg_Sw [%]* |
|---|---|---|---|---|---|---|---|---|---|---|---|---|
| 1 | ROCK | n.a. | n.a. | n.a. | n.a. | n.a. | n.a. | n.a. | n.a. | n.a. | n.a. | n.a. |
| 1 | RES | n.a. | n.a. | n.a. | n.a. | n.a. | n.a. | n.a. | n.a. | n.a. | n.a. | n.a. |
| 1 | PAY | n.a. | n.a. | n.a. | n.a. | n.a. | n.a. | n.a. | n.a. | n.a. | n.a. | n.a. |
| 2 | ROCK | 1311.959 | 1375.760 | 63.801 | 60.327 | 0.946 | 0.653 | 17.132 | 16.480 | 0.185 | 0.284 | 0.038 |
| 2 | RES | 1311.959 | 1375.760 | 63.801 | 59.616 | 0.934 | 0.652 | 17.122 | 16.470 | 0.184 | 0.287 | 0.038 |
| 2 | PAY | 1311.959 | 1375.760 | 63.801 | 59.616 | 0.934 | 0.652 | 17.122 | 16.470 | 0.184 | 0.287 | 0.038 |
| 4 | ROCK | 1379.545 | 1395.142 | 15.597 | 10.617 | 0.681 | 0.366 | 3.200 | 2.834 | 0.264 | 0.301 | 0.114 |
| 4 | RES | 1379.545 | 1395.142 | 15.597 | 10.109 | 0.648 | 0.361 | 3.167 | 2.805 | 0.265 | 0.313 | 0.114 |
| 4 | PAY | 1379.545 | 1395.142 | 15.597 | 9.601 | 0.616 | 0.344 | 3.017 | 2.673 | 0.254 | 0.314 | 0.114 |
| 5 | ROCK | 1395.142 | 1516.724 | 121.582 | 39.878 | 0.328 | 10.368 | 10.368 | 2.157 | 0.337 | 0.260 | 0.792 |
| 5 | RES | 1395.142 | 1516.724 | 121.582 | 39.243 | 0.323 | 10.322 | 10.322 | 2.195 | 0.336 | 0.263 | 0.787 |
| 5 | PAY | 1395.142 | 1516.724 | 121.582 | 0.940 | 0.008 | 0.235 | 0.235 | 0.126 | 0.383 | 0.250 | 0.463 |



Table 5.
The results from Archie/Clavaud water saturation are based on the same input as the Archie equation except for the resistivity, now using sand resistivity instead of formation resistivity. The overall porosity is comparable to the Archie equation in the oil zone and lower in the water zone. The water saturation is lower than both the Archie and Indonesia equations.

**Table 6. Results from Archie water saturation in zone 1 (gas zone) using neutron-density total porosity.**

| *Zone* | *Flag Name* | *Top [m]* | *Bottom [m]* | *Gross [m]* | *Net [m]* | *Net-Gross [ratio]* | *BVW* | *POR-TH [m]* | *HCPOR-TH [m]* | *Avg_Shale [%]* | *Avg_Porosity [%]* | *Avg_Sw [%]* |
|---|---|---|---|---|---|---|---|---|---|---|---|---|
| 1 | ROCK | 1275.855 | 1311.959 | 36.073 | 26.109 | 0.724 | 0.729 | 5.942 | 5.212 | 0.322 | 0.228 | 0.123 |
| 1 | RES | 1275.855 | 1311.959 | 36.073 | 25.397 | 0.704 | 0.721 | 5.910 | 5.189 | 0.327 | 0.233 | 0.122 |
| 1 | PAY | 1275.855 | 1311.959 | 36.073 | 25.397 | 0.704 | 0.721 | 5.910 | 5.189 | 0.327 | 0.233 | 0.122 |
| 2 | ROCK | n.a. | n.a. | n.a. | n.a. | n.a. | n.a. | n.a. | n.a. | n.a. | n.a. | n.a. |
| 2 | RES | n.a. | n.a. | n.a. | n.a. | n.a. | n.a. | n.a. | n.a. | n.a. | n.a. | n.a. |
| 2 | PAY | n.a. | n.a. | n.a. | n.a. | n.a. | n.a. | n.a. | n.a. | n.a. | n.a. | n.a. |
| 4 | ROCK | n.a. | n.a. | n.a. | n.a. | n.a. | n.a. | n.a. | n.a. | n.a. | n.a. | n.a. |
| 4 | RES | n.a. | n.a. | n.a. | n.a. | n.a. | n.a. | n.a. | n.a. | n.a. | n.a. | n.a. |
| 4 | PAY | n.a. | n.a. | n.a. | n.a. | n.a. | n.a. | n.a. | n.a. | n.a. | n.a. | n.a. |
| 5 | ROCK | n.a. | n.a. | n.a. | n.a. | n.a. | n.a. | n.a. | n.a. | n.a. | n.a. | n.a. |
| 5 | RES | n.a. | n.a. | n.a. | n.a. | n.a. | n.a. | n.a. | n.a. | n.a. | n.a. | n.a. |
| 5 | PAY | n.a. | n.a. | n.a. | n.a. | n.a. | n.a. | n.a. | n.a. | n.a. | n.a. | n.a. |

Table 6.
Zone 1, the gas zone, was investigated on water saturation using neutron-density porosity as input instead of density porosity as for zone 2, 4 and 5. The Archie water saturation equation for zone 1 uses total neutron-density porosity. The results reveal good reservoir porosity values of 0.233 and a water saturation of 0.122.

**Table 7: Results from Indonesia water saturation in zone 1 (gas zone) using neutron-density effective porosity and Clavier calculated Vsh.**

| *Zone* | *Flag Name* | *Top [m]* | *Bottom [m]* | *Gross [m]* | *Net [m]* | *Net-Gross [ratio]* | *BVW* | *POR-TH [m]* | *HCPOR-TH [m]* | *Avg_Shale [%]* | *Avg_Porosity [%]* | *Avg_Sw [%]* |
|---|---|---|---|---|---|---|---|---|---|---|---|---|
| 1 | ROCK | 1275.855 | 1311.959 | 36.073 | 35.278 | 0.978 | 0.486 | 4.087 | 3.601 | 0.228 | 0.116 | 0.119 |
| 1 | RES | 1275.855 | 1311.959 | 36.073 | 20.775 | 0.576 | 0.293 | 3.174 | 2.881 | 0.163 | 0.153 | 0.092 |
| 1 | PAY | 1275.855 | 1311.959 | 36.073 | 20.775 | 0.576 | 0.293 | 3.174 | 2.881 | 0.163 | 0.153 | 0.092 |
| 2 | ROCK | n.a. | n.a. | n.a. | n.a. | n.a. | n.a. | n.a. | n.a. | n.a. | n.a. | n.a. |
| 2 | RES | n.a. | n.a. | n.a. | n.a. | n.a. | n.a. | n.a. | n.a. | n.a. | n.a. | n.a. |
| 2 | PAY | n.a. | n.a. | n.a. | n.a. | n.a. | n.a. | n.a. | n.a. | n.a. | n.a. | n.a. |
| 4 | ROCK | n.a. | n.a. | n.a. | n.a. | n.a. | n.a. | n.a. | n.a. | n.a. | n.a. | n.a. |
| 4 | RES | n.a. | n.a. | n.a. | n.a. | n.a. | n.a. | n.a. | n.a. | n.a. | n.a. | n.a. |
| 4 | PAY | n.a. | n.a. | n.a. | n.a. | n.a. | n.a. | n.a. | n.a. | n.a. | n.a. | n.a. |
| 5 | ROCK | n.a. | n.a. | n.a. | n.a. | n.a. | n.a. | n.a. | n.a. | n.a. | n.a. | n.a. |
| 5 | RES | n.a. | n.a. | n.a. | n.a. | n.a. | n.a. | n.a. | n.a. | n.a. | n.a. | n.a. |
| 5 | PAY | n.a. | n.a. | n.a. | n.a. | n.a. | n.a. | n.a. | n.a. | n.a. | n.a. | n.a. |



Table 7.
The Indonesia equation use effective neutron-density porosity as input. The porosity is lower at 0.153 together with lower water saturation, 0.092, compared to the neutron-density porosity based Archie equation (Table 6).

**Table 8. Results from Archie/Clavaud water saturation in zone 1 (gas zone) using neutron-density total porosity.**

| *Zone* | *Flag Name* | *Top [m]* | *Bottom [m]* | *Gross [m]* | *Net [m]* | *Net-Gross [ratio]* | *BVW* | *POR-TH [m]* | *HCPOR-TH [m]* | *Avg_Shale [%]* | *Avg_Porosity [%]* | *Avg_Sw [%]* |
|---|---|---|---|---|---|---|---|---|---|---|---|---|
| 1 | ROCK | 1275.855 | 1311.959 | 36.073 | 26.109 | 0.724 | 0.369 | 5.942 | 5.573 | 0.322 | 0.228 | 0.062 |
| 1 | RES | 1275.855 | 1311.959 | 36.073 | 25.397 | 0.704 | 0.361 | 5.910 | 5.550 | 0.327 | 0.233 | 0.061 |
| 1 | PAY | 1275.855 | 1311.959 | 36.073 | 25.397 | 0.704 | 0.361 | 5.910 | 5.550 | 0.327 | 0.233 | 0.061 |
| 2 | ROCK | n.a. | n.a. | n.a. | n.a. | n.a. | n.a. | n.a. | n.a. | n.a. | n.a. | n.a. |
| 2 | RES | n.a. | n.a. | n.a. | n.a. | n.a. | n.a. | n.a. | n.a. | n.a. | n.a. | n.a. |
| 2 | PAY | n.a. | n.a. | n.a. | n.a. | n.a. | n.a. | n.a. | n.a. | n.a. | n.a. | n.a. |
| 4 | ROCK | n.a. | n.a. | n.a. | n.a. | n.a. | n.a. | n.a. | n.a. | n.a. | n.a. | n.a. |
| 4 | RES | n.a. | n.a. | n.a. | n.a. | n.a. | n.a. | n.a. | n.a. | n.a. | n.a. | n.a. |
| 4 | PAY | n.a. | n.a. | n.a. | n.a. | n.a. | n.a. | n.a. | n.a. | n.a. | n.a. | n.a. |
| 5 | ROCK | n.a. | n.a. | n.a. | n.a. | n.a. | n.a. | n.a. | n.a. | n.a. | n.a. | n.a. |
| 5 | RES | n.a. | n.a. | n.a. | n.a. | n.a. | n.a. | n.a. | n.a. | n.a. | n.a. | n.a. |
| 5 | PAY | n.a. | n.a. | n.a. | n.a. | n.a. | n.a. | n.a. | n.a. | n.a. | n.a. | n.a. |



Table 8.
The Archie/Clavaud equation uses the same input as the Archie water saturation equation except for the resistivity that differs now using sand resistivity. The porosity shows the same results as in the Archie equation and the water saturation is lower at 0.061.

# 4 Discussion

### Petrophysical interpretation

The overall quality of the logs is good and most of them cover the entire reservoir interval studied. In addition there is vast amount of log data from the 7220/8-1 well, and only a minor portion of this has been possible to analyze in this study. The logs analyzed are well suited for a study on the clay mineral influence on logging tools in a shaly sandstone reservoir. The desirable data from a special core analysis were, however, not provided in this study. If such material was at hand, the powerful clay quantification method, the Waxman-Smits water saturation equation (eq. 4) could have been performed. Since triaxial induction log tool data were available, the study was not limited to the Archie and Indonesia water saturation equations. The triaxial induction log data and the estimated sand resistivity served as a substitution for the Waxman-Smits equation resulting in a vigorous addition to the study.

Before calculating and summarizing the data selected for processing, a vital part of the work includes a determination and distinction of the reservoir intervals which was known prior to this study (Lindberg et al. 2013; Halland et al. 2013). All shale intervals in the reservoir will lower the mean hydrocarbon saturation results and were excluded from the study either by zonation of entire intervals or ruled out by cut off settings during result summation. The zonation of the dataset is based on the detectable fluid contacts. The intervals for Stø and Nordmela formations as well as the fluid contacts in the reservoir section are known in the 7220/8-1 well from company reports (Lindberg et al. 2013; Halland et al. 2013). The petrophysical framework leading up to reservoir determination are here briefly presented.

There are a number of resistivity peaks accompanied by high density and neutron readings visible at e.g. -1281 m, -1316 m and -1387 m depth (Appendix III). These peaks are interpreted to indicate densely calcite cemented sandstone beds and thus not considered as reservoir rocks. They are not displayed as separate zones but are ruled out by setting the cut-off values for total porosity at <10% when summarizing the results. The zones are interpreted as impermeable with a porosity <10% and thereby disregarded automatically by the software as reservoir intervals when not meeting reservoir conditions.

Low gamma ray accompanied by low resistivity values are an indication of sandstone containing formation water. These intervals are not considered as pay intervals unless there is an anisotropy occurring between the horizontal and vertical resistivity recorded by the triaxial induction tool. If that is the case, this might be an indication of a sandstone interval containing petroleum, and should thus be part of the pay interval. An example of this is visible in figure 21 derived from the petrophysical evaluation in Techlog.

Supposed sand intervals with decreasing resistivity indicate a transition from a clean sand formation to a formation containing more fine-grained particles. The resistivity of clay bound water in shaly intervals will lower the overall bulk resistivity measurements and indicate a water saturated reservoir even though the sand intervals may contain sufficient amounts of hydrocarbons. Higher sand resistivity compared to formation resistivity indicates petroleum in the sand intervals despite the vast shaliness (Figs. 21, 22).

Low gamma ray readings accompanied by high resistivity indicate clean hydrocarbon- saturated sandstone. Low gamma ray and low resistivity could be indicated as water-filled sandstone. Once again, low resistivity should always be compared to the sand resistivity derived from the triaxial induction log tool. Higher sand resistivity indicates laminated or isolated hydrocarbon filled sand intervals and are easily overlooked using formation resistivity only. This is handled by the software by setting the conditions of when the software should use sand or formation resistivity as input in water saturation calculations.

### Porosity

The Density porosity logging tool uses a robust and reliable technique. Zone 1 is interpreted as a gas zone due to the known fluid contacts. The neutron log confirms this having higher values in the gas zone compared to the oil zone accompanied by fairly constant density values. The gas, representing pore space, is not entirely detected by the density tool due to invasion or shale effects. These effects will mask the pay. A solution to this could be using equations for neutron-density porosity (eq. 16; 17), instead of density porosity (eq. 13; 14) allowing the neutron tool to read deeper in the formation. The neutron tool is sensitive to hydrogen and detects the gas, and hence pore space. Zone 1 is more comparable when using neutron-density porosity.

The porosity is expected to be lower using Indonesia equation since the formula uses effective porosity compared to total. The water saturation is expected to be lower, compared to the Archie water saturation equation, due to the exclusion of shale resistivity resulting in higher resistivity indicating petroleum opposite to water.

The results on total porosity from the log operations are comparable to the results from conventional core analysis (CCA). The difference between laboratory settings and subsurface conditions could be the explanation for any deviations (Appendix II). The core data contain values collected at a specific depth compared to the summary tables based on the average log data value for an entire zone.

### Water saturation

The results comparing the Indonesia or the Archie/Clavaud methods to the Archie water saturation method are consistent with what has been stated in the literature (e.g. Archie 1942, 1950, 1952; Waxman & Smits 1968; Poupon & Leveaux 1971; Boyd et al. 1995; Klein and Martin 1997; Tenchov 1998; Lasswell 2006; Anderson et al. 2005, 2008; Clavaud et al. 2005; Ellis & Singer 2008). Considering shale and excluding the effects of shale will lower the water saturation and increase pay giving results more comparable to the actual case. The shale effect using the Archie method masks the resistivity from petroleum indicating water which is false. A sudden water saturation decrease using the Indonesia and a greater difference using the

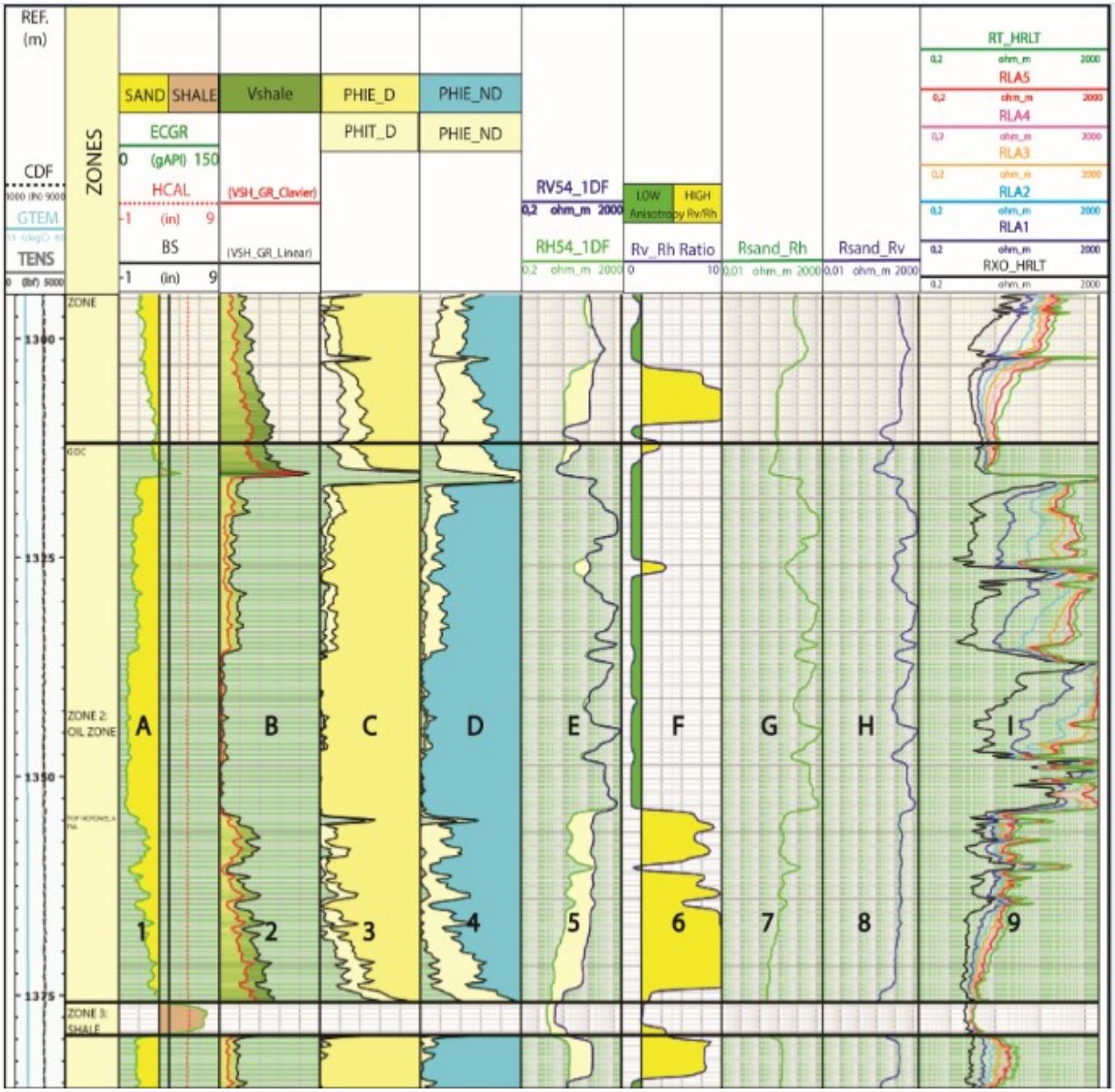


*Fig. 21. Original and computed well logs from well 7220/8-1.*

*At 1343 m: (A) Gamma ray response indicates a relatively clean sand unit. (B) Low volume of shale. (C) High density porosity and (D) high neutron-density porosity. (E) Overlying vertical and horizontal resistivity indicate a homogenous unit. (F) The computed resistivity anisotropy log indicates low values, interpreted as an isotropic unit. (G) Computed horizontal sand resistivity and (H) computed vertical sand resistivity show similar values. (I) Clear separation between the resistivity logs indicate a porous and permeable formation containing fluids not similar to the water based drilling fluids. Since the computed logs are reported as an isotropic unit the software use formation resistivity when calculating water saturation. The low clay mineral content verifies the interpretation. With low clay mineral content there is no need to compensate using another resistivity method.*

*At 1368 m: (1) Gamma ray log indicates a relatively lower sand content and higher clay mineral content compared to (A). (2) Computed shale volume are higher then (B). (3) Density porosity and (4) neutron-density porosity indicate a porous unit but less effective porosity compared to (C) and (D) indicating clay mineral. (5) The vertical and horizontal resistivities differ, verified by the computed resistivity anisotropy log (6) showing a relatively highly resistivity anisotropy. (7) Horizontal sand resistivity indicate lower resistivity compared to (8) vertical sand resistivity indicating horizontal layers with higher resistivity in an otherwise low resistivity unit. (9) Less separation compared to (I) indicates formation fluids different from drilling fluids, but the results are not as clear. This unit is interpreted as a shaly sand unit containing sand with clay minerals. The beds, containing clay minerals, are interpreted, from vertical and horizontal resistivity anisotropy, as horizontal layers. The clay mineral content makes the software choose sand resistivity that will exclude the clay minerals from the water saturation calculations focusing on the*

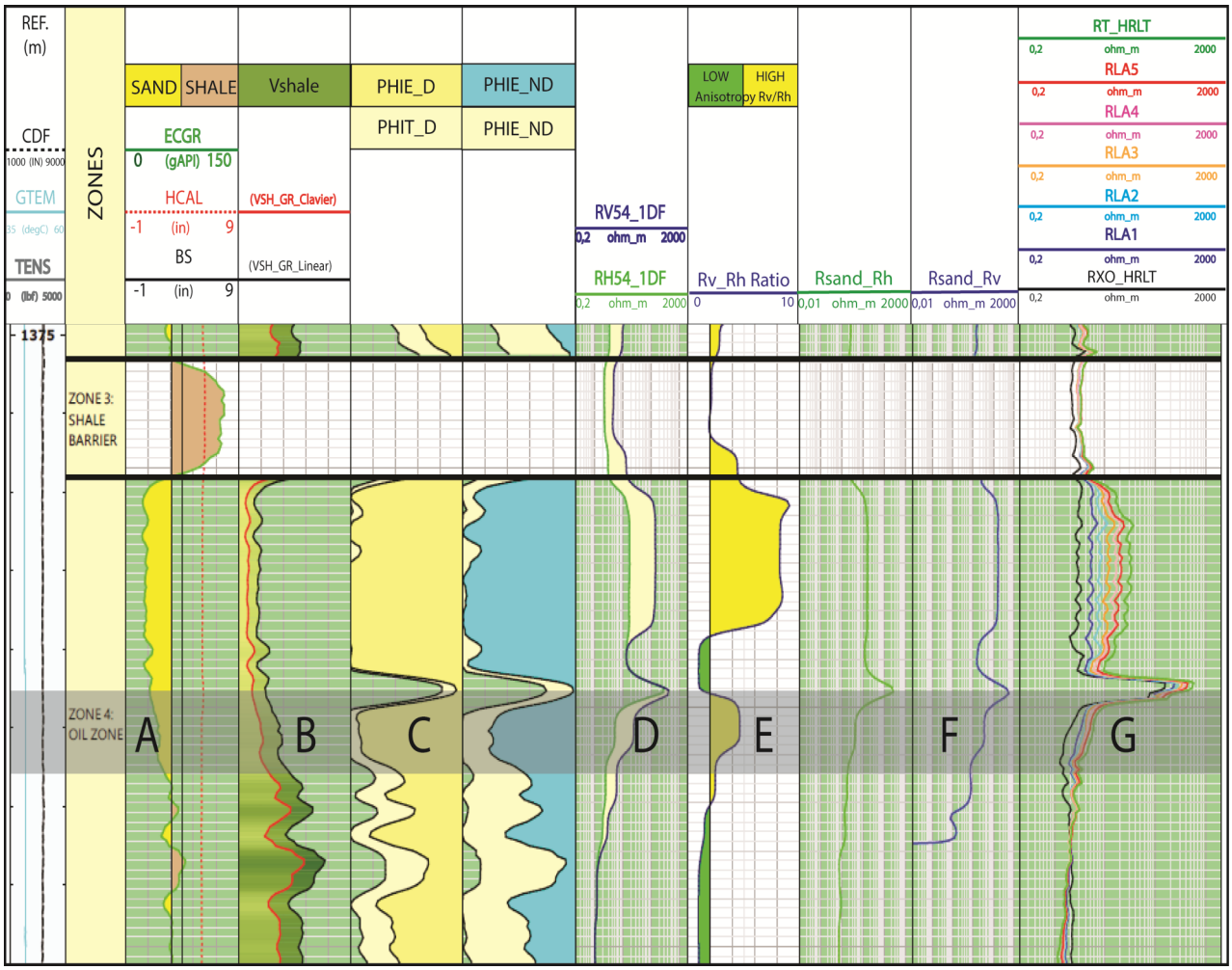


*Figure 22. A: Gamma Ray values indicate sandstone in a coarsening upward sequence. B: The volume of shale also indicates that shale is present in the sequence, an example of alternating thin beds of sand and shale. C: Density porosity indicates a formation with porosity, and effective porosity enhancing the alternating thin bed interpretation. D: There is a separation between the horizontal and vertical resistivity indicating a heterogeneous rock interval. E: The resistivity ratio indicates high anisotropy. F: The vertical sand resistivity shows higher values compared to formation resistivity indicating petroleum instead of water in the sand beds F: The resistivity data show lower values compared to vertical sand resistivity and to more obvious petroleum zones between e.g. 1325-1350 m (Appendix III). The scenario in the highlighted area on the log is an example of an interval with thin beds of sand and shale where the software would disregard formation resistivity and instead calculate water saturation based on the higher sand resistivity. This is an example of the challenge of not overlooking thin petroleum-bearing sand beds, being the basis of this study. Note: Higher resolution logs are available in Appendix III-V (Image generated, modified and retrieved from Techlog software).*

Archie/Clavaud is expected. This assumption goes well with the results of this study giving support to existing research (e.g. Archie 1942, 1950, 1952; Waxman & Smits 1968; Poupon & Leveaux 1971; Boyd et al. 1995; Klein and Martin, 1997; Tenchov 1998; Lasswell 2006; Anderson et al. 2005, 2008; Clavaud et al. 2005; Ellis & Singer 2008). Using sand resistivity compared to formation resistivity will reveal significantly more hydrocarbon saturated intervals and increase the total amounts of pay intervals.

The results are comparable to the results from the CCA using total porosity as input (Moosefinn 2011; Appendix II).

## The geological approach

The global energy consumption is vast and the demand for energy increases continuously. A lot of money and effort are spent on research and installation of renewable energy systems, but even combined; they could not match the effect of energy gained from petroleum. The demand and the lack of substitutes rely on the petroleum industry to deliver oil and gas on a daily basis. At the same time the tradition of producing petroleum with relative ease is vanishing. Throughout the history of petroleum production, the estimations of quantities did not have to be as accurate as of today. As an example related to this study, in order to estimate hydrocarbon volumes the water saturation calculations would rely on more simple equations such as the Archie water saturation equation. Receiving estimations based on the bulk rock was enough since the hydrocarbon volumes resulted in large revenues anyway. At the present, the petroleum companies operate in more and more geologically complex areas and the need to fully understand the complexity of the subsurface is an ongoing challenge.

This study examines the challenge of appraising

petroleum quantities in shaly sand reservoirs, a global challenge. The challenge lies within quantifying the clay mineral effects on logging tools in order to receive a correct interpretation of the reservoir. This is not able to do without using geological knowledge into the preparatory stages of petroleum exploration and production.

Extensive geological mapping of the sedimentary bedrock globally have been, and are still being, performed, none the least by the petroleum companies in certain areas. This information is available and has to be implemented when exploring potential petroleum discoveries. If there is an awareness of the geological condition in an area, and the history shaping the area, the planning to meet exploration and production challenges could be met.

The Stø and Nordmela formations, belonging to the Johan Skrugard field in the Barents Sea, have proven good reservoir conditions and the strata are well known in the 7220/8-1 well. Offshore operations, however, have large production costs. This makes it impossible for companies to invest in producing reservoirs that would be worth less in petroleum volumes sold, compared to the resources invested in the project. So in order for the Skrugard field to be produced, detailed evaluation of the petroleum volumes must be carried out.

With the knowledge of existing sandstone reservoirs containing shale, with more shale downward in the lenticular to flaser bedded Nordmela formation, preparations are vital. The petrophysical tool suite needed for formation evaluation should match the geological settings in the studied formation.

The petrophysical data available for this study meet the challenge of appraising the water saturation, and hence hydrocarbon saturation, in well 7220/8-1. The triaxial induction tool has been proven useful in order to include thin sandstone beds with petroleum potential in the hydrocarbon volume estimation. At the same time the shale-rich beds are excluded. The thin petroleum bearing sand beds would have been overlooked using Archie water saturation technique allowing the shale to influence the water saturation estimation.

Surprisingly, there were no special core analysis performed which provide data for quantifying the clay mineral content using the Waxman-Smits method. The need for a future project including work with sand resistivity from the triaxial induction tool together with special core analysis data, making a Waxman-Smits water saturation study possible, are requested. This would verify the validity of the triaxial induction tool as a means for correct water saturation estimations in shaly sand reservoirs. Using the triaxial induction tool instead of performing special core analysis would keep exploration costs relative low.

# 5 Conclusions

- Conventional water saturation estimations, such as the Archie method does not compensate for the effects from clay minerals.
- Clay minerals present in an alternating shaly sand sequence will mask pay intervals.
- The Indonesia water saturation equation detects and excludes the clay mineral effect based on shale volume.
- The Archie/Clavaud water saturation is based on an alternative resistivity, sand resistivity, as opposed to the formation resistivity in the Archie method. When vertical and horizontal resistivity anisotropy occurs, the sand resistivity is valid.
- The Archie/Clavaud method can be verified using the Waxman-Smits water saturation method as comparison. If proven valid, the Archie/Clavaud method should be preferred due to lower exploration costs.
- Rock physics are a consequence of geological evolution. Geological knowledge in the exploration area is vital to streamline drilling and petrophysical operations.

# 6 Acknowledgements

**Mikael Erlström**, Swedish Geological Survey, and **Per Ahlberg**, Lund University, Sweden
Mikael and Per supervised me during my thesis work. They are calm, thorough and professional. Their feedback on my thesis work has been very valuable, and will also be valuable later during a career within the field of geoscience.

**Erik Skogen**, Norwegian University of Science and Technology (NTNU)
Erik provided me with the well log data necessary to perform a formation evaluation in the well 7220/8-1. He also invited me to NTNU during my thesis work. I have been an exchange student at NTNU, which allowed me to perform the formation evaluation using Techlog at the Department of Petroleum Engineering and Applied Geophysics. This was vital for my thesis work.

**DISKOS,** Norway
Initially, the well log data came from the DISKOS database in Norway. I am grateful for the availability of such databases for students.

**Harry Brandt**, Statoil AS, Norway
I am indebted to Harry for inspirational lectures on the shaly sand topic during the spring of 2015 in Trondheim, as well as providing me with the core photos from well 7220/8-1 from the Statoil archive.

**My family**
The ongoing support from my family is vital for me to achieve my goals. They show appreciation and pride for my work and sacrifices. I hope that my excitement for the field of geoscience will influence them.

# 7 References


Al Saeed, M.M.A.M., Derks, J., Fuchs, T., Hantschel, T., Kauerauf, A., Neumaier, M., Schenk, O., Swientek, O., Tessen, N., Welte, D., Wygrala, B., Kornpihl, D. & Peters, K., 2009: Basin and petroleum system modeling. *Oilfield Review 21*, 2.

Anderson, B., Clavaud, J., Nelson, R., Guru, K.U. & Wang, H., 2005: Field examples of enhanced hydrocarbon estimation in thinly laminated formation with a triaxial array induction tool: A laminated sand-shale analysis with anisotropic shale: *Presented at the 46th Annual Logging Symposium, SPWLA*.

Andersson, B.I., Barber, T., Bastia, R., Clavaud J., Coffin, B., Das, M., Hayden, R., Klimentost, T., Minh, C.C. & Williams, S., 2008: *Triaxial induction – A new angle for an old measurement*. Schlumberger Oilfield Review, Summer edition. 84 pp.

Andersen, M.A., Duncan, B. & McLin, R., 2013: Core truth in formation evaluation. *Oilfield Review 25*, 16–23.

Archie, G.E., 1942: The Electrical resistivity log as an aid in determining some reservoir characteristics. *Petroleum Transactions of AIME 146*, 54–62.

Archie, G.E., 1950: Introduction to petrophysics of reservoir rocks. *American Association of Petroleum Geologists Bulletin 34*, 943–961.

Archie, G.E. 1952: Classification of carbonate reservoir rocks and petrophysical considerations. *American Association of Petroleum Geologists Bulletin 36,* 278–298.

Awuah, J.B., Wemazenu Adda, G., Mijinyawa, A., Andriamihhaja, S. & Siddiqui, N., 2013: 2D basin modelling and petroleum system analysis of the Triassic play in the Hammerfest Basin of the Norwegian Barents Sea. *Research Journal of Applied Sciences, Engineering and Technology 6,* 3137–3150.

Barrére, C., 2009: Integrated geophysical modelling and tectonic evolution of the western Barents Sea. *Doctoral thesis at NTNU 2009:267*.

Bassiouni, Z., 1994: *Theory, measurement and interpretation of well logs*. SPE Textbook Series Vol. 4, Society of Petroleum Engineers, Texas, 372 pp.

Bhuyan, K. & Passey, Q.R., 1994: Clay estimation from GR and Neutron-Density porosity logs. *SPWLA 35th Annual Logging Symposium, June 19–22.*

Bjørlykke, K., 2010: *Petroleum Gesocience.* Springer, 508 pp.

Boyd, A., Darling, H., Tabanou, T., Davis, B., Lyon, B., Flaum, C., Klein, J., Sneider, R.M., Sibbit, A. & Singer, J., 1995: The lowdown on low-resistivity pay. *Oilfield Review 7* (3), 4–18.

Catuneanu, O., Galloway, W.E., Kendall, C.G., Miall, A.D., Posamentier, H.W., Strasser, A. & Tucker, M.E., 2011: Sequence stratigraphy: methodology and nomenclature. *Newsletters on Stratigraphy 44 (3),* 173–245.

Cecchi, M., Markello, J. & Waite, L., 1995: Sequence stratigraphy architecture of Carboniferous-Permian sedimentary systems of the Norwegian Barents Sea with comparison to coeval systems of the USA. *Norwegian petroleum society special publications 5,* 545–569.

Clavaud, J., Nelson, R., Guru, K.U. & Wang, H., 2005: Field examples of enhanced hydrocarbon estimation in thinly laminated formation with a triaxial array induction tool: A laminated sand-shale analysis with anisotropic shale. *Presented at the 46th Annual Logging Symposium, SPWLA.*

Cocks, L.R.M. & Torsvik, T.H.., 2005: Baltica from the Late Precambrian to Mid-Palaeozoic Times: The gain and loss of a terrane's identity. *Earth-Science Review 72*, 39–66.

Cocks, L.R.M. & Torsvik, T.H. 2011: The Palaeozoic geography of Laurentia and western Laurussia: A stable craton with mobile margins. *Earth-Science Reviews 106*, 1–2, 1–51.

Dalland, A., Worsley, D. & Ofstad, K., 1988: A lithostratigraphic scheme for the Mesozoic and Cenozoic succession offshore mid-and northern Norway. *NPD-Bulletin 4,* 1–87.

Dengo, C.A. & Røssland, K.G., 1992: Extensional tectonic history of the western Barents Sea, *In* Larsen, R.M., Brekke, H., Larsen, B.T. & Talleraas, E., (eds.): Structural and tectonic modelling and its applications to petroleum geology. *Norwegian Petroleum Society (NPF) Special Pubblication 1*, 91–107.

Doré, A.G., 1991: The structural foundation and evolution of Mesozoic seaways between Europe and the Arctic. *Palaeogeography, Palaeoclimatology, Palaeoecology 87*, 441–492.

Doré, A., 1995: Barents Sea geology, petroleum resources and commercial potential. *Arctic 48*, 207 –221.

Edvardsen, I., Nyrnes, E., Johnsen, M.G., Hansen, T.L., Lövhaug, U.P. & Matzka, J., 2014: Improving the accuracy and reliability of MWD/magnetic-wellbore-directional surveying in the Barents Sea. *Society of petroleum engineers SPE-166226-PA*.

Eldholm, O., Thiede, J. & Taylor, E., 1987: Evolution of the Norwegian continental margin: Background and objectives. *In* Eldholm, O., Thiede, J. & Taylor, E. (eds.): Proceedings Oil Drilling Programme*, ODP Init. Repts.,104*, 5–25.

Ellis, D.V. & Singer, J.M., 2007: *Well logging for earth scientists*. 2nd Edition. Springer, 692 pp.

Faleide, J.I., Gudlaugsson, S.T. & Jacquart, G., 1984: Evolution of the western Barents Sea. *Marine and Petroleum Geology 1*, 123 –150.

Faleide, J.I., Vågnes, E. & Gudlaugsson, S.T.,1993: Late Mesozoic-Cenozoic evolution of the south-western Barents Sea in a regional rift-shear tectonic setting. *Marine and Petroleum Geology 10,* 186 –214.

Faleide, J.I., Tsikalas, F., Breivik, A.J., Mjelde, R., Ritzmann, O., Engen, O. & Eldholm, O., 2008: Structure and evolution of the continental margin of Norway and the Barents Sea. *Episodes 31,* 82.

Fanavoll, S., Gabrielsen, P.T. & Ellingsrud, S., 2014: CSEM as a tool for better exploration decisions: Case studies from the Barents Sea, Norwegian continental shelf (*in* Interpretation and integration of CSEM data ) *Interpretation (Tulsa)(August 2014) 2*: SH55 –SH66.

Fossen, H., 2000: Extensional tectonics in the Caledonides: Synorogenic or postorogenic? *Tectonics 19,*

213 –224.
Fossen, H., 2010: Extensional tectonics in the North Atlantic Caledonides: a regional view, *In* Law, R.D., Butler, R.W.H., Holdsworth, R.E., Krabbendam, M. & Strachan, R.A., (eds): Continental Tectonics and Mountain Building: The Legacy of Peach and Horne,. *Geological Society, London, Special Publications 335*, 767 –793.
Gabrielsen, R.H., 1990: Structural elements of the Norwegian continental shelf, Part 1: The Barents Sea region. *NPD-Bulletin 6,* 1–47.
Gernigon, L., Brönner, M., Roberts, D., Olesen,O., Nasuti, A. & Yamasaki, T., 2014: Crustal and basin evolution of the southwestern Barents Sea: From caledonian orogeny to continental breakup. *Tectonics 33*, 1–27.
Gjelberg, J. & Steel, R., 1981: An outline of Lower-Middle Carboniferous sedimentation on Svalbard: Effects of tectonic, climatic and sea level changes in rift basin sequences. *Canadian Society Petroleum Geologists Memoirs 7*, 543–561.
Gluyas, J. & Swarbrick, R., 2004: *Petroleum Geoscience*. Blackwell Publishing, 359 pp.
Glørstad-Clark, E., Faleide, J.I., Lundschien, B.A. & Nystuen, J.P., 2010: Triassic seismic sequence stratigraphy and paleogeography of the Western Barents Sea area. *Marine and Petroleum Geology 27,* 1448 –1475.
Halland, E., Mujezinovic, J., Riis, F., Bjørnestad, A., Tørneng Gjeldvik, I., Bjørheim, M., Magnus, C., Meling, I.M., Sande Rød, R., Pham, V.T.H. & Tappel, I., 2013: *$CO_2$ storage atlas, Barents Sea*. Norwegian Petroleum Directorate, 39 pp.
Harland, W. B., 1965: The tectonic evolution of the Artic-North Atlantic region. *Royal Society London. Philosophical Transactions 258*, 59 – 75.
Henriksen, E., Ryseth, A., Larssen, G., Heide, T., Rønning, K., Sollid, K. & Stoupakova, A., 2011: Tectonostratigraphy of the greater Barents Sea: Implications for petroleum systems. *Geological Society, London, Memoirs, 35,* 163–195.
Hill, H.J., Shirley, O.J. & Klein, G.E., 1979: Bound water in shaly sands – its relation to $Q_v$ and other formation properties. *Log Analyst May-June edition*.
Hochuli, P.A., Colin, J.P. & Vigran. I.O., 1989: Triassic biostratigraphy of the Barents Sea area. pp. 131-153 *In* Collinson. J.D. (ed ): *Correlation in Hydrocurbon Exploration.* Norwegian Petroleum Society. Graham & Trotman Ltd.
Hook, J.R., 2003: An Introduction to porosity. *Petrophysics 44*, 205–212.
Hürlimann, M.D., Venkataramanan, C., Flaum, C., Speier, P., Karmonik, C., Freedman, R. & Heaton, N., 2002: Diffusion-editing: New NMR measurement of saturation and pore geometry. *SPWLA 43rd Annual Logging Symposium, June 2–5.*
Johansen, S.E., Ostisty, B.K., Birkeland, Ø., Fedorovsky, Y.F., Martirosjan, V.N., Bruun Cristenssen, O., Cheredeev, S.I., Ignatenko, E.A. & Margulis, L.S., 1992: Hydrocarbon potential in the Barents Sea region: Play distribution and potential, *In* Vorren, T.O., Bergsager, E., Dahl-Stamnes, Ø.A., Holter, E., Johansen, B., Lie, E. & Lund, T.B. (eds.): *Arctic Geology and Petroleum Potential*, pp. 273–320, NPF Special Publication 2, Elsevier, Amsterdam.
Juhász, I., 1981: Normalised $Q_v$ – The key to shaly sand evaluation using the Waxman-Smits equation in the absence of core data. *SPWLA 22nd Annual Logging Symposium, June 23 –26.*
Klein, J.D., Martin P.R. & Allen D.F., 1997: The petrophysics of electrically anisotropic reservoirs. *The Log Analyst, May–June edition.*
Larssen, G., Elvebakk, G., Henriksen, L.B., Kristensen, S., Nilsson, I., Samuelsberg, T. & Worsley, D., 2002: Upper Palaeozoic lithostratigraphy of the southern Norwegian Barents Sea. *NPD-Bulletin 9*, 76.
Lasswell, P.M., 2006: Core analysis for electrical properties. *Petrophysics 47*, 191–213.
La Vigne, J., Herron, M. & Hertzog, R., 1994: Density-neutron interpretation in shaly sands. *SPWLA 35th Annual Logging Symposium, June 19 –22.*
Lindberg, B., Alzeni, F. & Holmboe, J.M., 2013: Skrugard – a new hydrocarbon province in the Barents Sea. *Society of Exploration Geophysicists 2013-0578*.
Lundin Oil, 2013: *Gohta: Et nytt oljefunn i Barentshavet*. Retrieved 151020, from http://lundin-norway.no/2013/10/16/gohta-et-nytt-oljefunn-i-barentshavet/.
Löseth, L.O., Wiik, T., Olsen, P.A., Becht, A. & Hansen, J.O., 2013: CSEM exploration in the Barents Sea, Part I: Detecting Skrugard from CSEM: *75th Annual and International Conference and Exhibition, EAGE, Extended Abstracts.*
Magoon, L. & Dow, W., 1991: The petroleum system - From source to trap. *AAPG Bulletin (American Association of Petroleum Geologists);(United States),75(CONF-910403).*
McKay, A., Mattsson, J. & Midgley, J., 2014: Towed streamer EM for success. *GEO ExPro 11*, 82–84.
McPhee, C., Reed, J. & Zubizarreta, I., 2015: *Core Analysis: A Best Practice Guide.* Developments in Petroleum Science 64. Elsevier, Amsterdam, 830 pp.
Mossefinn, J.F., 2011: *Core Analysis Well: 7220/8-1*. Weatherford Laboratories. Project No. 10746. Report No. 10746-11. 202 pp.
Mørk, A., Embry, A.F. & Weitschat, W., 1989: Triassic transgressive-regressive cycles in the Sverdrup basin, Svalbard and the Barents Shelf *In* Collinson, J.D. (ed.): Proceedings of the Conference Correlation in Hydrocarbon Exploration organized by the Norwegian Petroleum Society and held in Bergen, Norway, 3–5 October 1988, *Correlation in hydrocarbon exploration,*113 –130.
Norwegian Petroleum Directorate, 2013. *Factpages*. Collected at www.factpages.npd.no
Os Vigran, J., Mangerud, G., Mørk, A., Bugge, T. & Weitshat, W., 1998: Biostratigraphy and sequence stratigraphy of the Lower and Middle Triassic deposits from the Svalis dome, Central Barents Sea, Norway. *Palynology 22*, 89 –141.
Poupon, A. & Leveaux, J., 1971: Evaluation of water saturation in shaly formations. *Log Analyst 12*, 3–8.
Ritzmann, O. & Faleide, J.I., 2007: Caledonian basement of the western Barents Sea: *Tectonics 26*,

doi:10.1029/2006TC002059.
Roufosse, M.C., 1987: The formation and evolution of sedimentary basins in the western Barents Sea. *In* Brooks, J. & Glennie, K. (eds.), *Petroleum geology of north west Europe*, Graham & Trotman, London, 1149-1161.
Ryseth, A., Augustson, J.H., Charnock, M., Haugerud, O., Knutsen, S.M., Midbøe, P.S., Opsal, J.G. & Sundsbø, G., 2003: Cenozoic stratigraphy and evolution of the Sørvestsnaget basin, southwestern Barents Sea. *Norwegian Journal of Geology 83*, 107–130.
Rønnevik, H. & Jacobsen, H.P., 1984: Structural highs and basins in the western Barents Sea. *In* Spencer, A.M. (ed.)*:* Petroleum Geology of North European Margin*. Norwegian Petroleum Society*, Graham & Trotman, London, 19–32.
Sattar, N., Juhlin, C. & Ahmad, N., 2009: *Seismic stratigraphic framework of an early Cretaceous sand lobe at the slope of southern Loppa High, Barents Sea, Norway.* presented and published in AAPG-PAPG ATC 2009. Collected 160109 at: www.searchanddiscovery.com/abstracts/pdf/2012/papg2009/abstracts/ndx_sattar.pdf.
Schlumberger, 2009: *Log interpretation charts*. Schlumberger, Texas, 310 pp.
Serra, O., 1984: *Fundamentals of well log interpretation – Vol. 1: The acquisition of data*. Developments in Petroleum Science No. 15A, Elsevier, New York, 423 pp.
Serra, O., 1986: *Fundamentals of well log interpretation – Vol. 2: The interpretation of logging data.* Developments in Petroleum Science No. 15B, Elsevier Science Publishers, Amsterdam, 684 pp.
Smelror, M., 1994: Jurassic stratigraphy of the western Barents Sea region: A review. *Geobios 27*, 441–451.
Smelror, M., Petrov, O.V., Larsen, G.B. & Werner, S., 2009: *Atlas-geological history of the Barents Sea*, Geological Survey of Norway, Trondheim, 135 pp.
Spencer, A. M., Briskeby, P. I., Christensen, L. D., Foyn, R., Kjolleberg, M., Kvadsheim, E. & Williams, J. 2008: Petroleum geoscience in Norden-exploration, production and organization. *Episodes 31,* 115.
Stemmerik, L., Nilsson, I. & Elvebakk, G., 1995: Gzelian-Asselian depositional sequences in the western Barents Sea and north Greenland. *In* Steel, R.J., Felt, V.L., Johannessen, E.P. & Mathieu, C., (eds.), Sequence stratigraphy on the northwest European margin. *Norwegian Petroleum Society Special Publications 5*, 529–544.
Stemmerik, L. & Worsley, D., 2005: 30 years on - Arctic Upper Palaeozoic stratigraphy, depositional evolution and hydrocarbon prospectivity. *Norwegian Journal of Geology 85,* 151–168.
Tenchov, G.G., 1998: Evaluation of electrical conductivity of shaly sands using the theory of mixtures. *Journal of Petroleum Science and Engineering 21*, 263–271.
Tiab, D. & Donaldson, E.C., 1996: *Petrophysics: Theory and practice of measuring reservoir rock and fluid transport properties*, Gulf Publishing Co., Houston, Texas, 706 pp.
Van Veen, P.M., Skjold, L.J., Kristensen, S.E., Rasmussen, A., Gjelberg, J. & Stølan, T., 1993: Triassic sequence stratigraphy in the Barents Sea. *Norwegian Petroleum Society Special Publications 2,* 515–538.
Waxman, M.H. & Smits, L.J.M., 1968: Electrical conductivities in oil bearing shaly sands. *Society of Petroleum Engineers Journal 8*, 107–122.
Wood, R.J., Edrich, S.P. & Hutchison. I., 1989: Influence of north Atlantic tectonics on the large scale uplift of the Stappen High and the Loppa High, western Barents Shelf. *American Association of Petroleum Geologists Memoir 46*, 559—566.
Worsley, D., 2006: The post-Caledonian geological development of Svalbard and the Barents Sea. *Norwegian Geological Society, Abstracts and Proceedings, 3,* 5–21.
Ziegler, P.A., 1986: Geodynamic model for the Palaeozoic crustal consolidation of western and central Europe: *Tectonophysics 126*, 303–328.

# 8 Appendix

## Appendix I. General drilling operational data from well 72208-1

| | |
|---|---|
| **Wellbore Name** | 7220/8-1 |
| **Type** | EXPLORATION |
| **Purpose** | WILDCAT |
| **Status** | P&A (Plugged & Abandoned) |
| **Main Area** | BARENTS SEA |
| **Discovery** | 7220/8-1 JOHAN CASTBERG |
| **Seismic Location** | 3D survey WG08 –inline 1530 & crossline 3470 |
| **Drilled in production license** | 532 |
| **Drilling Operator** | Statoil Petroleum AS |
| **Drill Permit** | 1327-L |
| **Drilling Facility** | POLAR PIONEER |
| **Drilling Days** | 65 |
| **Entered date** | 27.02.2011 |
| **Completed date** | 02.05.2011 |
| **Release date** | 02.05.2011 |
| **Publication date** | 02.05.2011 |
| **Content** | OIL/GAS |
| **Discovery Wellbore** | YES |
| **1st Level with HC, Age** | MIDDLE JURASSIC |
| **1st Level with HC, Formation** | STØ FORMATION |
| **2nd Level with HC, Age** | EARLY JURASSIC |
| **2nd Level with HC, Formation** | NORDMELA FORMATION |
| **Kelly Bushing Elevation [m]** | 23.0 |
| **Water Depth [m]** | 374.0 |
| **Total Depth [m]** | 2222.0 |
| **Final Vertical Depth [m]** | 2221.0 |
| **Maximum Inclination [°]** | 3.2 |
| **Oldest penetrated age** | LATE TRIASSIC |
| **Oldest penetrated formation** | SNADD FORMATION |
| **Geoedic Datum** | ED50 |
| **NS degrees** | 72° 29' 28.92'' N |
| **EW degrees** | 20° 20' 2.25'' E |
| **NS UTM [m]** | 8051910.71 |
| **EW UTM [m]** | 678908.52 |
| **UTM Zone** | 33 |
| **NPDID Wellbore** | 6484 |

## Appendix II. Saturation results from conventional core analysis (after Mossefinn 2011)

| Depth [m] | Porosity [%] | Grain Density [g/cc] | Water Saturation [%] |
|---|---|---|---|
| 1293,18 | 27,5 | 2,64 | 6,6 |
| 1294,07 | 0,70 | 2,67 | 21,4 |
| 1295,07 | 25,4 | 2,65 | 33,2 |
| 1296,06 | 24,8 | 2,64 | 15,2 |
| 1298,05 | 25,4 | 2,64 | 9,8 |
| 1299,05 | 26,6 | 2,64 | 50,5 |
| 1300,05 | 25,5 | 2,64 | 51,2 |
| 1301,05 | 26,4 | 2,64 | 52,3 |
| 1302,05 | 26,3 | 2,64 | 58,6 |
| 1303,05 | 26,5 | 2,64 | 14,0 |
| 1304,05 | 23,5 | 2,64 | 50,9 |
| 1305,05 | 25,3 | 2,64 | 49,0 |
| 1306,05 | 22,8 | 2,65 | 52,9 |
| 1307,05 | 24,0 | 2,64 | 31,7 |
| 1308,05 | 22,4 | 2,65 | 46,5 |
| 1309,05 | 22,7 | 2,65 | 53,4 |
| 1310,05 | 20,9 | 2,66 | 54,2 |
| 1311,05 | 22,9 | 2,66 | 49,7 |
| 1312,05 | 21,6 | 2,65 | 50,1 |
| 1313,05 | 21,0 | 2,65 | 35,3 |
| 1314,05 | 21,3 | 2,65 | 38,3 |
| 1315,05 | 0,90 | 2,67 | 36,2 |
| 1316,05 | 24,8 | 2,69 | 41,8 |
| 1317,05 | 25,6 | 2,64 | 7,0 |
| 1318,05 | 24,9 | 2,64 | 5,4 |
| 1319,05 | 24,5 | 2,64 | 9,6 |
| 1320,05 | 26,0 | 2,64 | 9,7 |
| 1321,05 | 26,1 | 2,64 | 4,5 |
| 1322,05 | 26,3 | 2,64 | 4,6 |
| 1323,05 | 25,8 | 2,65 | 5,2 |
| 1324,09 | 25,8 | 2,64 | 8,1 |
| 1325,05 | 26,1 | 2,64 | 6,5 |
| 1326,05 | 25,8 | 2,64 | 4,1 |
| 1327,05 | 26,9 | 2,64 | 3,7 |
| 1328,05 | 26,1 | 2,64 | 4,1 |
| 1329,05 | 26,5 | 2,64 | 3,3 |
| 1330,05 | 26,4 | 2,64 | 3,7 |
| 1331,05 | 26,3 | 2,64 | 4,9 |
| 1332,05 | 26,4 | 2,64 | 5,0 |
| 1333,05 | 26,8 | 2,64 | 5,6 |
| 1334,05 | 26,8 | 2,64 | 5,5 |
| 1335,05 | 27,4 | 2,64 | 5,8 |
| 1336,05 | 23,0 | 2,64 | 36,7 |
| 1337,05 | 24,3 | 2,64 | 46,1 |
| 1338,05 | 26,7 | 2,64 | 4,5 |
| 1339,05 | 26,9 | 2,63 | 8,6 |
| 1340,05 | 27,5 | 2,63 | 11,3 |
| 1341,05 | 26,9 | 2,64 | 9,2 |
| 1342,05 | 27,0 | 2,64 | 21,3 |
| 1343,05 | 26,0 | 2,64 | 8,4 |
| 1344,05 | 27,0 | 2,64 | 11,6 |
| 1345,05 | 26,9 | 2,64 | 7,9 |
| 1346,05 | 26,3 | 2,64 | 14,5 |
| 1347,05 | 26,4 | 2,64 | 6,3 |
| 1348,03 | 26,9 | 2,64 | 22,0 |
| 1349,05 | 26,7 | 2,63 | 11,4 |
| 1350,05 | 27,4 | 2,66 | 7,6 |
| 1351,23 | 26,5 | 2,64 | 7,7 |
| 1352,05 | 26,9 | 2,64 | 46,6 |
| 1353,05 | 26,7 | 2,63 | 11,3 |
| 1354,05 | 26,1 | 2,63 | 8,2 |
| 1355,05 | 28,7 | 2,64 | 57,2 |
| 1356,05 | 30,1 | 2,64 | 11,2 |
| 1357,10 | 29,2 | 2,65 | 13,0 |
| 1358,06 | 29,7 | 2,64 | 12,6 |
| 1359,03 | 27,1 | 2,64 | 6,6 |
| 1360,12 | 25,5 | 2,64 | 27,9 |
| 1361,10 | 27,4 | 2,64 | 7,0 |
| 1362,07 | 29,0 | 2,64 | 10,5 |
| 1363,07 | 28,8 | 2,65 | 11,2 |
| 1364,07 | 25,4 | 2,64 | 18,7 |
| 1365,13 | 29,3 | 2,64 | 12,0 |
| 1366,06 | 24,3 | 2,66 | 40,9 |
| 1367,08 | 27,1 | 2,65 | 16,5 |
| 1368,10 | 25,9 | 2,66 | 19,3 |
| 1369,08 | 21,9 | 2,65 | 39,5 |
| 1370,10 | 27,4 | 2,65 | 12,0 |
| 1371,07 | 24,1 | 2,65 | 40,7 |
| 1372,11 | 27,2 | 2,65 | 19,4 |
| 1373,05 | 17,9 | 2,69 | 77,2 |
| 1374,07 | 26,3 | 2,65 | 26,5 |
| 1375,06 | 20,5 | 2,66 | 67,3 |
| 1376,07 | 6,30 | 2,69 | 87,8 |
| 1377,05 | 15,5 | 2,77 | 98,6 |
| 1379,10 | 13,7 | 2,69 | 99,9 |
| 1380,05 | 27,4 | 2,64 | 14,5 |

| | | | |
|---|---|---|---|
| 1381,05 | 31,3 | 2,64 | 12,1 |
| 1382,05 | 30,2 | 2,64 | 15,0 |
| 1383,05 | 30,6 | 2,64 | 16,6 |
| 1384,08 | 31,1 | 2,64 | 17,4 |
| 1385,08 | 28,1 | 2,64 | 31,3 |
| 1386,08 | 3,4 | 2,67 | 66,2 |
| 1387,08 | 30,2 | 2,64 | 37,7 |
| 1388,08 | 30,7 | 2,64 | 36,5 |
| 1389,06 | 27,0 | 2,65 | 57,2 |
| 1390,08 | 25,4 | 2,65 | 58,5 |
| 1391,07 | 29,0 | 2,64 | 46,2 |
| 1392,07 | 22,1 | 2,65 | 82,9 |
| 1393,06 | 29,1 | 2,64 | 56,7 |
| 1394,08 | 24,1 | 2,65 | 75,2 |

# Appendix III. Initial logs from well 7220/8-1 used in formation evaluation (Covering Stø & Nordmela formations)

**From left to right the log panel display the following logs**: ECGR (Environmentally Corrected Gamma Ray), HCAL (Caliper), BS (Borehole Size), PEFZ (Photoelectric Factor), NPHI (Neutron), RHOZ (Density), RT_HRLT (Formation resistivity), RLA 1-5 (Resistivity @ different penetration depths from the borehole wall), RXO_HRLT (Mud resistivity), RH54_1DF (Horizontal resistivity), RV54_1DF (Vertical resistivity), DTSM (Delta Time Share/Sonic log) and DTCO (Delta Time Compressional/Sonic log).

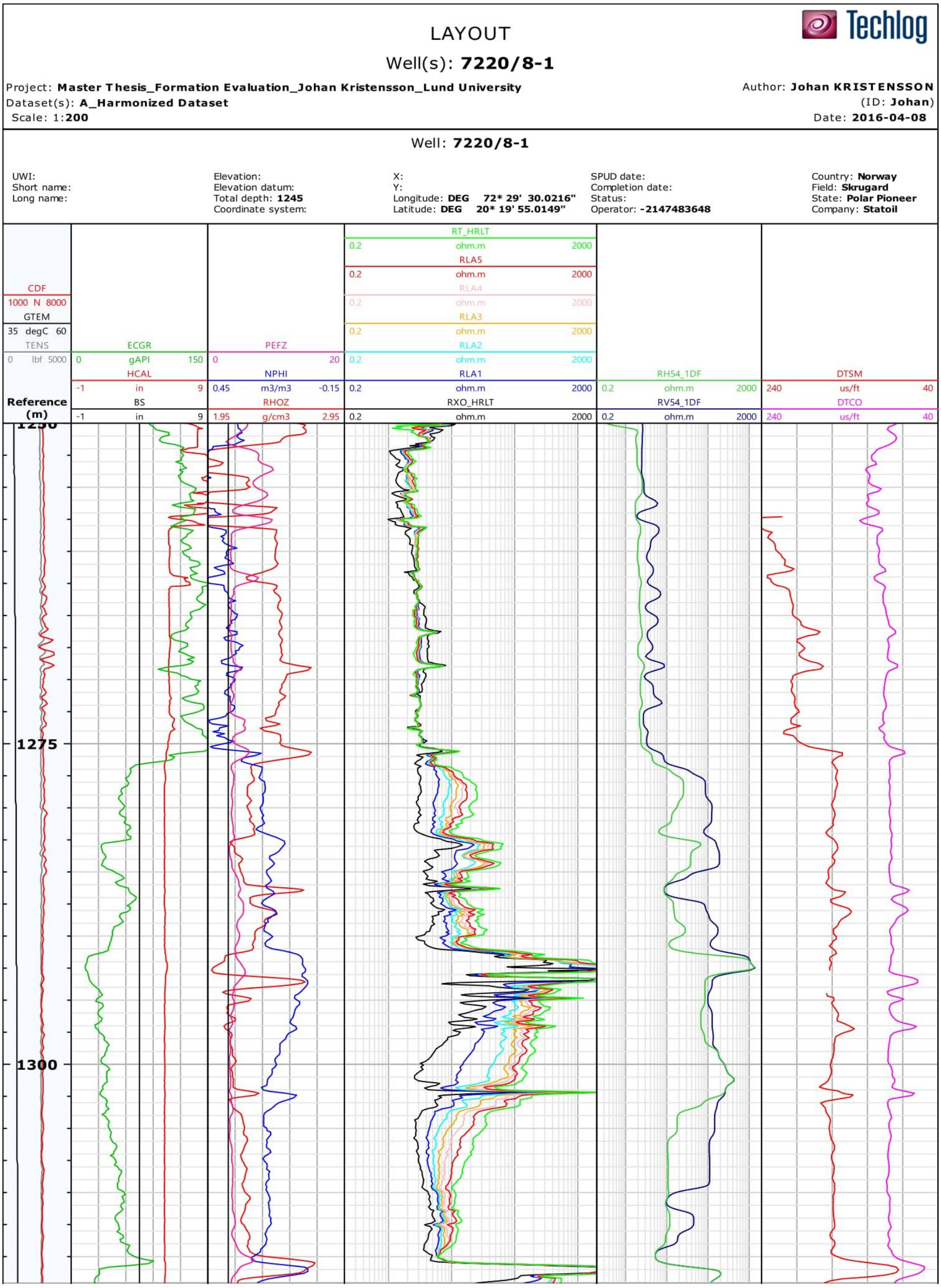

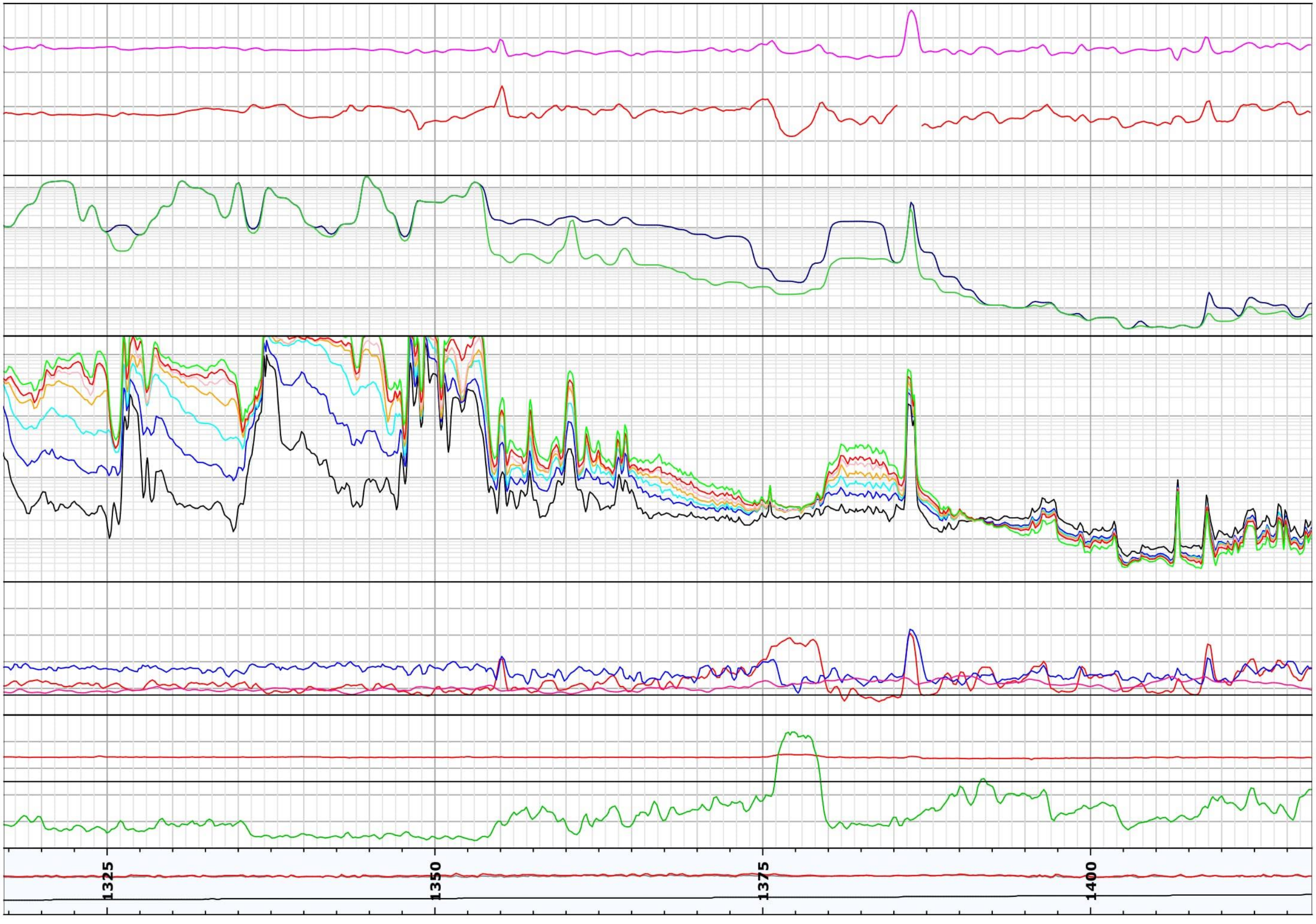
1325
1350
1375
1400

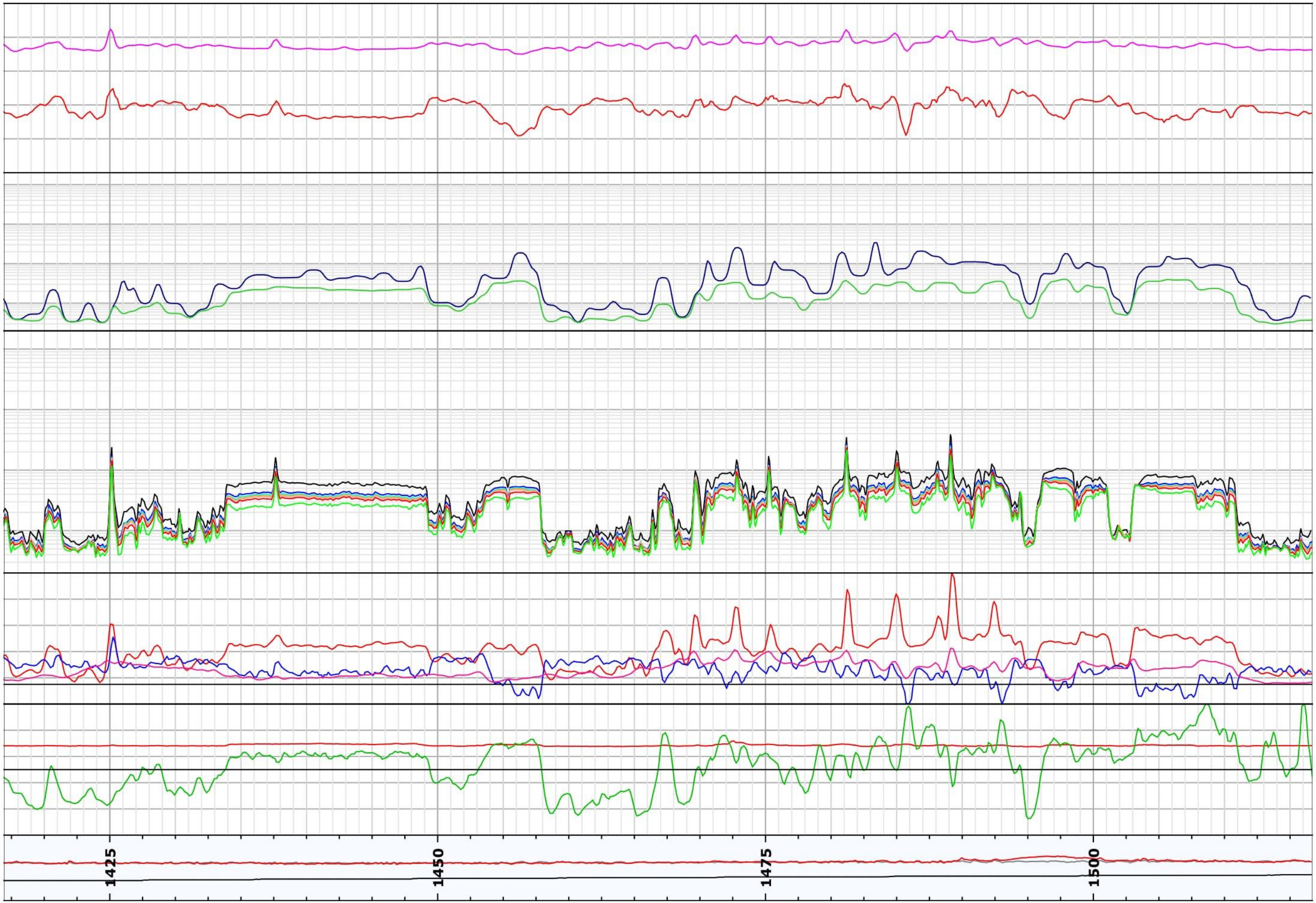
1425
1450
1475
1500

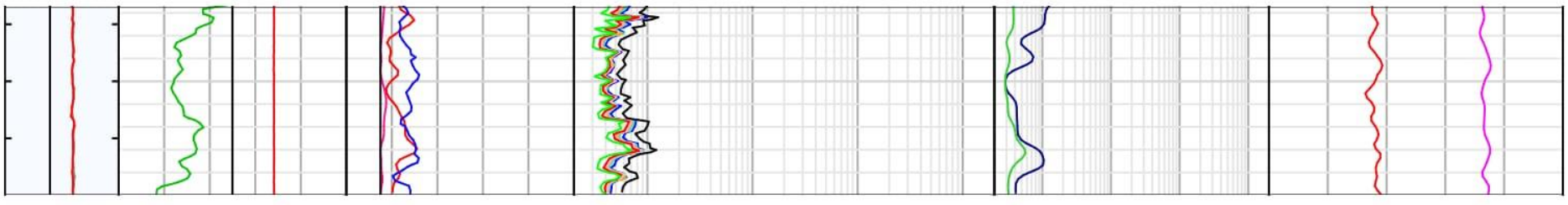

# Appendix IV. Logs interpreted and computed from the initial log suite (Appendix III)

**From left to right the log panel display the following logs**: ECGR (Environmentally Corrected Gamma Ray – Yellow shading interpreted as sand and brown shading interpreted as shale), HCAL (Caliper), BS (Borehole Size), VSH_GR (Volume of Shale computed from ECGR), PHIE_D (Effective porosity from RHOZ), PHIT_D (Total porosity from RHOZ), PHIE_ND (Effective porosity from RHOZ & NPHI), PHIT_ND (Total porosity from RHOZ & NPHI), RH54_1DF (Horizontal resistivity), RV54_1DF (Vertical resistivity – Light yellow shading interpreted as sections where horizontal/vertical resistivity anisotropy occur), Rv_Rh_Ratio (Low resistivity anisotropy [<2] vs. High resistivity anisotropy [>2]), Rsand [Rh] (Horizontal sand resistivity), Rsand [Rv] (Vertical sand resistivity), ), RT_HRLT (Formation resistivity), RLA 1-5 (Resistivity @ different penetration depths from the borehole wall) and RXO_HRLT (Mud resistivity)

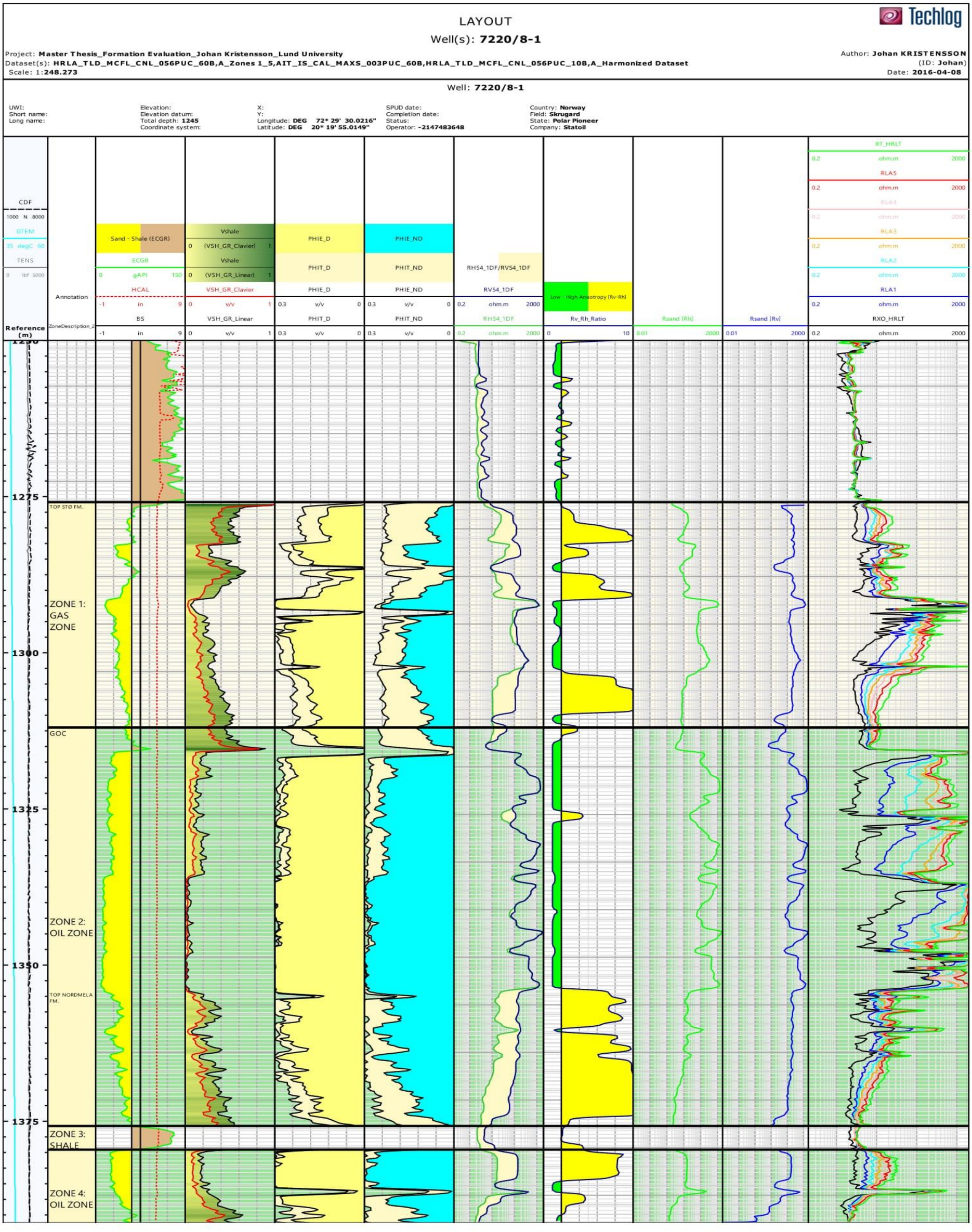


OWC
ZONE 5: WATER ZONE
ZONE 5: WATER ZONE
TOP TUBAEN FM.
1400
1425
1450
1475
1500

# Appendix V. Logs comparing the results from the Archie, Indonesia and Archie/Clavaud water saturation calculations

**From left to right the log panel display the following logs**: ECGR (Environmentally Corrected Gamma Ray), - Results from the Archie equation using PHIT_D, - Results from the Indonesia equation using PHIE_D, - Results from the Archie/Clavaud equation using PHIT_D, - Results from the Archie equation using PHIT_ND, - Results from the Indonesia equation using PHIE_ND and - Results from the Archie/Clavaud equation using PHIT_ND.

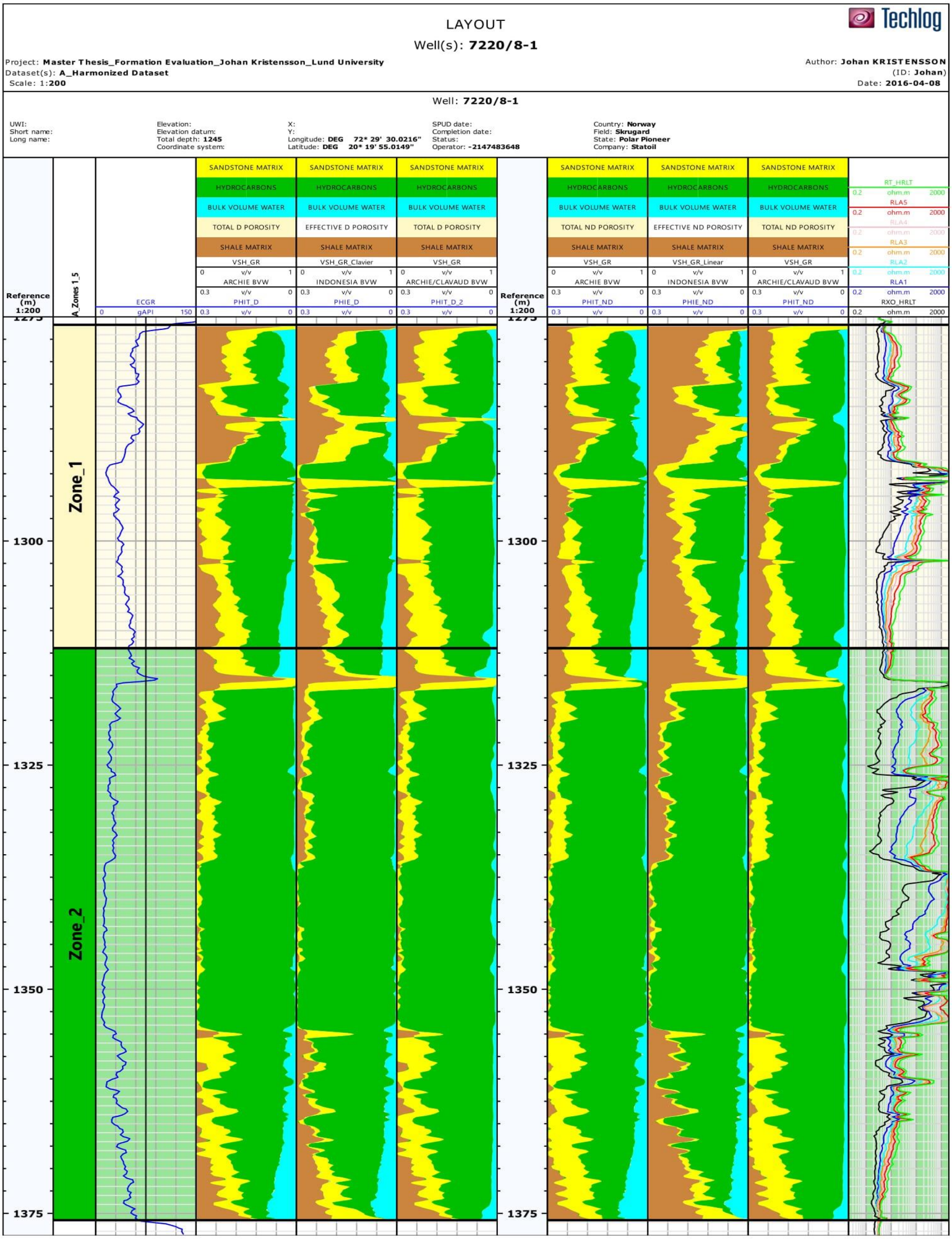


1500
1475
1450
1425
1400
Zone_5
Zone_4

## Tidigare skrifter i serien ”Examensarbeten i Geologi vid Lunds universitet”:

443. Lönsjö, Emma, 2015: Utbredningen av PFOS i Sverige och världen med fokus på grundvattnet – en litteraturstudie. (15 hp)
444. Asani, Besnik, 2015: A geophysical study of a drumlin in the Åsnen area, Småland, south Sweden. (15 hp)
445. Ohlin, Jeanette, 2015: Riskanalys över pesticidförekomst i enskilda brunnar i Sjöbo kommun. (15 hp)
446. Stevic, Marijana, 2015: Identification and environmental interpretation of microtextures on quartz grains from aeolian sediments - Brattforsheden and Vittskövle, Sweden. (15 hp)
447. Johansson, Ida, 2015: Is there an influence of solar activity on the North Atlantic Oscillation? A literature study of the forcing factors behind the North Atlantic Oscillation. (15 hp)
448. Halling, Jenny, 2015: Inventering av sprickmineraliseringar i en del av Sorgenfrei-Tornquistzonen, Dalby stenbrott, Skåne. (15 hp)
449. Nordas, Johan, 2015: A palynological study across the Ordovician Kinnekulle. (15 hp)
450. Åhlén, Alexandra, 2015: Carbonatites at the Alnö complex, Sweden and along the East African Rift: a literature review. (15 hp)
451. Andersson, Klara, 2015: Undersökning av slugtestsmetodik. (15 hp)
452. Ivarsson, Filip, 2015: Hur bildades Bushveldkomplexet? (15 hp)
453. Glommé, Alexandra, 2015: $^{87}Sr/^{86}Sr$ in plagioclase, evidence for a crustal origin of the Hakefjorden Complex, SW Sweden. (45 hp)
454. Kullberg, Sara, 2015: Using Fe-Ti oxides and trace element analysis to determine crystallization sequence of an anorthosite-norite intrusion, Älgön SW Sweden. (45 hp)
455. Gustafsson, Jon, 2015: När började plattektoniken? Bevis för plattektoniska processer i geologisk tid. (15 hp)
456. Bergqvist, Martina, 2015: Kan Ölands grundvatten öka vid en uppdämning av de utgrävda dikena genom strandvallarna på Ölands östkust? (15 hp)
457. Larsson, Emilie, 2015: U-Pb baddeleyite dating of intrusions in the south-easternmost Kaapvaal Craton (South Africa): revealing multiple events of dyke emplacement. (45 hp)
458. Zaman, Patrik, 2015: LiDAR mapping of presumed rock-cored drumlins in the Lake Åsnen area, Småland, South Sweden. (15 hp)
459. Aguilera Pradenas, Ariam, 2015: The formation mechanisms of Polycrystalline diamonds: diamondites and carbonados. (15 hp)
460. Viehweger, Bernhard, 2015: Sources and effects of short-term environmental changes in Gullmar Fjord, Sweden, inferred from the composition of sedimentary organic matter. (45 hp)
461. Bokhari Friberg, Yasmin, 2015: The paleoceanography of Kattegat during the last deglaciation from benthic foraminiferal stable isotopes. (45 hp)
462. Lundberg, Frans, 2016: Cambrian stratigraphy and depositional dynamics based on the Tomten-1 drill core, Falbygden, Västergötland, Sweden. (45 hp)
463. Flindt, Anne-Cécile, 2016: A pre-LGM sandur deposit at Fiskarheden, NW Dalarna - sedimentology and glaciotectonic deformation. (45 hp)
464. Karlatou-Charalampopoulou, Artemis, 2016: Vegetation responses to Late Glacial climate shifts as reflected in a high resolution pollen record from Blekinge, south-eastern Sweden, compared with responses of other climate proxies. (45 hp)
465. Hajny, Casandra, 2016: Sedimentological study of the Jurassic and Cretaceous sequence in the Revinge-1 core, Scania. (45 hp)
466. Linders, Wictor, 2016: U-Pb geochronology and geochemistry of host rocks to the Bastnäs-type REE mineralization in the Riddarhyttan area, west central Berglsagen, Sweden. (45 hp)
467. Olsson, Andreas, 2016: Metamorphic record of monazite in aluminous migmatitic gneisses at Stensjöstrand, Sveconorwegian orogen. (45 hp)
468. Liesirova, Tina, 2016: Oxygen and its impact on nitrification rates in aquatic sediments. (15 hp)
469. Perneby Molin, Susanna, 2016: Embryologi och tidig ontogeni hos mesozoiska fisködlor (Ichthyopterygia). (15 hp)
470. Benavides Höglund, Nikolas, 2016: Digitization and interpretation of vintage 2D seismic reflection data from Hanö Bay, Sweden. (15 hp)
471. Malmgren, Johan, 2016: De mellankambriska oelandicuslagren på Öland - stratigrafi och faciestyper. (15 hp)
472. Fouskopoulos Larsson, Anna, 2016: XRF -studie av sedimentära borrkärnor - en metodikstudie av programvarorna Q-spec och Tray-sum. (15 hp)
473. Jansson, Robin, 2016: Är ERT och Tidsdomän IP potentiella karteringsverk-

tyg inom miljögeologi? (15 hp)

474. Heger, Katja, 2016: Makrofossilanalys av sediment från det tidig-holocena undervattenslandskapet vid Haväng, östra Skåne. (15 hp)
475. Swierz, Pia, 2016: Utvärdering av vattenkemisk data från Borgholm kommun och dess relation till geologiska förhållanden och markanvändning. (15 hp)
476. Mårdh, Joakim, 2016: WalkTEM-undersökning vid Revingehed provpumpningsanläggning. (15 hp)
477. Rydberg, Elaine, 2016: Gummigranulat - En litteraturstudie över miljö- och hälsopåverkan vid användandet av gummigranulat. (15 hp)
478. Björnfors, Mark, 2016: Kusterosion och äldre kustdyners morfologi i Skälderviken. (15 hp)
479. Ringholm, Martin, 2016: Klimatutlöst matbrist i tidiga medeltida Europa, en jämförande studie mellan historiska dokument och paleoklimatarkiv. (15 hp)
480. Teilmann, Kim, 2016: Paleomagnetic dating of a mysterious lake record from the Kerguelen archipelago by matching to paleomagnetic field models. (15 hp)
481. Schönström, Jonas, 2016: Resistivitets- och markradarmätning i Ängelholmsområdet - undersökning av korrosiva markstrukturer kring vattenledningar. (15 hp)
482. Martell, Josefin, 2016: A study of shock-metamorphic features in zircon from the Siljan impact structure, Sweden. (15 hp)
483. Rosvall, Markus, 2016: Spår av himlakroppskollisioner - bergarter i nedslagskratrar med fokus på Mien, Småland. (15 hp)
484. Olausson, My, 2016: Resistivitets- och IP -mätningar på den nedlagda deponin Gustavsfält i Halmstad. (30 hp)
485. Plan, Anders, 2016: Markradar- och resistivitetsmätningar – undersökningar utav korrosionsförhöjande markegenskaper kring fjärrvärmeledningar i Ängelholm. (15 hp)
486. Jennerheim, Jessica, 2016: Evaluation of methods to characterise the geochemistry of limestone and its fracturing in connection to heating. (45 hp)
487. Olsson, Pontus, 2016: Ekologiskt vatten från Lilla Klåveröd: en riskinventering för skydd av grundvatten. (15 hp)
488. Henriksson, Oskar, 2016: The Dynamics of Beryllium 10 transport and deposition in lake sediments. (15 hp)
489. Brådenmark, Niklas, 2016: Lower to Middle Ordovician carbonate sedimentology and stratigraphy of the Pakri peninsula, north-western Estonia. (45 hp)
490. Karlsson, Michelle, 2016: Utvärdering av metoderna DCIP och CSIA för identifiering av nedbrytningszoner för klorerade lösningsmedel: En studie av Färgaren 3 i Kristianstad. (45 hp)
491. Elali, Mohammed, 2016: Flygsanddyners inre uppbyggnad – georadarundersökning. (15 hp)
492. Preis-Bergdahl, Daniel, 2016: Evaluation of DC Resistivity and Time-Domain IP Tomography for Bedrock Characterisation at Önneslöv, Southern Sweden. (45 hp)
493. Kristensson, Johan, 2016: Formation evaluation of the Jurassic Stø and Nordmela formations in exploration well 7220/8-1, Barents Sea, Norway. (45 hp)

LUNDS UNIVERSITET

**Geologiska institutionen**
**Lunds universitet**
**Sölvegatan 12, 223 62 Lund**